Contaminant Transfer in a Run-Around Membrane Energy Exchanger

A Thesis Submitted to the College of

Graduate Studies and Research

In Partial Fulfillment of the Requirements

For the Degree of Master of Science

In the Department of Mechanical Engineering

University of Saskatchewan

Saskatoon

By

Hiren Patel

Permission to Use

In presenting this thesis in partial fulfillment of the requirements for a postgraduate degree from the University of Saskatchewan, I agree that the Libraries of this University may make it freely available for inspection. I further agree that permission for copying of this thesis in any manner, in whole or in part, for scholarly purposes may be granted by the professors who supervised my thesis work or, in their absence, by the Head of the Department or the Dean of the College in which my thesis work was done. It is understood that any copying or publication or use of this thesis or parts thereof for financial gain shall not be allowed without my written permission. It is also understood that due recognition shall be given to me and to the University of Saskatchewan in any scholarly use which may be made of any material in my thesis.

Requests for permission to copy or to make other use of material in this thesis in whole or part should be addressed to:

Head of the Department of Mechanical Engineering

University of Saskatchewan

Saskatoon, Saskatchewan (S7N 5A9)

ABSTRACT

Volatile Organic Compounds (VOCs) constitute an important class of indoor air contaminants and they may cause adverse health effects for occupants in buildings. Indoor generated contaminants may be transferred between the supply and exhaust air streams of the building's Heating, Ventilation and Air-conditioning (HVAC) system when air-to-air energy recovery devices are used. The run-around membrane energy exchanger (RAMEE) is a novel exchanger, which uses aqueous magnesium chloride ($MgCl_2$) salt solution (34-35 wt%) as a liquid desiccant to transfer heat and moisture between remote supply and exhaust air streams. In the RAMEE, a gas-phase porous membrane is placed between the air stream and the liquid desiccant stream in each exchanger and the membrane prevents the salt solution from entering the air stream but still allows the transfer of water vapor through the semi-permeable membrane.

In the RAMEE, VOCs may transfer between the exhaust and supply air streams due to (i) air leakage or (ii) due to dissolution of VOCs into the liquid desiccant in the exhaust exchanger and their subsequent evaporation into the air stream of the supply exchanger. These two transfer mechanisms were tested in the laboratory using two counter-cross-flow RAMEE prototypes (Prototype #4 and Prototype #6). Tests were conducted at different air and desiccant flow rates at AHRI standard summer and winter operating conditions. Sulfur hexafluoride (SF_6) was used as a tracer gas to test air leakage and toluene (C_7H_8) and formaldehyde (HCHO) were used to test VOC dissolution and transfer. From an external source, a known concentration of VOC was injected into the exhaust air inlet stream and the transfer fraction of VOC to the supply air stream was calculated. This transfer fraction or Exhaust Air Transfer Ratio (*EATR*) defined by ANSI/ASHRAE Standard 84 (2012) at steady state conditions was used to quantify and compare

the transfer fraction of contaminants in both prototypes. The uncertainty in the transfer fraction was calculated and all the uncertainty bounds were calculated for 95% confidence interval.

The transfer fraction of sulfur hexafluoride was $0.02 \pm 3.6\%$ for both prototypes tested, which means that the air leakage between the air streams is negligible. The transfer of toluene, which has a low solubility in water, was less than the uncertainty in the measurement. *EATR** values for toluene were 2.3-3.4% and the uncertainties were 3.4-3.6%. The transfer of formaldehyde between the exhaust and the supply air streams was the highest and the *EATR** values just exceeded the uncertainties in the *EATR** measurement. The highest *EATR** values for the transfer of formaldehyde in Prototype #4 and Prototype #6 were $6.4\% \pm 3.6\%$ and $5.3 \pm 3.6\%$, respectively. At steady state, the measured *EATR** values for both prototypes were insensitive to changes in the air flow rate, the liquid desiccant flow rate, the latent effectiveness and the environmental conditions but time delays to reach steady state were significant. These results imply that there is a negligible transfer of contaminants due to air leakage between the air streams, a negligible transfer of low water soluble VOCs (such as toluene), but possibly a small detectable transfer of very water soluble VOCs (such as formaldehyde) between the exhaust and supply air streams of the RAMEE.

ACKNOWLEDGEMENTS

It would not have been possible to write this thesis without the help and support of the kind people around me, to only some of whom it is possible to give particular mention here.

Above all, I would like to thank my supervisors, Prof. Carey Simonson and Prof. Robert Besant, for their wealth of knowledge and continuing support throughout this research program. I am very grateful for their motivation, patience and understanding. Their good advice has been invaluable on both an academic and a personal level. I would also like to thank Dr. Gazi Mahmood for his recommendations and suggestions. I would like to extend my gratitude to the RAMEE research team but in particular Khizir Mahmud and David Beriault for all their help.

A special thanks to my committee members Prof. David Sumner and Prof. David Torvi for their comments and suggestions. I also acknowledge the invaluable assistance of Mr. Rick Retzlaff and Mr. Dave Deutscher in facilitating the laboratory experiments.

Most importantly, my parents have given me their unequivocal support throughout, as always, for which my mere expression of thanks does not suffice. I would like to thank Mr. Jim Hanson for his kindness and support in completion of this thesis. I would also like to thank my friends Shivani Trivedi, Aditya Manek, Geeta Dinani and Nayan Patel for their support and prayers.

Last, but by no means least, I would like to acknowledge the financial support from the Natural Science and Engineering Research Council of Canada (NSERC) and Venmar CES Inc., Saskatoon.

Dedication

I dedicate this thesis to my parents Niranjanbhai Patel and Bhagvatiben Patel.

I could not have succeeded without your love and blessings.

TABLE OF CONTENTS

Page

LIST OF TABLES

Table **Page**

LIST OF FIGURES

Figure **Page**

NOMENCLATURE

ACRONYMS

ACGIH	American Conference of Governmental Industrial Hygienists
AHRI	Air-conditioning Heating and Refrigerating Institute
ANSI	American National Standard Institute
ASHRAE	American Society of Heating, Refrigerating and Air-Conditioning Engineers
CRD	Collaborative Research and Development
DAQ	Data Acquisition
DSP	Digital Signal Processor
EATR	Exhaust Air Transfer Ratio
ECA	European Collaborative Action
EE	Exhaust Exchanger
EI	Exhaust Inlet
ePTFE	Expanded Polytetrafluoroethylene
ER	Energy Recovery
FFT	Fast Fourier Transform
FID	Flame Ionization Detection
FTIR	Fourier Transform Infrared Spectroscopy
GC	Gas Chromatography
HPLC	High Performance Liquid Chromatography
HVAC	Heating, Ventilation and Air-Conditioning
IR	Infrared Spectroscopy

ISO	International Organization for Standardization
LAMEE	Liquid-to-Air Membrane Energy Exchanger
MS	Mass Spectroscopy
NI	National Instruments
NIOSH	National Institute for Occupational Safety and Health
NSERC	Natural Science and Engineering Research Council of Canada
PI	Process Inlet
POM	Particulate Organic Matter
PTC	Performance Test Code
PVC	Polyvinyl Chloride
RAHE	Run-Around Heat Exchanger
RAMEE	Run-Around Membrane Energy Exchanger
RH	Relative Humidity
RO	Regeneration Outlet
RTD	Resistance Temperature Detector
SE	Supply Exchanger
SI	Supply Inlet
ST	Short Term
SVOC	Semi Volatile Organic Compound
TVOC	Total Volatile Organic Compound
TWA	Time Weighted Average
VOC	Volatile Organic Compound
VVOC	Very Volatile Organic Compound

WHO	World Health Organization

English Symbols

a	Absorptivity (m^2/mol)
A	membrane surface area (m^2)
A	absorbance
b	optical path length (m)
B	bias uncertainty
C	heat capacity rate (W/K)
C_0	solubility of the compound in the distilled water (g/L)
C_{air}	heat capacity rate of air (W/K)
C_d	discharge coefficient
C_i	concentration (ppm)
C_p	specific heat capacity (J/kgK)
C_r	ratio of minimum to maximum heat capacity rate
C_s	saturation concentration (g/L)
C_{salt}	solubility of the compound in the salt solution (g/L)
C_{sol}	heat capacity rate of liquid desiccant (W/K)
d	diameter of orifice plate opening (m)
D	inside diameter of pipe (m)
D_{AB}	diffusivity of component A through component B (m^2/s)
h	enthalpy (J/kg)
h_G	gas specific parameter

h_i	ion specific parameter
H	height of the exchanger (m)
H_{mem}	height of the membrane surface (m)
I	intensity of infrared radiation
k	Boltzman's constant (J/K)
k_s	absorption coefficient (mol/Latm)
K_s	salting or setschenow constant
L	length (m)
$L_{sol,e}$	entrance length of the desiccant solution (m)
$\dot{m}$	mass flow rate (kg/s)
M	mass balance inequality
M	molecular weight (g/mol)
NTU	number of heat transfer units
NTU_m	number of mass transfer units
P	precision uncertainty
P	pressure (kPa)
P_i	partial pressure of individual component (kPa)
P_v	partial pressure of vapor (kPa)
$P_{v,sat}$	saturation vapor pressure (kPa)
q	volumetric flowrate (m^3/s)
r_{AB}	molecular separation at collision (nm)
R	thermal resistance (K/W)
R	universal gas constant (kJ/kgK)

R_m	mass transfer resistance
S	salt concentration
t	t-student distribution constant
T	temperature (^oC)
T	transmittance
T_b	normal boiling point (^oC)
U	overall heat transfer coefficient (W/m^2K)
V	volume (L)
W	humidity ratio (kg_w/kg_{da})
x	mole fraction
X	air properties (temperature, humidity ratio and enthalpy)

Greek Symbols

β	orifice plate diameter ratio
ΔP	pressure drop across an orifice plate (kPa)
ε	effectiveness
ε_{AB}	energy of molecular attraction
ε_l	latent effectivenes
ε_s	sensible effectiveness
ρ	density (kg/m^3)

Subscripts

air	air

atm	atmosphere
avg	average
da	dry air
f	formaldehyde
m	mixture
max	maximum
mem	membrane
min	minimum
sat	saturation
sol	desiccant solution
t	toluene
v	vapor

CHAPTER 1

INTRODUCTION

1.1 Overview

In cold and moderate climate countries, people spend up to 90% of their time indoors (Brown et al., 1994). Hence, for the majority of time people are exposed to various contaminants present in indoor air. There are several sources of indoor air contaminants in buildings which include building materials (e.g. airborne emissions from insulation, paint, plywood, adhesives), furnishing materials (e.g. emissions from furniture, floor and wall coverings), consumer products (e.g. air fresheners, cleaning and personal care products), equipment (e.g. emissions from laser printers, photocopiers, computers, other office equipment), indoor activities (e.g. from cooking, tobacco smoke, use of solvents), and ventilation systems (e.g. transmission through air filters for heating, ventilation and air-conditioning (HVAC) systems) Additionally, outdoor ventilation air may be contaminated by traffic and neighboring industrial sources (Wolkoff et al., 1997). Air contamination is a concern for ventilation engineers when it causes indoor health problems for building occupants.

Air contaminants are classified as particles or gases (e.g. Very Volatile Organic Compounds (VVOCs), Volatile Organic Compounds (VOCs), Semi Volatile Organic Compounds (SVOCs) and Particulate Organic Matter (POM) (WHO, 1989)). Among these indoor contaminants, VOCs have attracted considerable attention in nonindustrial environments as many of them have adverse health effects on occupants (e.g. causing headache, drowsiness

and difficulties in breathing). Above certain threshold concentrations, they are either known, or suspected, to cause allergic, carcinogenic, neurotoxic, immunotoxic and irritant reactions among people (Molhave, 1991). More than 307 compounds of VOCs have been identified in indoor air in different countries (Berglund et al., 1989). Each compound seldom exceeds a concentration level of 50 $\mu g/m^3$, which is 100 to 1000 times lower than relevant occupational health threshold limit values (TLVs) listed by the American Conference of Governmental Industrial Hygienists (ACGIH, 1988). The total concentration of all VOCs in non-industrial environments is normally well below 1 mg/m^3 (Molhave, 1986).

Several researchers have studied the effects of VOC exposure on human health under a variety of design conditions (Kjaergaard et al., 1991; Hundell et al., 1993; Molhave et al., 1993a, 1993b; Otto et al., 1993; Prah et al., 1993). In most of these studies, humans were exposed to a specified mixture of 22 different VOCs. Total Volatile Organic Compound (TVOC) concentration, the indicative measure for total measurable level of mixture of 22 VOCs, was investigated. The TVOC concentrations investigated in these studies ranged from 1 to 25 mg/m^3. Experimenters reported that there is no discomfort or irritation at TVOC concentration below 0.2 mg/m^3. Irritation of the eyes, nose and mouth was observed at TVOC concentration from 3 to 25 mg/m^3. Air quality was found to be substantially reduced causing headache and neurotoxic effects above 25 mg/m^3 or 0.02% of the air mass TVOC concentration.

Ventilation is the primary method for controlling air quality in the buildings as it brings in fresh air to dilute the contaminants. This can provide a healthy environment for building occupants and reduces the risk of contracting air transmitted diseases. Fresh air also plays an important role in worker productivity (Fang et al., 2000; Kosonen and Tan, 2004). This need for supply of fresh air results in a substantial need for energy to condition the supply air to comfort

conditions. Up to 50% of the energy consumed in a building is used to condition fresh air supply (D&R International, 2009). The recent emphasis on energy conservation has led to the construction of tighter buildings through better building envelope design and sealing.

Higher fractions of recirculated air are often used along with minimum fractions of fresh air. This reduces the amount of ventilation air that has to be heated or cooled. However, the combination of a tighter building with a low fresh air flow rates produces an indoor environment with relatively high level of contaminants and, as implied by the discussion above, this affects occupant health (Redlich et al., 1997). There are several ways to reduce energy consumption of HVAC systems while maintaining adequate supply of fresh air. One widely used technique is recuperation of the waste energy from the HVAC system exhaust air by the use of air-to-air energy recovery systems; however, concerns have been expressed that some types of air-to-air energy recovery systems also transfer contaminants between the exhaust and the supply air streams (Andersson et al., 1993). Consequently, there is a trade-off for the HVAC designers to provide a healthy indoor environment while minimizing the energy consumption and cost.

1.2 Air-to-Air Energy Recovery Systems

Fresh air needs to be supplied and an equivalent volume of air needs to be exhausted from the building continuously to provide adequate ventilation to the occupants of buildings. The exhaust air from buildings is close to the thermal comfort conditions for temperature and humidity (ANSI/ASHRAE Standard 55, 2004). An air-to-air energy recovery system is used to precondition the supply air close to the desired temperature and humidity in the space by transferring energy between the supply and exhaust air streams. Figure 1.1 shows schematic of a typical HVAC system with an air-to-air energy recovery system.

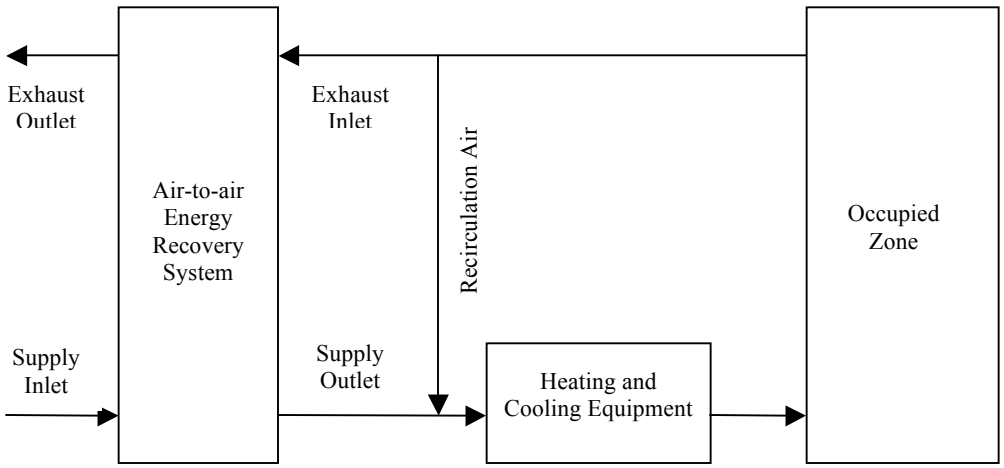

Figure 1.1: A schematic of a typical HVAC system with an air-to-air energy recovery system

As shown in Figure 1.1, an energy recovery device is installed between the supply and exhaust air duct and it transfers energy by transferring heat and moisture between the supply and exhaust air streams. The preconditioning of the incoming air saves some heating or cooling energy of the HVAC system. Depending on the outdoor conditions, the energy recovery device heats and humidifies or cools and dehumidifies the supply air. In summer, when the outdoor air is hot and humid, the transfer of heat and moisture from the supply air to the exhaust air will reduce the cooling loads on the HVAC system. In winter, the outdoor air is cold and dry; hence heat and moisture transfer from the exhaust air to the supply air can reduce the heating and specified humidification loads on the HVAC system.

Some indoor generated contaminants may transfer through air-to-air energy recovery devices from the exhaust air to the supply air along with the transfer of heat and moisture. This reduces the HVAC system's effectiveness for control of the concentration of these indoor contaminants. The transfer mechanism of contaminants varies by the type of air-to-air energy recovery device used. Hence, it is a challenge to design an air-to-air energy recovery device that

can recover the maximum amount of energy while minimizing the transfer of indoor generated contaminants.

1.2.1 Existing Energy Recovery Systems

Currently, there are several types of air-to-air energy recovery devices commercially available. Some of them, such as flat plate exchangers (Mishra et al., 2004; Srihari and Das, 2008; Spiga and Spiga, 1987), heat pipe exchangers (Wu et al., 1997), and glycol run-around loops (Fan et al., 2005; Johnson et al., 1995) can only transfer heat (sensible energy). A sensible energy recovery device is also called a heat exchanger. However, rotary energy wheels (Simonson, 2007), enthalpy plates (Zhang and Niu, 2002) and twin tower enthalpy recovery loops (Ali et. al., 2004; Mesquita et. al., 2006; Park et. al., 1994) can transfer both heat and moisture (sensible and latent energy). Hence, they are also known as energy or enthalpy exchangers. Larson (2006) introduced a new method to classify currently available energy recovery devices by categorizing them according to their modes of energy transfer as well as ducting arrangements. Larson (2006) divided all the energy recovery devices in four different categories as shown in Figure 1.2.

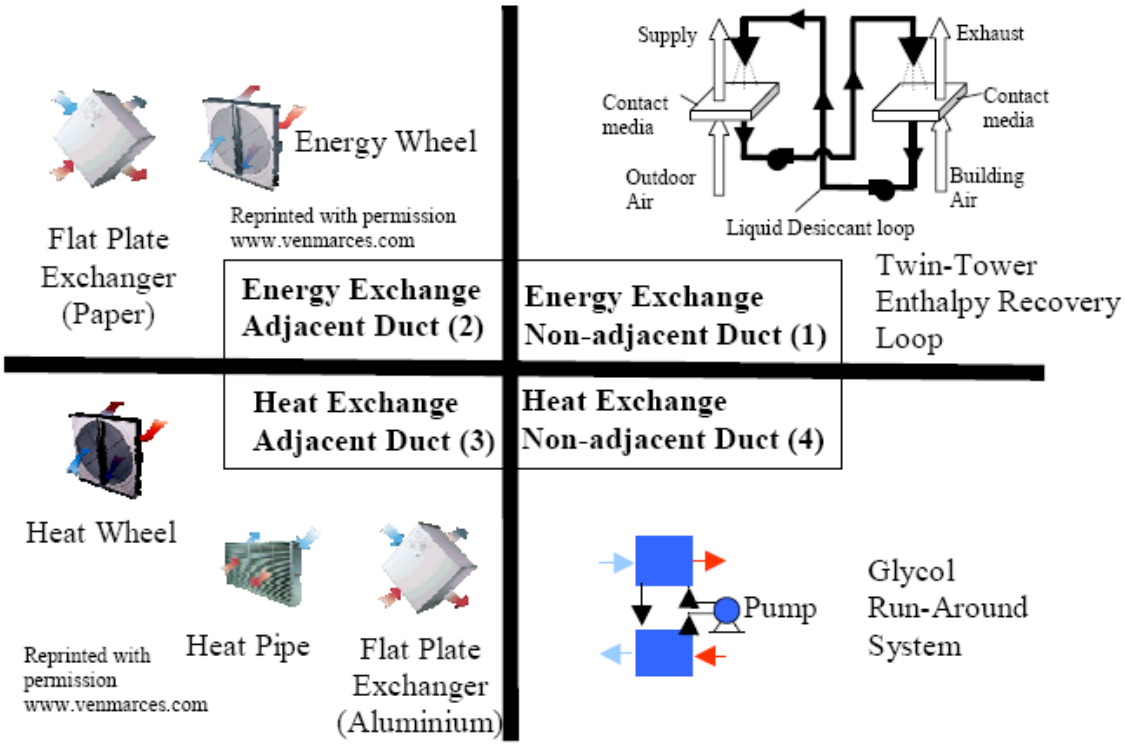

Figure 1.2: Four main categories of existing air-to-air energy recovery systems (Larson, 2006)

Some of these energy recovery devices (e.g. energy (enthalpy) wheels, heat wheels, heat pipes, and flat plate exchangers) can be installed only when there is an adjacent ducting arrangement. Hence, this requirement limits their application to mostly new buildings, as the cost of changing the ducting is often a problem for retrofitting existing buildings. According to ASHRAE (2008), the ideal air-to-air energy recovery system is capable of transferring both sensible and latent energy without any significant transfer of air contaminants. Transfer of contaminants between air streams can occur by air leakage, even in exchangers that are not designed for moisture transfer; however, in enthalpy exchangers there may be additional mechanisms for contaminant transfer. Hence, it requires careful selection of the energy recovery devices depending on the application as each of these energy recovery devices is not capable of transferring both heat and moisture (e.g. heat wheel, heat pipe, and glycol run-around loops).

1.3 Contaminant Transfer in Energy Recovery (ER) systems

Contaminant transfer in air-to-air energy recovery device may happen due to air leakage between the air streams, carry-over in rotating parts of the energy recovery device or sorption of contaminants on regenerative exchanger surfaces or liquids (Andersson et al., 1993). Contaminant transfer by air leakage happens due to pressure differentials between the adjacent supply and exhaust air duct, whereas carry-over is the fraction of entrained exhaust air transferred to the supply duct by the rotation of the energy (enthalpy) wheel (Shang et al., 2001). The transfer of contaminants by sorption mechanism occurs due to adsorption and desorption of contaminants along with water vapor and it is observed only in the case of energy (enthalpy) wheels. Significant transfer by sorption would appear most likely for contaminants (e.g. formaldehyde) that have a molecular-atomic structure chemically similar to that for water. These types of polar molecules are most soluble in water, aqueous solutions such as salt solutions and desiccant surfaces with several layers of attached adsorbed water molecules.

Increasing the pressure in the supply duct can minimize the contaminant transfer from the exhaust air to the supply air due to air leakage. However, it is difficult to reduce the contaminant transfer due to carry-over and sorption mechanisms, as they are complex mechanisms dependent on parameters such as rotational speed of the energy recovery device and solubility of contaminants. The mechanisms for contaminant transfer in various energy exchangers are discussed in the following sections.

1.3.1 Enthalpy Plate Exchanger

Enthalpy plate exchangers consist of a series of parallel plates with spaces between the adjacent plates. Typically, the supply and the exhaust air flows through these plates in a cross-flow direction. The enthalpy plate exchangers are made with a core fabricated from semi-

permeable hygroscopic membrane unlike the thin solid and non-permeable plates in flat plate exchangers. Cellulose, polymers and synthetic membranes are some of the most common types of hygroscopic materials. The semi-permeable membrane allows the transfer of heat as well as moisture and hence, enthalpy plate exchangers have relatively higher energy performance compared to flat plate heat exchangers.

From theoretical considerations, the contaminant transfer process in enthalpy plate exchangers can be divided into two stages. First, gas molecules must be transferred to the surface of the membrane by convection and molecular diffusion through the airstream. This transfer rate is dependent on the convection coefficient and the diffusion coefficient of the gas through air. The second stage, transfer through the membrane, may be due to more than one mechanism (Treybal, 1980). If the diameter of the pores of the membrane is greater than about 20 times the mean free path of the diffusing molecule, then ordinary molecular diffusion occurs at a rate that is proportional to the diffusion coefficient of the gas in air (Fisk et al., 1985). If the pore diameters are less than about 0.2 times the mean free path, the rate of diffusion through the membrane is controlled by collisions with the walls of the pores (Fisk et al., 1985). This process of diffusion is called Knudsen diffusion. The size, shape, and number of pores of the membrane are generally not known. Hence, the diffusion rate through the membrane is determined experimentally and characterized by an effective diffusion coefficient, which is based on the area of the solid in contrast to the area of pores.

Fisk et al. (1985) measured the transfer of formaldehyde (HCHO) and two tracer gases, propane (C_3H_8) and sulfur hexafluoride (SF_6), in an enthalpy plate exchanger, containing a cross-flow core fabricated from a treated paper. Only 5-8% of the two tracer gases and 8-12% of the formaldehyde injected into the exhaust air stream was transferred to the supply air stream. The

measured transfer fractions of propane and sulfur hexafluoride were nearly identical, whereas the predicted transfer fraction of propane by ordinary or Knudsen diffusion through pores was approximately 1.7 times the predicted transfer fraction of sulfur hexafluoride. This discrepancy between the experimental and theoretical predictions suggested that the primary transfer mechanism for propane and sulfur hexafluoride was leakage of air between the air streams. The transfer fraction of formaldehyde was measured significantly higher than those for propane and sulfur hexafluoride tracer gases. These differences cannot be caused by leakage of air or the two diffusion processes. Hence, it was concluded that formaldehyde must be transferred at a significant rate by an additional process of sorption.

Sparrow et al. (2001) tested the transfer of water vapor (H_2O) and carbon dioxide (CO_2) in a cross-flow enthalpy exchanger. This exchanger was made of a novel permeable material, which was manufactured by applying a thin layer of hydrophilic polymer film on top of a commercially available polymer membrane. The first set of experiments was conducted to measure the mass transfer effectiveness of water vapor and carbon dioxide through the composite membrane in a wind-tunnel test facility. Mass transfer effectiveness for water vapor was measured to be 20% at the exchanger face velocity of 1.27-2.29 m/s (250-450 fpm). The second set of experiments on the enthalpy exchanger was carried out as a simulated field test. The exchanger was placed in the ventilation of a commercial house and the water vapor transfer effectiveness was measured to be in the range of 50% at the exchanger face velocity of 0.25-0.76 m/s (50-150 fpm). The mass transfer effectiveness for carbon dioxide was measured to be lower than 1% at the face velocity of 1.52 m/s (300 fpm). It was concluded that the thin coating of polymer film prevented the transfer of carbon dioxide for the test conditions used while allowing the transfer of water vapor by solution diffusion. The authors recommended that the enthalpy

exchangers with this kind of composite polymer membrane could be used in the applications where indoor air quality is of primary importance along with energy conservation.

1.3.2 Energy Wheel

Energy wheels are the most common type of rotary air-to-air energy recovery devices used in buildings. The rotating wheel energy exchanger, also known as an enthalpy wheel, is composed of a rotating cylinder constructed from corrugated aluminum, plastic or synthetic fibers. A coating of desiccant such as silica gel, molecular sieve or zeolite desiccant is applied to the wheel for the purpose of humidifying or dehumidifying the air stream. Figure 1.3 shows a rotary air-to-air energy exchanger installed between the supply air stream and the exhaust air stream.

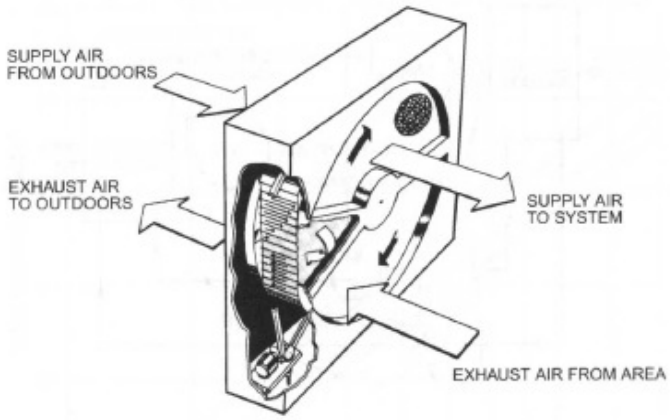

Figure 1.3: Rotary energy wheel (ASHRAE, 2008)

The two airstreams pass through the energy wheel such that one half of the wheel is in the supply air stream and the other half is in the exhaust air stream. As the energy wheel rotates, it picks up the heat and moisture (sensible and latent energy) from the exhaust air stream in one half of the rotation, and gives up to the supply air stream in the other half of the rotation. Since air can bypass at the interface between the two air streams at the energy exchanger boundary,

brushed flow channel seals are required to separate the two air streams. However, a higher pressure gradient between the two air streams often results in a cross-leakage of up to 10% of total airflow and it can cause the unwanted contamination of the supply air (ASHRAE, 2008). Furthermore, cross contamination due to carry-over can also occur as a small quantity of exhaust air is entrained in the core as the rotor passes from the exhaust air stream to the supply air stream. However, carry-over can be minimized by the inclusion of a purging sector in the rotor.

Energy wheels may transfer contaminants by additional mechanism of sorption as they are coated with desiccants. Popescu and Ghosh (1999) investigated the adsorption of toluene (C_7H_8), 1,1,1-trichloroethane ($C_2H_3Cl_3$) and formaldehyde (HCHO) by 1M type proprietary desiccant, which was prepared from a mixture of silica gel, molecular sieves 13x, and a hydrophobic molecular sieve. A stainless steel tube having 3.75 cm ID and 30 cm length was packed with 1M type desiccant to be used as an adsorption column. Air mixture containing toluene (62 ppm), 1,1,1-trichloroethane (218 ppm), formaldehyde (4.54 ppm), carbon dioxide (830 ppm) and water (7220 ppm) was passed through the adsorption column at the flow rate of 6 m^3/h (3.53 cfm). It was found that the desiccant material immediately started to adsorb the contaminants and the adsorption column reached to its saturation limit within 1-6 minutes. Similarly, the enthalpy wheel coated by the desiccant may transfer contaminants by adsorption and desorption process.

Fisk et al. (1985) conducted laboratory experiments on an energy wheel constructed from a blend of natural and synthetic fibers and coated with lithium chloride. The energy wheel was installed in a sheet metal case with improved set of seals to minimize leakage between airstreams. Transfer fraction of propane (C_3H_8), sulfur hexafluoride (SF_6) and formaldehyde (HCHO) were measured. Only 5-7% of propane and sulfur hexafluoride were transferred;

however, the transfer fraction of formaldehyde was measured 9-15%. It was concluded that due to very high water solubility of formaldehyde, it was transferred at a significantly higher rate by absorption and desorption on the rotor surface along with water vapor. Andersson et al. (1993) measured the transfer of nitrous oxide (N_2O) and formaldehyde (HCHO) in six rotary energy exchangers. Nitrous oxide was used as a tracer gas to check for any leakage due to improper installation of enthalpy exchangers. The level of re-entrainment for nitrous oxide was not more than 1%; however, the calculated re-entrainment of formaldehyde was 1-9% with a relative standard deviation of 15-29%, which is in agreement with values obtained by Fisk et al. (1985).

Schaeffler et al. (1988) measured the carry over rate of nitrous oxide (N_2O) in a heat wheel. The influences of the air flow rate, rotational speed of heat wheel and pressure differences between the supply and exhaust air streams on carry over rate were investigated in these experiments. The transfer of nitrous oxide by carry over was increased by 10-20% when the air volume flow was increased from 3000 m^3/h (1765 cfm) to 3500 m^3/h (2060 cfm). An increase of differential pressure between the supply and exhaust air stream from 50 Pa to 400 Pa resulted in an increase of nitrous oxide carry over rate of 20-39%. Further experiments showed a quadratic dependency between the carry over rate of nitrous oxide and rotation speed of the heat wheel within the tested range of 2-8 rpm. It was concluded that the rotational speed of the rotor has significant impact on the amount of contaminants transferred between the supply and exhaust air streams due to its quadratic dependency.

Wolfrum et al. (2008) investigated the transfer of toluene (C_7H_8) and n-hexane (C_6H_{14}) in a desiccant wheel. Desiccant wheels are structurally similar to energy wheels; however, desiccant wheels are divided into two sections known as the process side and the regeneration side. Unlike energy wheels, the regeneration stream is heated to improve moisture transfer ability

before supplying to the desiccant wheel. The desiccant wheel used for contaminant transfer experiments was made from synthetic substrate and coated with silica-based desiccant. Process stream was supplied at 30^{o}C and regeneration stream was heated to 88^{o}C before supplying to the desiccant wheel. At 24 rph desiccant wheel rotation speed, approximately 71% of toluene and 22% of n-hexane were transferred from the process inlet (PI) stream to the regeneration outlet (RO) stream. Toluene was transferred at higher rate than n-hexane due to its lower volatility and higher vapor pressure, which helped in better adsorption of toluene by the desiccant wheel. Effects of various process parameters on contaminant transfer were also studied during these experiments. Increasing the inlet concentration of toluene (50-130 ppb) and n-hexane (60-150 ppb) did not increase the transfer fraction of contaminants. This led to a conclusion that the desiccant wheel's contaminant transfer performance was limited by the adsorption equilibrium of contaminants and not by the absolute wheel capacity.

Contaminant transfer was reduced by approximately 12-15% when the inlet relative humidity was increased from 40% to 70%. It was concluded that at higher relative humidity, water vapor adsorption increased and therefore, there were fewer adsorption sites available on the desiccant wheel for contaminants. Consequently, increasing the regeneration inlet temperature from 60^{o}C to 108^{o}C, increased the contaminant transfer by 15-17% because at higher regeneration temperature the desiccant wheel became drier as it was regenerated, and, therefore had more adsorption capacity for both water and contaminants. The contaminant transfer was increased by about 13-15% when the wheel rotation speed was increased from 12 to 36 rph. The dependency between wheel rotation speed and contaminant transfer was found to be linear rather than quadratic as found by Schaeffler et al. (1988).

1.3.3 Twin Tower Enthalpy Recovery Loop

This system is an air-to-liquid, liquid-to-air enthalpy recovery system. It is the only system currently available on the market that provides both heat and moisture transfer (sensible and latent energy recovery) between two remotely located air streams. It consists of two contactor towers coupled by an aqueous salt solution. The supply and exhaust air streams pass through the contact surface in a counter flow direction to the salt solution flow to achieve high contact effectiveness. Alternatively, the salt solution is in direct contact with the air flowing through the towers, which allows for higher moisture transfer rates. However, this causes entrainment of small droplets of the salt solution in the air and these droplets are transported downstream into the ducts. Demister pads are used to remove most of the entrained droplets in the air; nevertheless, they are not 100% effective. There are no chances of cross contamination by air leakage due to remotely located air streams; however, there may be some transfer of contaminants by sorption as the air stream is in direct contact with the salt solution.

1.3.4 Summary

The literature review for the contaminant transfer in different kinds of air-to-air energy recovery systems is summarized and shown in Table 1.1. It shows the comparison of the transfer mechanism of contaminants, the transfer fraction of contaminants and also the effect of change in various process parameters on contaminant transfer fraction.

Table 1.1: Summary of contaminant transfer in different air-to-air energy recovery systems literature review (Fisk et al., 1985; Sparrow et al., 2001; Schaeffler et al., 1988; Wolfrum et al., 2008)

	Enthalpy plate	Energy wheel	Heat wheel	Desiccant wheel	Twin towers
Transfer mechanism of contaminants	Convection and molecular diffusion through the air and the diffusion through the membrane wall Air leakage between the air streams	Air leakage between the air streams Carry-over from one air stream to the other air stream Adsorption and subsequent desorption from one air stream to the other air stream	Air leakage between the air streams Carry-over from one air stream to the other air stream	Air leakage between the air streams Carry-over from one air stream to the other air stream Adsorption and subsequent desorption from one air stream to the other air stream	Absorption and subsequent evaporation from one air stream to the other
Transfer fraction of contaminants	C_3H_8: 5-8% SF_6: 5-8% HCHO: 8-12%	C_3H_8: 5-7% SF_6: 5-7% HCHO: 9-15%	N_2O: 0.05-0.3%	C_7H_8: 71% n-C_6H_{14}: 22%	---
Effect of change in the process parameters on the transfer fraction	---	---	Transfer fraction of N_2O was increased by 10-20% when the air flow rate was increased from 3000 m^3/h to 3500 m^3/h Transfer fraction of N_2O was increased by 20-39% when the differential pressure between the air stream was increased from 50 Pa to 400 Pa N_2O transfer fraction was increased by 4 times when the rotational speed of the wheel was increased from 2 to 8 rpm	Transfer fraction of contaminants was reduced by 12-15% with increase in the inlet relative humidity from 40% to 70% Transfer fraction of contaminants was increased by 15-17% when the regeneration inlet temperature was increased from 60^{o}C to 108^{o}C Transfer fraction of contaminants was increased by 13-15% with increase in the wheel rotational speed from 12 to 36 rph	---

1.4 Energy Recovery (ER) Effectiveness and Exhaust Air Transfer Ratio (*EATR*)

ANSI/ASHRAE Standard 84 (2012) has prescribed guidelines for performance testing of the air-to-air heat/energy exchangers. The performance provides an indication of the amount of energy recovered or transferred by the energy recovery system for a given operating condition. The performance of the air-to-air heat/energy exchanger is primarily determined by the effectiveness (ε) as shown in equation (1.1), which is the ratio of the actual energy transfer (sensible, latent, or total) to the maximum possible energy transfer. The sensible effectiveness accounts for the ability of an exchanger to transfer heat, whereas the latent effectiveness refers to the moisture/water vapor transfer ability of an exchanger. The total effectiveness includes the effect of both the heat and moisture transfer phenomena.

$$\varepsilon = \frac{q_{\text{actual}}}{q_{\text{maximum}}} = \frac{C_{\text{supply}}(X_{in,S} - X_{out,S})}{C_{\min}(X_{in,S} - X_{in,E})} = \frac{C_{\text{exhaust}}(X_{in,E} - X_{out,E})}{C_{\min}(X_{in,S} - X_{in,E})} \tag{1.1}$$

Here,

ε = sensible, latent or total effectiveness (%),

X = T (°C), the dry bulb temperature for sensible energy effectiveness,

= W (kg_w/kg_{da}), the humidity ratio for latent energy effectiveness,

= h (J/kg), the enthalpy for total energy effectiveness,

C = the capacity rate for supply or exhaust air stream (W/K),

= $\dot{m}C_p$ for the dry bulb temperature in the supply or exhaust,

= $\dot{m}h_{fg}$ for the humidity ratio in the supply or exhaust,

= $\dot{m}$ for the enthalpy in the supply or exhaust,

$C_{\min}$ = minimum capacity rate between the supply and exhaust air stream, and

$\dot{m}$ = the average dry air mass flow rate in the supply and exhaust air stream (kg/s).

Equation (1.1) is based on the assumption of steady state test conditions and no heat gain/loss between the energy recovery system and its surrounding. Johnson et al. (1995) showed that for the steady state conditions, the overall effectiveness of the system is given by the average of the supply and exhaust exchanger effectiveness. ANSI/ASHRAE Standard 90.1 (2007) requires minimum of 50% overall effectiveness for the energy recovery system; however, currently available ER systems have the total overall effectiveness between 40-85% (Besant and Simonson, 2003).

The Exhaust Air Transfer Ratio (*EATR*) defined in ANSI/ASHRAE Standard 84 (2012) for an inert tracer gas is the ratio of the bulk mean concentration difference in the supply air divided by maximum bulk mean concentration difference between the exhaust and supply air inlets.

$$EATR = \frac{C_2 - C_1}{C_3 - C_1} \tag{1.2}$$

Here,

C_1, C_2 and C_3 = the chemically inert tracer gas concentrations at the supply inlet (1), supply outlet (2) and exhaust inlet (3), respectively (ppm).

According to ANSI/ASHRAE Standard 84 (2012), exhaust air transfer is given as the air quantity transferred from the exhaust to the supply air stream when the mass flow rates of dry air are equal at the supply inlet and the exhaust inlet. It accounts for both air leakage and carry-over in the energy recovery devices but not transfer due to sorption and chemical reactions. If there is no transfer of bulk flow through the air-to-air energy recovery system, the tracer gas concentrations at the supply inlet and supply outlet will be equal resulting in *EATR* = 0.0. During

testing to determine *EATR*, the mass balance data should satisfy the following mass balance inequality suggested by ANSI/ASHRAE Standard 84 (2012).

$$M = \frac{\left|\dot{m}_1 C_1 - \dot{m}_2 C_2 + \dot{m}_3 C_3 - \dot{m}_4 C_4\right|}{\dot{m}_{\min(1,3)}\left|C_1 - C_3\right|} < 0.15 \tag{1.3}$$

Here,

$\dot{m}_1, \dot{m}_2, \dot{m}_3$ and $\dot{m}_4$ = the dry air mass flow rates at the supply inlet (1), supply outlet (2), exhaust inlet (3) and exhaust outlet (4), respectively (kg/s), and

C_1, C_2, C_3 and C_4 = the inert tracer gas concentrations at the supply inlet (1), supply outlet (2), exhaust inlet (3) and exhaust outlet (4), respectively (ppm).

Equations (1.2) and (1.3) imply steady and equal, or nearly equal, inlet air mass flow rates ($\dot{m}_1$ and $\dot{m}_3$) and steady state conditions that are only applicable to chemically inert tracer gases (e.g. SF_6, N_2O) because these equations pertain to bulk air leakage within the energy recovery devices. Hence, there will be a reasonable conservation of mass in case of bulk mass transfer of tracer gases and equation (1.3) is satisfied. However, *EATR* equations cause problems when they are used to measure the transfer fraction of the airborne contaminants (e.g. HCHO). This airborne contaminant adsorbs onto certain surfaces (e.g. desiccants) and dissolves in aqueous solution within the energy recovery devices. After a step change for the inlet conditions, sorption interactions are accompanied by long time delays before steady state conditions are reached. To reach steady state, these time delays can range from hours to days or weeks, for bulk mass transfer of airborne contaminants. These time delays are known to be a function of the cycle time for the liquid desiccant bulk mean flow to complete one cycle in Run-Around Membrane Energy

Exchanger (RAMEE) (e.g. it may be 5 to 50 cycle times to reach steady state). Conservation of mass (equation (1.3)) may not be satisfied for a short duration of testing because transient time delays in the response dominate. Hence, a modified *EATR* (i.e., $EATR^*$) as shown in equation (1.4) is used to characterize the quasi-steady-state bulk mass transfer of airborne contaminants. *EATR** differs from equation (1.2) and (1.3) for *EATR* and its mass balance given by ANSI/ASHRAE standard 84 (2012) in that it is postulated that it can be used for water soluble gases such as HCHO when a reasonable mass balance of HCHO is provided.

$$EATR^* = \frac{C_2 - C_1}{C_3 - C_1} \tag{1.4}$$

Here,

C_1, C_2 and C_3 = the airborne contaminant concentrations at the supply inlet (1), supply outlet (2) and exhaust inlet (3) respectively (ppm).

It is interesting to note the similarities among equations (1.1), (1.2) and (1.4). Equation (1.1) can be for water vapor transfer while the other two equations are for some tracer gas transfer, i.e., each of these defines a mass transfer ratio. Indeed, a similarity might be expected between the water vapor transfer effectiveness in equation (1.1) and *EATR** in equation (1.4) when the water solubility of HCHO is considered. Hence, it may be postulated that *EATR** will be a function of latent effectiveness (ε_l) and the solubility of HCHO in water. Furthermore, it may be postulated that the time required to reach steady state, or a defined steady state, after a step change in the tracer gas concentration will be a multiple of the time required for the bulk mean flow in the RAMEE to complete one cycle.

Table 1.2 shows the comparison of sensible effectiveness, latent effectiveness, total effectiveness and Exhaust Air Transfer Ratios for different kinds of air-to-air energy recovery devices.

Table 1.2: Comparison of air-to-air energy recovery devices (ASHRAE, 2008)

	Fixed Plate	Enthalpy Plate	Heat Wheel	Energy Wheel	Heat Pipe	RAHE*	Twin Towers
Typical sensible effectiveness (%)	50 to 80	50 to 75	50 to 85	50 to 85	45 to 65	55 to 65	40 to 60
Typical Latent effectiveness (%)	---	50 to 72	---	50 to 85	---	---	---
Total effectiveness (%)	---	50 to 73	---	50 to 85	---	---	---
EATR (%)	0 to 5	0 to 5	0.5 to 10	0.5 to 10	0 to 1	0	0

*RAHE = Run-Around Heat Exchanger

From the above comparison it is evident that the heat and energy wheels have the highest sensible, latent and total effectiveness; however, they also have highest *EATR* compared to any other ER device. The fixed plate and enthalpy plate exchanger have slightly lower effectiveness compared to heat wheel and energy wheel but the contaminant transfer is reduced by 50% in the plate exchangers compared to heat or energy wheels. The Heat pipe, RAHE and twin towers have lower effectiveness values; nevertheless, the contaminant transfer is almost negligible in these ER devices.

1.5 Run-Around Membrane Energy Exchanger (RAMEE)

The Run-Around Membrane Energy Exchanger (RAMEE) system is a novel design proposed by Prof. Carey Simonson and Prof. Emeritus Robert Besant in collaboration with Venmar CES Inc. The requirement of developing an effective energy recovery system for retrofit applications initiated the RAMEE project. The concept of RAMEE started with the idea of modifying the Run Around Heat Exchanger (RAHE) system to include moisture transfer ability. Unlike RAHE, the exchangers are made using a semi-permeable membrane instead of copper or aluminum, resulting in a transfer of both heat and moisture between air and the circulating liquid.

A liquid desiccant can be used as a circulating fluid in a closed loop between the two exchangers because it has the ability to absorb and desorb the moisture to/from the air stream. Since the system is a Run-Around system and it uses a membrane as an exchanger interface, it is called Run-Around Membrane Energy Exchanger (RAMEE). Each individual exchanger in the RAMEE is known as Liquid-to-Air Membrane Energy Exchanger (LAMEE). Thus, the RAMEE uses the liquid desiccant as a coupling fluid between the two LAMEEs as shown in Figure 1.4. An aqueous magnesium chloride ($MgCl_2$) solution is used as a liquid desiccant. Heat and moisture are transferred to and from the aqueous liquid desiccant in the two LAMEEs.

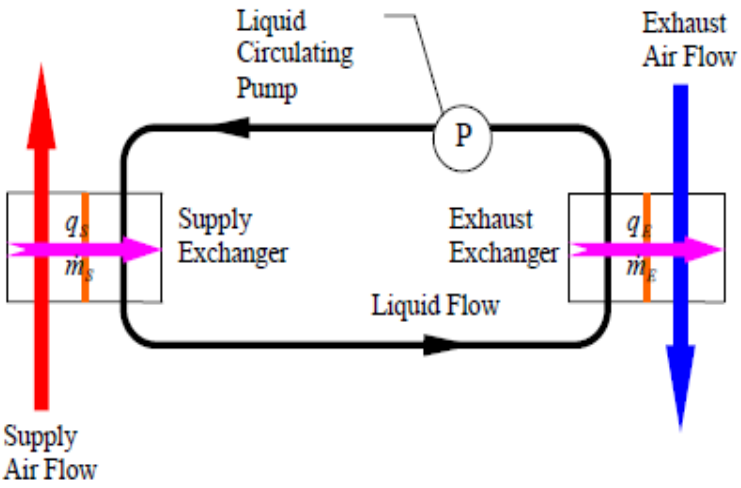

Figure 1.4: A schematic of a Run-Around Membrane Energy Exchanger (RAMEE) (Fan, 2005)

A microporous membrane is placed between the air stream and the liquid desiccant in each LAMEE. The membrane separates the liquid desiccant and the air stream allowing only moisture transfer through the pores. The moisture transfer in each LAMEE is achieved due to water vapor pressure differences between the liquid desiccant and the air stream in each exchanger. Similarly, it is expected that some contaminants present in the exhaust air stream can be transferred to the liquid desiccant along with the water vapor transfer in the exhaust LAMEE. Such contaminants dissolved in the liquid desiccant at the exhaust LAMEE may be then pumped

to the supply exchanger where some of them may be transferred into the supply air due to partial pressure differences of the contaminants in the liquid desiccant and that in the supply air. Thus, contaminants may be returned to the indoor space increasing the indoor concentration of contaminants and increasing the risk of negative health effects on the occupants of the building. Therefore, it is necessary to determine the transfer ratio of contaminants, which gives the amount of contaminants that are transferred between the exhaust and supply air streams of the RAMEE.

1.6 Past RAMEE Research

Since the inception of the RAMEE project in 2002, there has been a lot of research work done on the RAMEE at the Department of Mechanical Engineering, University of Saskatchewan. This project is in partnership with a local HVAC company, Venmar CES Inc. and it is funded by a NSERC Collaborative Research and Development (CRD) Grant. A number of students have worked on this project exploring the various aspects of the RAMEE. A brief description of previous research work done on the RAMEE is given in the following sections.

1.6.1 Fan (2005)

Fan (2005) developed a numerical model of a cross-flow RAMEE and simulated the temperature and moisture content properties of a cross-flow LAMEE shown in Figure 1.5 at the steady state operating conditions.

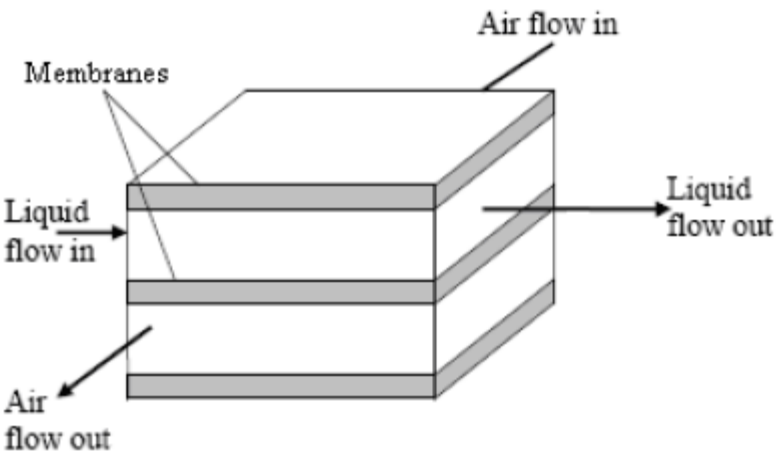

Figure 1.5: A schematic of a cross-flow LAMEE with membrane separating the air stream and the liquid desiccant (Fan, 2005)

Fan (2005) showed that the maximum effectiveness for the RAMEE occurs at a heat capacity ratio $C_r = 3$ for the AHRI Standard summer test conditions and is dependent on variations of the Number of Transfer Units (NTU). C_r and NTU are defined as follows for heat exchangers (Incropera and Dewitt, 2002),

$$NTU = \frac{UA}{C_{\min}} = \frac{1}{R(\dot{m}C_p)_{\min}},\ C_r = \frac{C_{\min}}{C_{\max}} \tag{1.5}$$

Here,

U = the overall heat transfer coefficient (W/m^{2}K),

A = the total membrane surface area (m^2),

C_{min} = minimum heat capacity rate between air and the liquid desiccant (W/K),

= $(\dot{m}C_p)_{\min}$

R = the overall thermal resistance of the membrane equivalent to the product UA (K/W), and

C_r = the ratio of minimum to maximum heat capacity rate.

1.6.2 Hemingson (2005)

Hemingson (2005) built and tested the **Prototype #1** of the RAMEE at the University of Saskatchewan. Figure 1.6 shows the first RAMEE prototype. The objective of this project was to compare the experimental results of the RAMEE with the numerical results of Fan (2005). Two cross-flow exchangers were made using Tyvek® as a membrane and lithium bromide was used as a liquid desiccant. The testing of this prototype was not successful because many problems associated with the construction of the prototype became clear. The first problem was the membrane deformation caused by the liquid desiccant pressure that resulted in substantially blocked air channels and reduced system effectiveness. Reducing the operating pressure of the liquid desiccant introduced more complications and created non-uniform liquid flow distributions in the liquid desiccant channels of the LAMEEs. Additionally, there were also some issues with the liquid desiccant leaking through the membrane into the air stream.

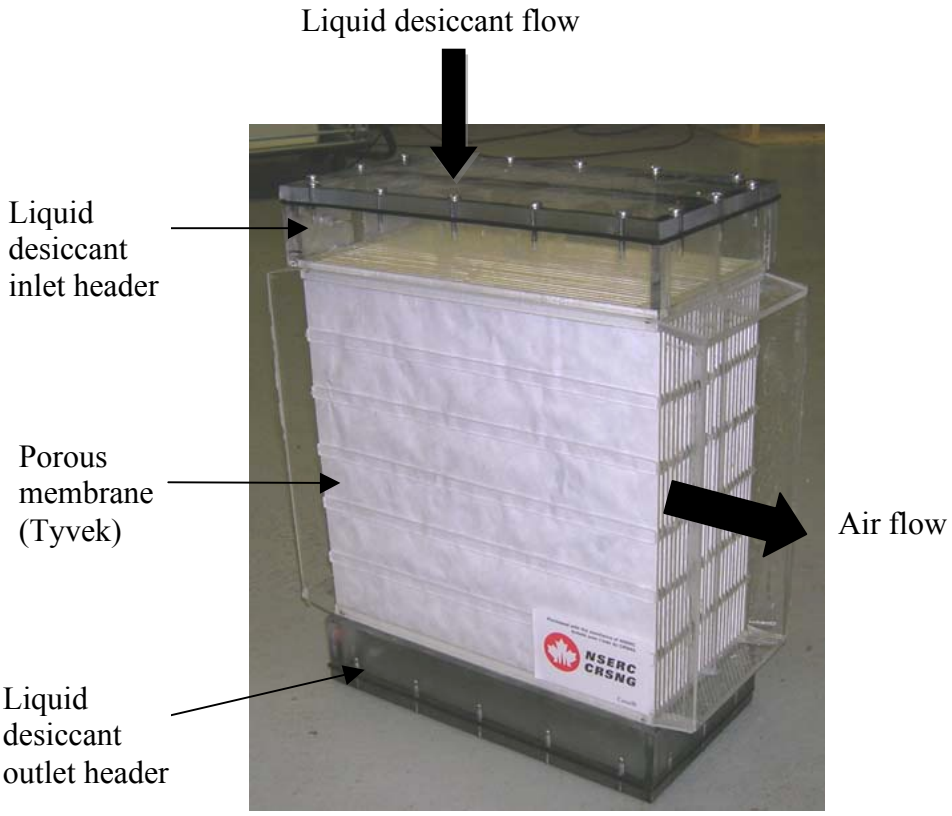

Figure 1.6: First prototype of cross-flow LAMEE developed and tested by Hemingson (2005)

1.6.3 Larson (2006)

The challenges associated with the construction and membrane selection of **Prototype #1** initiated the research work on membranes by Larson (2006). He investigated various semi-permeable membranes and tested them for properties such as vapor diffusion resistance, air permeability, liquid penetration pressure, elastic modulus and degradation. The experimental results showed that a two-layer polypropylene laminated material known as Propore™ had lower vapor diffusion resistance (i.e. higher moisture transfer effectiveness), lower air permeability (i.e. higher air flow resistance), higher liquid penetration pressure and lower modulus of elasticity (i.e. higher structural strength) compared to a spunbonded polyolefin membrane known as Tyvek®. Larson also suggested the use of a metal screen with the square openings of 12.7 mm to minimize the membrane deflections.

1.6.4 Erb (2007)

Prototype #2 was a cross-flow RAMEE built and tested by Erb (2007) at the University of Saskatchewan. Larson's recommendations were implemented in the manufacturing of the new prototype. The major difference between the prototype #1 and the prototype #2 was the addition of an outer screen and the use of the new membrane Propore™ instead of Tyvek®. Figure 1.7 shows the two cross-flow LAMEEs designed and built by Erb (2007).

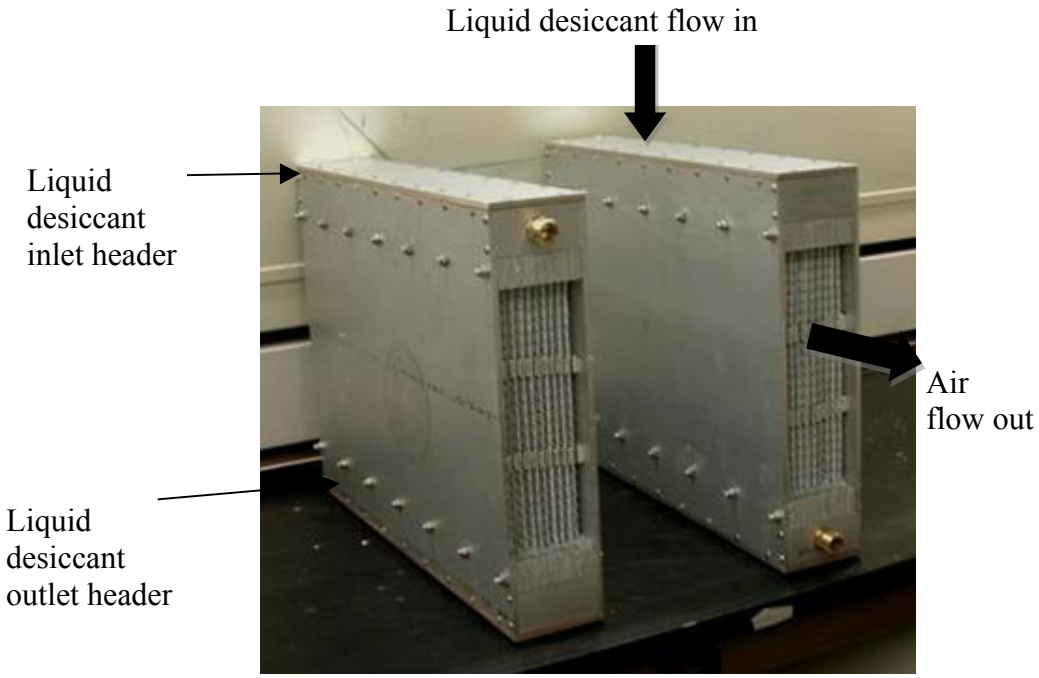

Figure 1.7: Two cross-flow LAMEEs built and tested by Erb (2007)

The **Prototype #2** showed higher structural strength and reduced membrane deflections compared to those in the **Prototype #1**. However, it introduced a few more challenges to the design of the RAMEE. Each liquid panel was manufactured by wrapping a plastic screen with a semi-permeable membrane Propore™. This inner screen increased the resistance to the desiccant flow in the panels. Initially, the desiccant flow direction was kept from top-to-bottom and the maximum effectiveness ($\varepsilon_{o,total}$ = 36% at NTU = 9.5 and C_{sol}/C_{air} = 10) of prototype #2 was

measured 25% lower than the predicted effectiveness of Larson (2006) who employed Fan's (2005) model. The lower effectiveness was suggested to be due to the non-uniform flow distribution of the liquid desiccant in the LAMEE. The experiments were repeated but this time the desiccant flow direction was reversed so that it would flow from bottom-to-top to overcome the mal-distribution problems. This time the maximum effectiveness ($\varepsilon_{o,total}$ = 41% at NTU = 9.8 and C_{sol}/C_{air} = 10.7) was found to be higher by 5% indicating the better performance than earlier testing.

1.6.5 Seyed Ahmadi (2008)

A two-dimensional, transient numerical model for a cross-flow RAMEE was developed by Seyed Ahmadi (2008). Comparing the numerical results with the experimental results of prototype #2 (Erb, 2007) validated the numerical model. A good agreement between numerical results and experiments for both sensible and latent effectiveness was found at different operating conditions. However, there were discrepancies during the transient times because maximum average differences of 7.5% and 10.3% were shown between the experimental and numerical transient effectiveness for summer and winter operating conditions, respectively. The effect of various dimensionless parameters like the Number of Transfer Units (NTU), thermal capacity ratio (C_{sol}/C_{air}), heat loss/gain ratio, storage volume ratio and initial salt solution concentration were also studied. It was concluded that the heat loss/gain ratio has a significant impact on the quasi-steady state effectiveness of the RAMEE and the initial salt solution concentration and the storage volume of the salt solution drastically changes the transient behavior of the system.

1.6.6 Vali (2009)

Vali (2009) developed a two-dimensional steady state numerical model to predict the performance of the RAMEE using $MgCl_2$ as a coupling fluid. The model used Propore™ as the membrane in the LAMEEs. However, this model was developed for a new configuration of the air-liquid flow arrangement in the LAMEEs known as the counter-cross-flow exchanger. The counter-cross-flow exchanger consists of a small cross-flow inlet and outlet header located at the opposite ends of the exchanger. This arrangement of liquid headers cause the air and liquid flow to be in the cross-flow arrangement near the flow entrance and exit regions and nearly counter-flow arrangement in the rest of the LAMEE. Vali (2009) showed that the RAMEE using counter-cross-flow configuration had 6% higher effectiveness than the cross-flow configuration and 1.5% lower effectiveness than the counter-flow configuration. The study also showed that the overall effectiveness of the counter-cross-flow RAMEE was largely influenced by the entrance ratio (the ratio of desiccant solution entrance length to the length of the exchanger, $L_{sol,e}/L$) and the aspect ratio (the ratio of membrane surface height to the length of the exchanger, H_{mem}/L).

1.6.7 Mahmud (2009)

Mahmud (2009) performed experimental testing of the counter-cross flow RAMEE **Prototype #3** and compared the results with the numerical simulations of Vali (2009). Each LAMEE was manufactured using Propore™ and magnesium chloride ($MgCl_2$) was used as the liquid desiccant in a closed loop. Each LAMEE had an exchanger membrane surface aspect ratio of 1/9 and the desiccant solution entrance ratio of 1/24. Mahmud (2009) measured the maximum total effectiveness of 45% during summer outdoor conditions and 50% during winter outdoor condition, respectively. Some agreement between the experimental measurements and the numerical simulations was found with an average absolute discrepancy of 3% to 8% for the

overall total system effectiveness. The amount of discrepancy was observed to be higher at higher *NTU* values; however, the counter-cross-flow RAMEE showed 10% to 20% higher effectiveness than the cross-flow RAMEE.

1.7 Thesis Objective and Overview

While previous studies have been focused on the design and performance testing of the RAMEE prototypes, it is equally important to look at the other aspects of the RAMEE. Contaminant transfer in the RAMEE is one such major aspect yet to be explored. Like any other air-to-air energy recovery device, the RAMEE may also transfer contaminants between the supply and exhaust air streams. Hence, it is essential to determine the transfer ratio of contaminants in the RAMEE. Experimental work was carried out to measure the Exhaust Air Transfer Ratio (*EATR*) for the RAMEE. The explicit objectives of this research work were as follows:

1. Select the most significant contaminants (Volatile Organic Compounds (VOCs)) for testing of the RAMEE prototypes and design injection and sampling mechanism for VOCs;
2. Measure the concentration of contaminants and $EATR^*$, which quantifies the fraction of the contaminants in the exhaust air stream that are transferred to the supply air stream by the RAMEE, for selected contaminants;
3. Experimentally measure $EATR_i^*$ (where *i* denotes the chemical number for each gas or VOC tested) for two different RAMEE prototypes (Prototype #4 and Prototype #6) under different operating conditions.

The counter-cross-flow design of RAMEE prototypes and the test facility used for testing of the RAMEE are described in **Chapter 2**. The instruments used to measure air and liquid

desiccant properties are also described. The criteria used for selection of the contaminants are explained in **Chapter 3**. The injection and sampling mechanism of contaminants are also explained in detail in this chapter. $EATR_i^*$, experimental test results and analysis for the counter-cross flow RAMEE prototypes are discussed in **Chapter 4**. Finally, **Chapter 5** presents the conclusions based on the findings in this thesis. Recommendations for future RAMEE research are also presented.

CHAPTER 2

RAMEE PROTOTYPE DESIGN AND TEST FACILITY

2.1 Introduction

In order to understand the mechanism of contaminant transfer between the inlet and exhaust airstreams of a RAMEE, it is important to understand the construction and design of each LAMEE prototype that was used for VOC transfer tests. This chapter describes the design of two different prototypes (Prototype #4 and Prototype #6) of counter-cross-flow LAMEE including their membrane and desiccant solution properties. It also presents the RAMEE testing apparatus used to measure the transfer of contaminants in both prototypes including all of the instrumentation and sensors. The measurement of air properties (e.g. temperature, humidity ratio, mass flow rate) and desiccant properties (e.g. temperature, mass flow rate) are presented in this chapter. These measurements are taken using the RAMEE test facility. The modifications of the facility used for contaminant transfer measurements are discussed in Chapter 3.

For counter-flow heat exchangers under steady state operating conditions, the relationship between the heat exchanger effectiveness ε_s, and the *NTU* and C_r parameters are given by equation (2.1) (Incropera and DeWitt, 2002).

$$\varepsilon_s = \frac{1-\exp\left[-NTU(1+C_r)\right]}{1-C_r\exp\left[-NTU(1-C_r)\right]} \tag{2.1}$$

Here, the heat exchanger effectiveness (ε_s) refers to the sensible energy effectiveness of the exchanger and it is a function of *NTU* and C_r of the heat exchanger. *NTU* and C_r for a heat

exchanger are defined in equation (1.5). Similar relationship exists for the run-around heat exchangers, where the effectiveness of each individual heat exchanger ($\varepsilon_{s,1,}\ \varepsilon_{s,2}$) is a function of NTU_1, NTU_2, $C_{r,1}$ and $C_{r,2}$. Subscripts 1 and 2 denotes values for the two individual heat exchangers of the run-around system. For the two identical heat exchangers of the run-around system with the same mass flow rate of air and liquid through each exchanger, NTU_1 is same as NTU_2 and $C_{r,1}$ is same as $C_{r,2}$. Similarly, the sensible effectiveness (ε_s), for the counterflow RAMEE with two identical LAMEEs having the same mass flow rate of air and liquid desiccant through each exchanger, is a function of *NTU* and *Cr**. *Cr** for the RAMEE is given by equation (2.2) and defined as the ratio of the heat capacity rate of liquid desiccant to that of the air.

$$C_r^* = \frac{\left(\dot{m}C_p\right)_{liq}}{\left(\dot{m}C_p\right)_{air}} \tag{2.2}$$

Using the heat and mass transfer analogy for the RAMEE, it can be shown that the latent effectiveness (ε_l) of RAMEE is a function of NTU_m and *Cr**. NTU_m refers to the number of mass transfer units and it is given as shown in equation (2.3) (Sparrow et al., 2001).

$$NTU_m = \frac{1}{R_m(\dot{m}_a)_{\min}} \tag{2.3}$$

Here,

R_m = the total membrane mass transfer resistance, (i.e., it includes the air and liquid convection resistances as well as the membrane resistance each in units of $1/m_a$)

$\dot{m}_a$ = the mass flow rate of air (kg/s).

The mass transfer of contaminants across the membrane occurs in a similar physical manner to that for mass transfer of water vapor in the RAMEE. Hence, *EATR** for each contaminant is a function of its solubility in water and the latent effectiveness of the RAMEE. Thus it is necessary to know the RAMEE latent effectiveness as well as contaminant transfer (*EATR**).

2.2 LAMEE Prototype Design

The RAMEE comprising of two separate liquid-to-air membrane energy exchangers (LAMEE) was investigated for contaminant transfer. Two different prototypes (Prototype #4 and Prototype #6) of LAMEE were tested for contaminant transfer. The design of both prototypes is described in the following sections.

2.2.1 Design of Prototype # 4

Prototype # 4 was built by Beriault (2011) at the Thermal Science Laboratory in the University of Saskatchewan. A counter-cross-flow configuration was chosen in the construction of this prototype, which allowed the direct comparison of the experimental results with those from Prototype # 3 (Mahmud, 2009) and also with the counter-cross-flow numerical model (Vali, 2009). The LAMEEs constructed by Beriault (2011) were 52 inches (1.32 m) long, 15 inches (0.38 m) high and 3.3 inches (0.083 m) wide with each of them containing 10 liquid desiccant panels as shown in Figure 2.1 (a). The two side walls of the liquid desiccant panel were made of AY Tech^{TM} ePTFE laminated membrane. The corrugated plastic, the inner screen and the desiccant spacers were encapsulated between two membrane walls and Delrin air spacers as shown in Figure 2.1 (b). A thin felt layer and perforated plastic screen were used as the inner spacer in the liquid desiccant panel. The air spacers and the desiccant spacers were used to create

about 1/4 inch (6.35 mm) of air gap between adjacent panels and 1/8 inch (3.18 mm) of desiccant solution gap in each panel.

(a) (b)

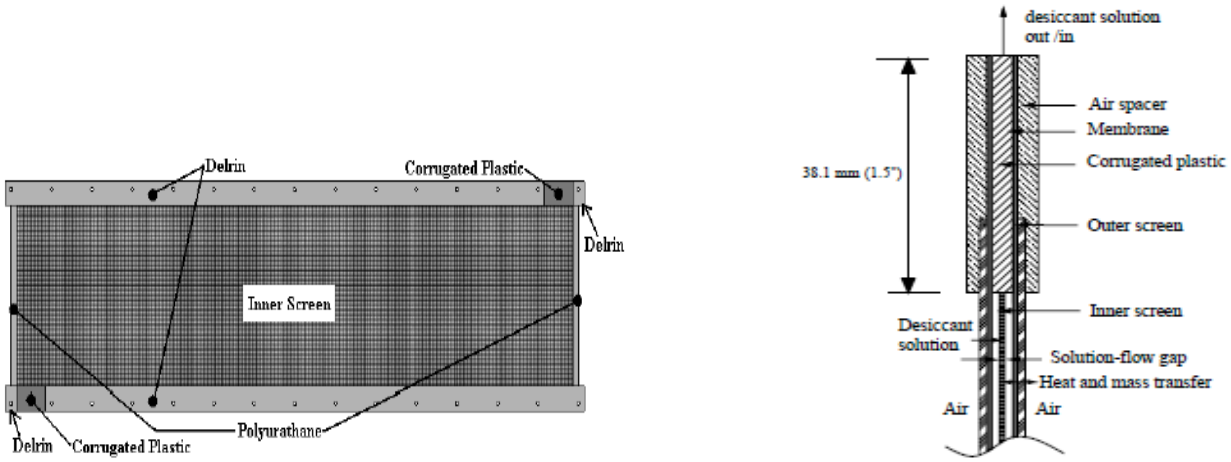

Figure 2.1: (a) Liquid desiccant panel construction (Beriault, 2011) (b) Cross-sectional view of a liquid panel (Mahmud, 2009)

The corrugated plastic was used for the liquid desiccant entrance and exit to and from the liquid panel at two diagonal opposite locations (Figure 2.1 (a)). The inner screen was inserted between the two membrane side walls to prevent the membranes from collapsing inwards and blocking the liquid desiccant channel. The desiccant spacer of a felt layer was used to create a constant gap for the liquid desiccant flow in the liquid panel. As shown in Figure 2.1 (b), the two outer metal screens (one on each side) were attached to the membrane to reduce the membrane deflections into the air stream under liquid pressure. The four air spacers (two on the top and two on the bottom) were used to hold the outer screens against the membrane walls. When two such liquid panels were attached side by side, they created an air channel in between them. Cylindrical rods placed longitudinally in the air channel served as spacers and prevented the metal screen from deflecting into the air channel under liquid pressure. Placing 10 liquid panels side by side and assembling them together inside the metal casing constructed the LAMEEs as shown in

Figures 2.2 (a) and (b). The LAMEE casings were insulated with spray foam to minimize the heat losses/gain to/from the surroundings.

(a) (b)

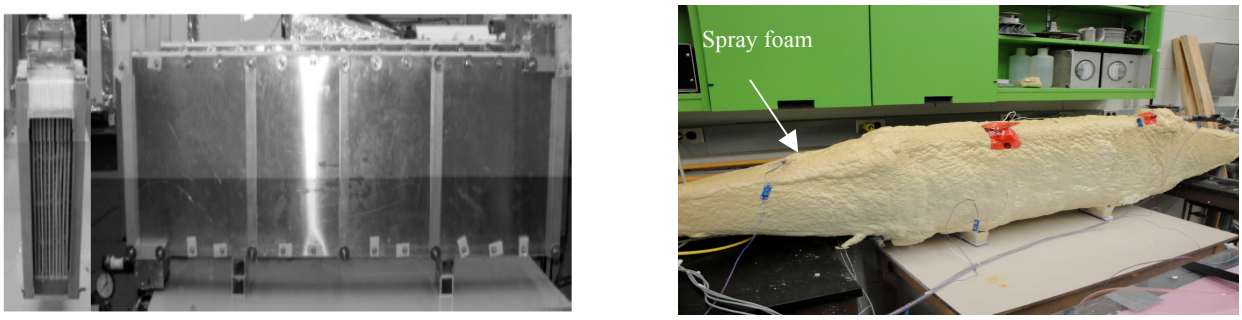

Figure 2.2: (a) Side view and front view of assembled LAMEE Prototype # 4 (Beriault, 2011) (b) LAMEE Prototype # 4 coated with spray foam

2.2.2 Design of Prototype # 6

The Prototype # 6 was constructed by Venmar CES Inc., the collaborating company for the RAMEE project, at its manufacturing facility in Saskatoon, SK. This prototype was also built with a counter-cross-flow configuration; however, a few design modifications were implemented for improved performance in this prototype. The basic construction of the liquid panel and air channel was same in the Prototype # 4 and Prototype # 6; however, the biggest differences between the two prototypes were the membrane materials and changes in the physical dimensions of the LAMEEs. Figure 2.3 shows the assembled Prototype # 6.

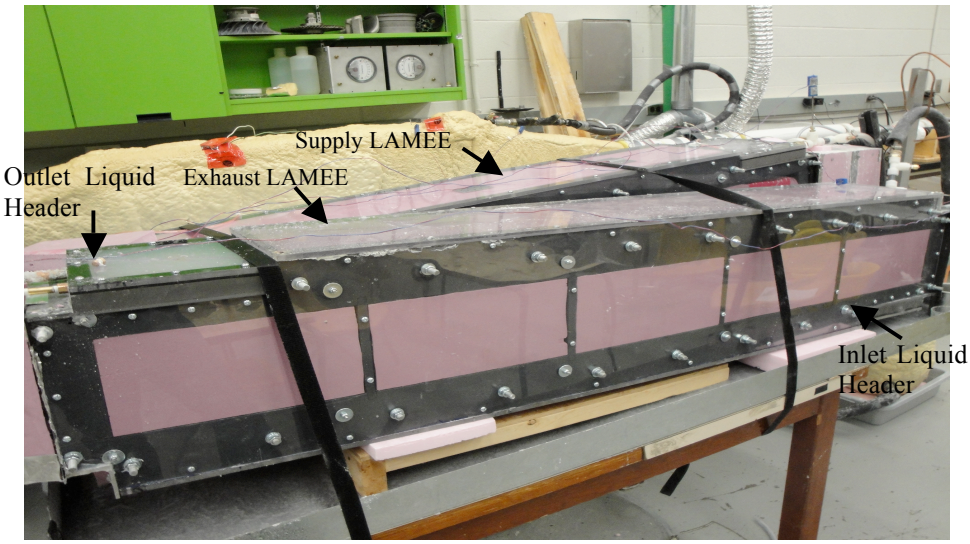

Figure 2.3: Assembled supply and exhaust LAMEEs of Prototype # 6 installed in the Thermal Science Laboratory

As shown in Figure 2.3, the liquid desiccant flows from the bottom to the top liquid header and air flow inlet was chosen accordingly to create a counter-cross flow arrangement in each LAMEE. The Prototype # 6 was built longer (70 inches (1.78 m) long) and wider (11.125 inches (0.28 m) wide) than the Prototype # 4, but the height of both prototypes was almost similar. The longer air/liquid channels in Prototype # 6 provided a better counter flow configuration than that in Prototype # 4. Due to its wider construction, Prototype # 6 had more air channels (1/4 inch (6.35 mm) thick 24 air channels) and liquid desiccant channels (1/16 inch (1.59 mm) thick 23 desiccant channels). The liquid panel of the Prototype # 6 was constructed with GE ePTFE QL822^{TM} membrane. A sinusoidal metal screen was used in the air channel as spacers in the Prototype # 6 instead of the cylindrical rods used in Prototype # 4. The sinusoidal screen helped to create a constant air gap between the adjacent liquid panels. The LAMEEs were covered with extruded polystyrene insulation and then sealed in a Lexan case to minimize the heat losses/gain to/from the surroundings.

2.2.3 Liquid Desiccant Circulation Loop

The two LAMEE modules of the same prototype are coupled together using a liquid desiccant running in a closed loop between the two LAMEEs. Many liquid desiccants such as magnesium chloride ($MgCl_2$), calcium chloride ($CaCl_2$), lithium chloride (LiCl), and lithium bromide (LiBr) were considered to be used in the RAMEE. Afshin et al. (2010) investigated the properties of various liquid desiccants in the RAMEE and suggested that magnesium chloride ($MgCl_2$) is the most suitable choice considering its cost and performance in a variety of climates. Therefore, an aqueous magnesium chloride ($MgCl_2$) salt solution with an initial concentration of 33% was used as the liquid desiccant in both prototypes (Prototype # 4 and Prototype # 6). The liquid desiccant pumps provided desiccant circulation between the LAMEEs. Details of the desiccant circulation are provided later in the Section 2.4.

2.3 Instrumentation and Properties Measurement

It is important to measure the inlet and outlet air properties (temperature (T_{air}), humidity ratio (W_{air}), and mass flow rate ($\dot{m}_{air}$)) and the inlet and outlet liquid desiccant properties (temperature (T_{sol}), salt concentration (C_{sol}) and mass flow rate ($\dot{m}_{sol}$)) in order to determine the testing conditions and to calculate the RAMEE effectiveness (sensible, latent and total) based on the equation (1.1). Figure 2.4 shows the locations required for all air and the liquid desiccant properties measurement.

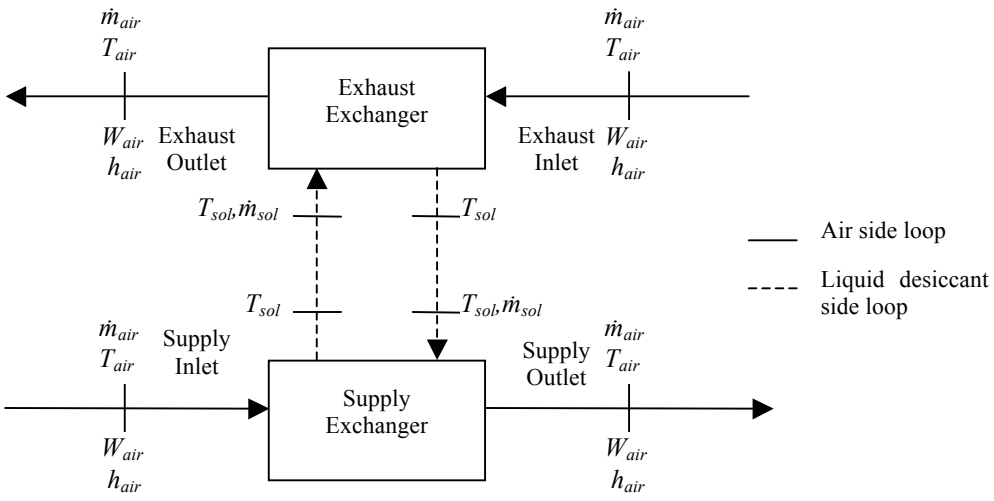

Figure 2.4: Schematic diagram of locations for the air and the liquid desiccant properties measurement of the RAMEE

All the air properties (temperature, humidity ratio, and mass flow rate) and the temperature of the liquid desiccant were measured at the inlet and outlet of each exchanger (i.e. supply and exhaust LAMEEs). The mass flow rate of the liquid desiccant was measured at the inlet of each exchanger to assure the constant supply of the liquid desiccant. Among all of these properties, temperature and moisture content were the only properties measured directly. The mass flow rate and enthalpy were calculated from other directly measured properties. Instruments required to measure the temperature, humidity ratio of the air and the temperature of the liquid desiccant are described along with their calibration procedures in the following sections.

2.3.1 Temperature of Air and Liquid Desiccant (T_{air}, T_{sol})

Temperature of the air (T_{air}) and the liquid desiccant (T_{sol}) at the inlet and outlet of each exchanger was measured using T-type thermocouples. T_{sol} was measured using specially shielded thermocouples. The Hart Scientific (model: 9107) thermocouple calibrator was used for calibration of the thermocouples as shown in Figure 2.5. The thermocouple calibrator operates

over the range of -45°C to 140°C and it uses precision platinum RTD as a sensor and thermoelectric modules to produce the desired temperature within the constant temperature aluminum block. The aluminum block was used to calibrate the thermocouples with various probe diameters. The Hart Scientific thermocouple calibrator has a bias uncertainty of ±0.1 °C.

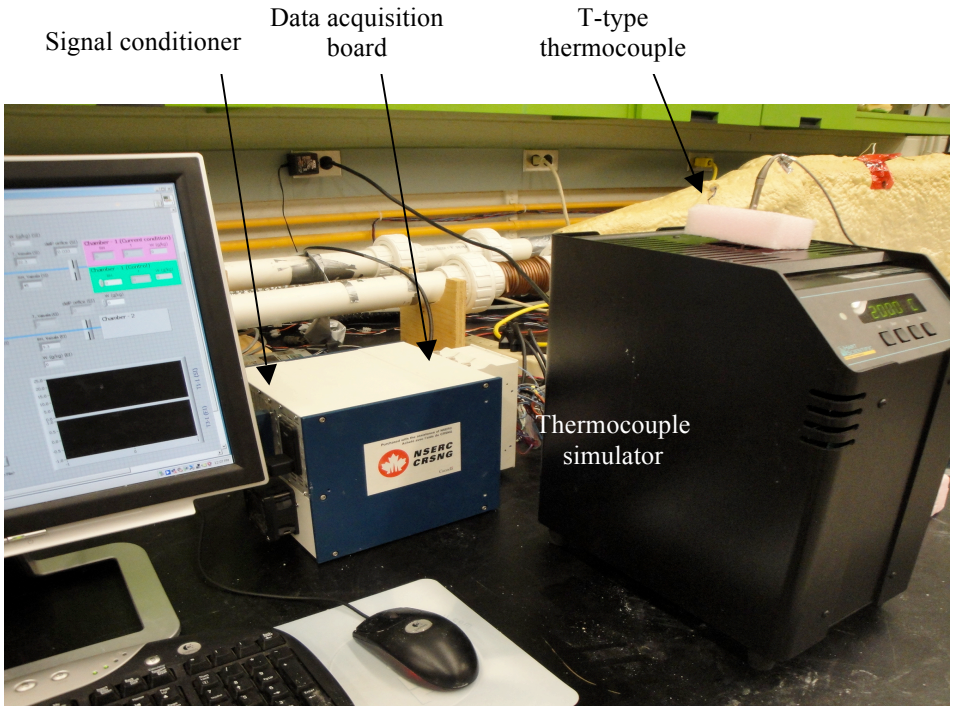

Figure 2.5: Calibration of T-type thermocouple using thermocouple simulator

As shown in Figure 2.5, the thermocouples were connected to the National Instruments (NI) data acquisition board (DAQ) and the computer through the signal conditioner. When a specific temperature was set in the thermocouple calibrator, thermocouples sent the corresponding output voltage signals to the NI data acquisition board. Using an internal cold junction temperature and calibrations, the signal conditioner converted the voltage signal to temperature. The computer then recorded the response from the signal conditioner using an in-house built LabVIEW program. Data were recorded continuously for 20 minutes at the frequency

of 1 kHz for 1 sec. The steady-state temperature values obtained by thermocouple at each of the reference temperatures were used to obtain the average measured temperatures. These average measured temperatures are plotted against the reference temperatures to obtain a calibration curve. A typical calibration curve for one of the T-type thermocouples is shown in Figure 2.6.

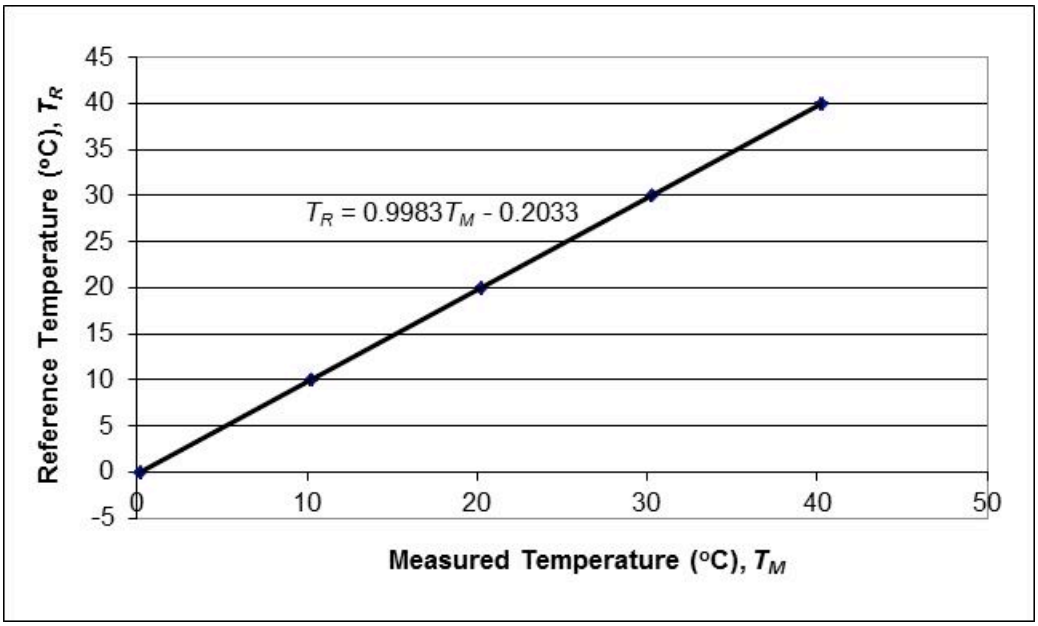

Figure 2.6: Typical calibration curve for one T-type thermocouple

The linear relationship between the calibrator (reference temperature) and the thermocouple reading (measured temperature) gives the bias uncertainty for the thermocouple reading (measured temperature) because it is going to remain constant in repeated measurements of the reference temperature. This bias uncertainty of the thermocouple reading (measured temperature) can be reduced by equation (2.4) obtained from the calibration curve.

$$T_M = \frac{T_R + 0.2033}{0.9983} \tag{2.4}$$

Here,

T_M = the measured temperature (°C), and

T_R = the reference temperature (^oC).

The maximum precision uncertainty in the thermocouple reading (measured temperature) was calculated by finding the standard deviation of individual thermocouple reading from the average thermocouple reading. The maximum precision uncertainty in thermocouple reading was found to be $\pm 0.07\,^oC$ and was calculated using equation (2.5) (ASME PTC 19.1, 1998).

$$P = \sqrt{\sum_{i=1}^{N} \frac{(X_k - \overline{X})^2}{N-1}} \tag{2.5}$$

Here,

X_k = the individual thermocouple reading (^oC),

$\overline{X}$ = the average thermocouple reading (^oC), and

N = the number of measurements.

The bias uncertainty of the calibrator/reference temperature ($\pm 0.1\,^oC$) and the precision uncertainty of thermocouple reading/measured temperature ($\pm 0.07\,^oC$) were used to calculate the overall uncertainty at 95% confidence interval for one T-type thermocouple using equation (2.6) (ASME PTC 19.1, 1998) and it was found to be $\pm 0.17\,^oC$.

$$U_{95} = (B^2 + (tS)^2)^{1/2} \tag{2.6}$$

Here,

U_{95} = the 95% confidence interval measurement uncertainty,

B = the bias uncertainty in the measurement,

t = the t-student distribution constant (2), and

S = the precision uncertainty in the measurement.

2.3.2 Humidity Ratio of Air (W_{air})

The humidity ratio of air (W_{air}) was calculated from the measured temperature and relative humidity (RH) of the air. According to ASHRAE Fundamentals (2005), the humidity ratio of the air is defined as

$$W_{air} = 0.62198\left(\frac{P_v}{P - P_v}\right) \tag{2.7}$$

Here,

P = the atmospheric pressure (kPa), and

P_v = the partial pressure of water vapor in air (kPa).

The atmospheric pressure (P) was measured using a mercury manometer. The partial pressure of water vapor (P_v) was calculated from the relative humidity (RH) and the saturation vapor pressure ($P_{v,sat}$) of air as shown below.

$$P_v = P_{v,sat}(RH) \tag{2.8}$$

The saturation vapor pressure ($P_{v,sat}$) is a function of T_{air} and it is calculated using the following correlation when air temperature is greater than 0^oC (ASHRAE, 2005).

$$P_{v,sat} = \exp\left(\frac{C_1}{T} + C_2 + C_3T + C_4T^2 + C_5T^3 + C_6\ln(T)\right) \tag{2.9}$$

where the saturation vapor pressure is in kPa when the temperature is in K. Here,

$P_{v,sat}$ = the saturation vapor pressure (kPa),

T = the measured dry bulb temperature of the air stream (K),

C_1 = -5800.2206,

C_2 = 1.3914993,

C_3 = $-4.8640239*10^{-2}$,

C_4 = $4.1764768*10^{-5}$,

C_5 = $-1.4452093*10^{-8}$,

C_6 = 6.5459673.

In order to calculate the humidity ratio (W_{air}) of the air, it is necessary to measure the temperature (T_{air}) and the relative humidity (RH) of the air at the same point and at the same time. Vaisala temperature and humidity transmitters (model: HMP 233) are microprocessor based instruments and they were used to measure the temperature and the relative humidity of the air at the same time. The temperature in Vaisala transmitters was measured using a Pt 100 Resistance Temperature Detector (RTD) sensor. Vaisala transmitters were equipped with the HUMICAP® sensor for measuring the relative humidity of the air. The HUMICAP® incorporates a thin polymer film which absorbs the water molecules resulting in the change in capacitance of the sensor. The HMP 233 model of the Vaisala transmitters has the temperature measuring range of -40°C to +120°C and the humidity measuring range of 0 to 100% RH.

The Vaisala temperature and humidity transmitter was calibrated using a Thunder Scientific humidity generator (model: 1200) that produces accurate humidity using the "two-pressure" principle. The humidity generator consists of a constant air supply, a saturator, an expansion valve and a constant humidity chamber as shown in Figure 2.7.

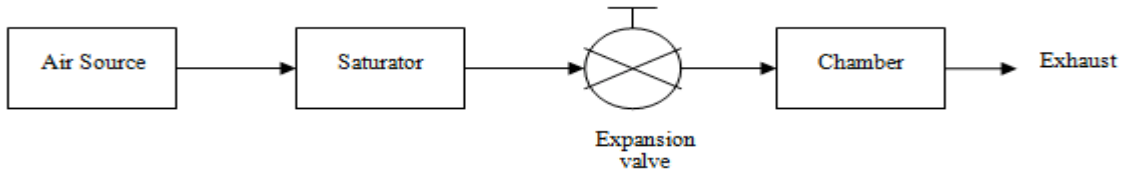

Figure 2.7: Schematic diagram of a humidity generator

Initially, the air is saturated with water vapor at a known temperature and pressure. The saturated high-pressure air flows through an expansion valve where it is isothermally expanded to the test pressure. As the pressure is reduced, the RH of the air drops. Thus, the humidity generator maintains the desired RH in the humidity chamber by controlling the pressure change through the expansion valve. It is capable of generating the RH in the range of 10 to 95% (at 10 to 60^{o}C) in the humidity chamber. The Thunder Scientific humidity generator has a bias uncertainty of $\pm 0.5\%$.

Vaisala humidity and temperature transmitters were placed inside the humidity chamber of the humidity generator for calibration. The HUMICAP® sensor produced the output voltage of 0 to 1 V corresponding to the input RH (0-100%). The Pt 100 RTD sensor converted the measured temperature (-40 to +120^{o}C) to an output voltage ranging from 0 to 10 V. The computer and the NI data acquisition system were used to record the responses from the humidity sensor that was converted to the measured relative humidity reading. A typical calibration curve for RH sensor of Vaisala humidity and temperature transmitter is shown in Figure 2.8.

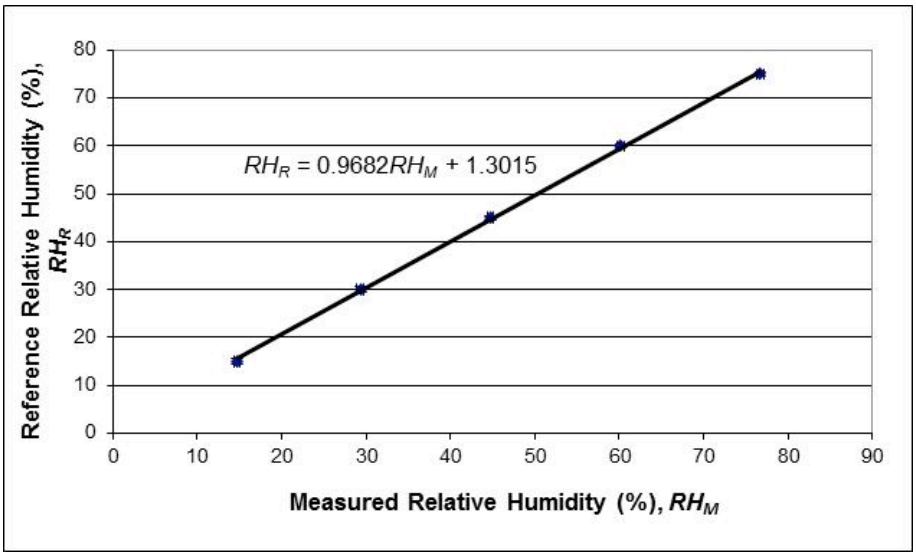

Figure 2.8: Typical calibration curve for one Vaisala humidity and temperature transmitter

The bias uncertainty in Vaisala's RH sensor (measured relative humidity) can be reduced by equation (2.10) obtained from the linear relationship between the humidity chamber reading (reference relative humidity) and Vaisala RH sensor reading (measured relative humidity).

$$RH_M = \frac{RH_R - 1.3015}{0.9682} \tag{2.10}$$

Here,

RH_M = the measured relative humidity, and

RH_R = the reference relative humidity.

The precision uncertainty was found to be $\pm 0.4\,\%$ for the RH sensor. Using the same procedure described in Section 2.3.1, the overall uncertainty in the measured relative humidity of Vaisala at 95% confidence interval was calculated to be $\pm 0.9\,\%$. The Pt 100 RTD sensor was calibrated using the Hart Scientific thermocouple calibrator (model: 9107) similar to the thermocouple calibration. The Vaisala temperature and humidity transmitter was placed inside the calibrator and measurements were recorded using the NI data acquisition system. The overall uncertainty in Vaisala's RTD temperature sensor in the worst case scenario of 95% confidence was found to be $\pm 0.2\,^{o}C$.

2.3.3 Enthalpy of Air (h_{air})

The enthalpy of air (h_{air}) was required to calculate the total effectiveness of the RAMEE and according to ASHRAE Fundamentals (2005), it is calculated using equation (2.11).

$$h_{air} = 1.006T_{air} + W_{air}(2501 + 1.86T_{air}) \tag{2.11}$$

Here,

h_{air} = enthalpy of air (kJ/kg),

T_{air} = temperature of air (^{o}C), and

W_{air} = humidity ratio of air (kg_w/kg_{da}).

The temperature of the air (T_{air}) was measured using the T-type thermocouples (section 2.3.1) and the humidity ratio of the air (W_{air}) was measured using the Vaisala temperature and humidity transmitter (Section 2.3.2).

2.3.4 Mass Flow Rate of Air ($\dot{m}_{air}$)

The mass flow rate of dry air ($\dot{m}_{air}$) was used to calculate the sensible, latent and total effectiveness (equation (1.1)) of the RAMEE and also to determine the EATR mass balance inequality (equation (1.3)). Dry air mass flow rate ($\dot{m}_{air}$) was measured before and after each exchanger (Figure 2.4) and it is calculated as shown in equation (2.12).

$$\dot{m}_{air} = \rho_{da} q_{air} \tag{2.12}$$

Here,

ρ_{da} = the dry air density (kg/m^3), and

q_{air} = the volume flow rate of air (m^3/s).

The ideal gas law is used to calculate the dry air density as shown in equation (2.13).

$$\rho_{da} = \frac{P - P_v}{RT_{air}} \tag{2.13}$$

Here,

P = the atmospheric pressure (kPa),

P_v = the water vapor pressure (kPa),

R = the universal gas constant (kJ/kgK), and

T_{air} = the temperature of air (K).

The volumetric flow rate of air (q_{air}) is calculated using equation (2.14) where the measured pressure drop across an orifice plate is ΔP.

$$q_{air} = C_d \frac{\pi}{4} d^2 \left[\frac{2\Delta P}{\rho_{air}(1-\beta^4)} \right]^{1/2} \tag{2.14}$$

Here,

C_d = the discharge coefficient (approx. 0.61),

d = the diameter of the orifice plate opening (m),

ΔP = the pressure drop across an orifice plate (Pa),

ρ_{air} = the density of the humid air (kg/m^3),

$$= \frac{P}{RT_{air}}, \text{ and} \tag{2.15}$$

β = the diameter ratio

$$= \frac{d}{D} \text{ where } D \text{ is the inside diameter of the pipe.} \tag{2.16}$$

From equation (2.12) to equation (2.16), it is evident that the pressure drop (ΔP) across an orifice plate is required to calculate the mass flow rate of the air ($\dot{m}_{air}$). The differential pressure across the orifice plate was measured using a TSI DP-CALC™ micromanometer (model: 8705). The micromanometer has the measurement range of -5 to +15 inches of H_2O (-1.25 to 3.74 kPa) with a bias uncertainty of 1% of reading ± 0.005 inches of H_2O. The micromanometer was calibrated using a high precision DPI 605 Druck pressure calibrator featuring the reading bias of $\pm 0.025\%$ and the barometric bias of ± 0.0044 inches of Hg (± 14.9 Pa). An integral hand pump and volume adjuster were used to achieve the desired pressure in the Druck pressure calibrator. The known pressure from the Druck pressure calibrator was then applied to the TSI DP-CALC™ micromanometer and the pressure shown by the micromanometer was recorded. Figure 2.9 shows a typical calibration curve of the TSI DP-CALC™ micromanometer.

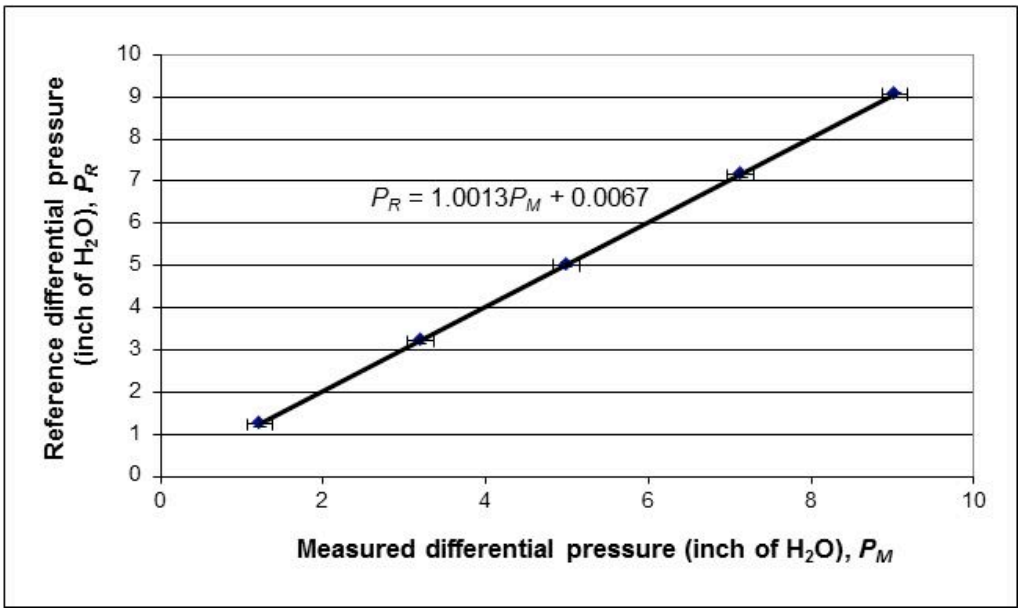

Figure 2.9: Typical calibration curve of the TSI micromanometer

Using the Druck pressure calibrator bias uncertainty and the precision uncertainty of ±0.72 inch of H_2O (±0.18 kPa) calculated from different set of readings, the worst case scenario of 95% uncertainty in the measured differential pressure of the TSI micromanometer was calculated to be ±0.18 inch H_2O (±0.04 kPa).

2.3.5 Mass Flow Rate of Liquid Desiccant ($\dot{m}_{sol}$)

It is necessary to measure the mass flow rate of the liquid desiccant in order to investigate the effects of change in liquid desiccant flow rate on the effectiveness and the *EATR* value for the RAMEE system. Omega FMG 220 magnetic flow meters were used in conjunction with the electronically actuated flow control valves to accurately control the flow rate of the liquid desiccant. Here, 1/8 hp (65 W) AC magnetic drive centrifugal pumps (model: LAING series SM 909/959) pumps were used to pump the liquid desiccant through the magnetic flow meter and the flow control valve. The flow meters were calibrated for five different flow rates of the liquid desiccant. A known voltage was applied to the flow control valve and the resulting flow of liquid

desiccant was diverted in to the bucket of known volume. The time required to fill the bucket up to certain volume was noted using a stopwatch. In the end, the bucket was weighted and the density of the liquid desiccant was measured using the Anton Paar densitometer (model: DMA 4500M) to find out the flow rate of the liquid desiccant corresponding to the voltage applied. The resulting calibration curve for the mass flow meter is shown in Figure 2.10. The measurement uncertainty at 95% confidence interval is found to be 0.3 L/min.

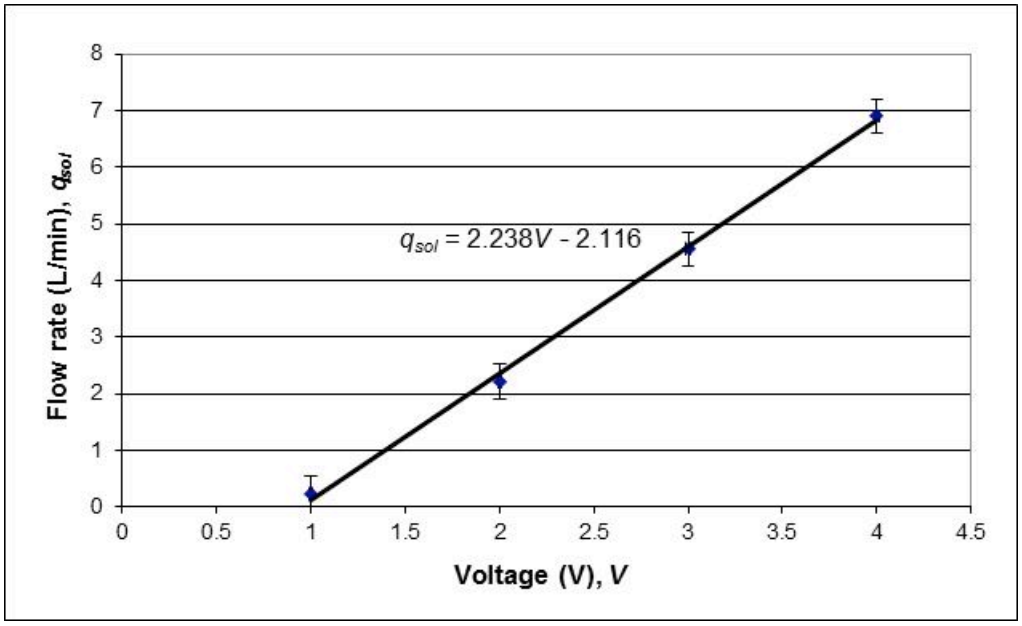

Figure 2.10: Calibration curve of the liquid desiccant flow meter

2.4 Test Facility

The test facility at the Thermal Science Laboratory in the University of Saskatchewan was used to measure the effectiveness and the contaminant transfer in the RAMEE. Erb (2007) developed this test facility based on the ISO standard 5167-1 (1991). The RAMEE test facility consists of two distinct parts (air flow ducts and liquid desiccant loop), which are discussed in detail in the following sections. Figure 2.11 shows the RAMEE test facility used for testing of the LAMEE prototypes (Prototype # 4 and Prototype # 6). The supply exchanger (SE) and exhaust exchanger (EE) in the Figure 2.11 represent the LAMEE of the same prototype. The air

and liquid desiccant property measurement locations in the test facility were already shown in Figure 2.4.

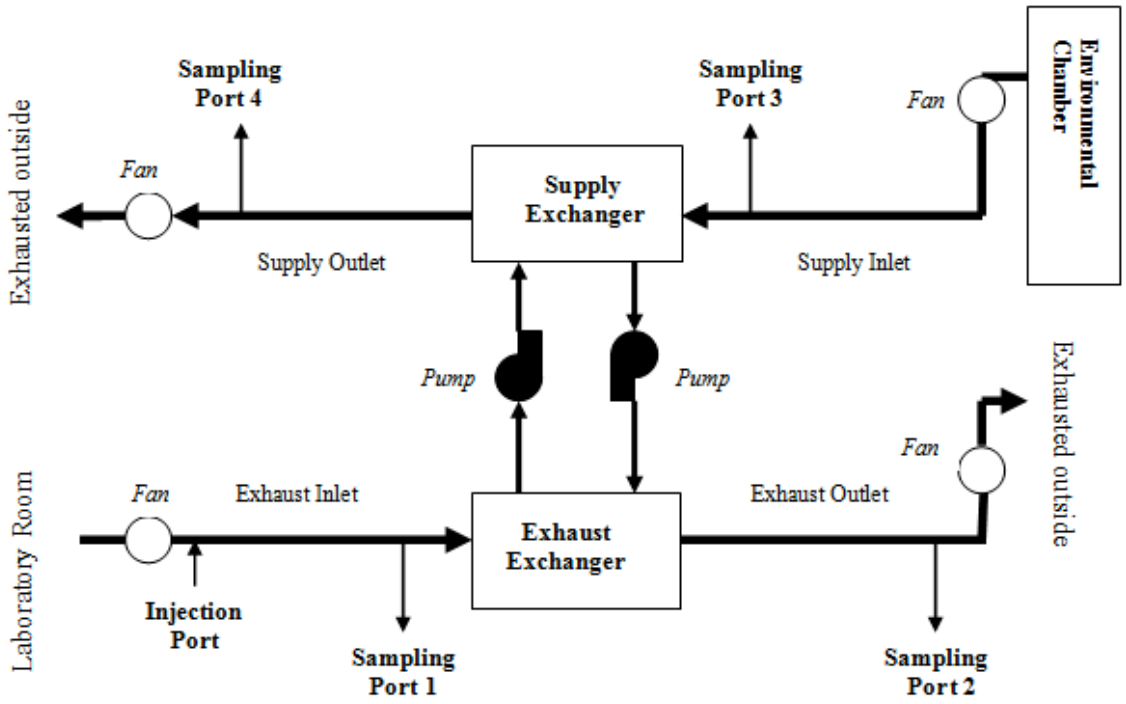

Figure 2.11: The RAMEE test facility used for the testing of LAMEE prototypes

2.4.1 Air Flow Ducts

The environmental chamber shown in Figure 2.11 was used to condition air to represents the outdoor air. It was used to condition the supply air temperature and relative humidity according to AHRI 1060 (2011) standard test conditions presented in Table 2.1 below. The laboratory room in Figure 2.11 acts as an indoor space in a typical HVAC system. Thus the supply exchanger and exhaust exchanger LAMEEs in the RAMEE test facility represent the energy recovery exchangers in a HVAC system.

Table 2.1: American Heating and Refrigeration Institute (AHRI) 1060-2005 standard test conditions

Test Condition	Supply Inlet	Exhaust Inlet
Summer	$35 \pm 0.2^{o}C$ & $50\% \pm 0.9\%RH$	$24 \pm 0.2^{o}C$ & $50\% \pm 0.9\%RH$
Winter	$1.7 \pm 0.2^{o}C$ & $80\% \pm 0.9\%RH$	$21 \pm 0.2^{o}C$ & $50\% \pm 0.9\%RH$

The environmental chamber is capable of conditioning the supply air temperature in the range of -40^{o}C to +40^{o}C. A Nortec humidifier (NH electrode steam humidifier) was used to inject the steam into the environmental chamber and it can produce an RH of up to 90% in the environmental chamber. A Vaisala temperature and humidity transmitter kept inside the environmental chamber controled the operation of the humidifier. The feedback of the RH sensor was recorded and compared to the set value of required RH by the NI data acquisition system, which either turned on or off the operation of the humidifier. Such conditioned air was supplied from the environmental chamber to the supply exchanger through the supply inlet duct.

The air entered the supply exchanger through a transition piece used to connect the duct with the exchanger. The air leaving the supply exchanger flowed through the supply outlet duct and was exhausted outside of the laboratory. The exhaust air from the laboratory room was supplied through the exhaust inlet duct to the exhaust exchanger and was also exhausted outside through the exhaust outlet duct. Five (5) hp (3.73 kW) vacuum fans were located in all four segments of the air streams (supply inlet, supply outlet, exhaust inlet and exhaust outlet) to supply the air and balance the pressure loss across each exchanger. Variable transformers were used to control the voltage supplied to the vacuum fans resulting in the control of the flow rate of the vacuum fans. Each of these piping segments of the air streams was designed to follow the ISO Standard 5167-1 (Erb, 2007). Figure 2.12 shows the details of the exhaust inlet pipe as an example. The ports used for injection and samplings of the contaminants are also shown in Figure 2.12. The other three pipe sections have the similar configuration as shown in Figure 2.12, but without the injection port.

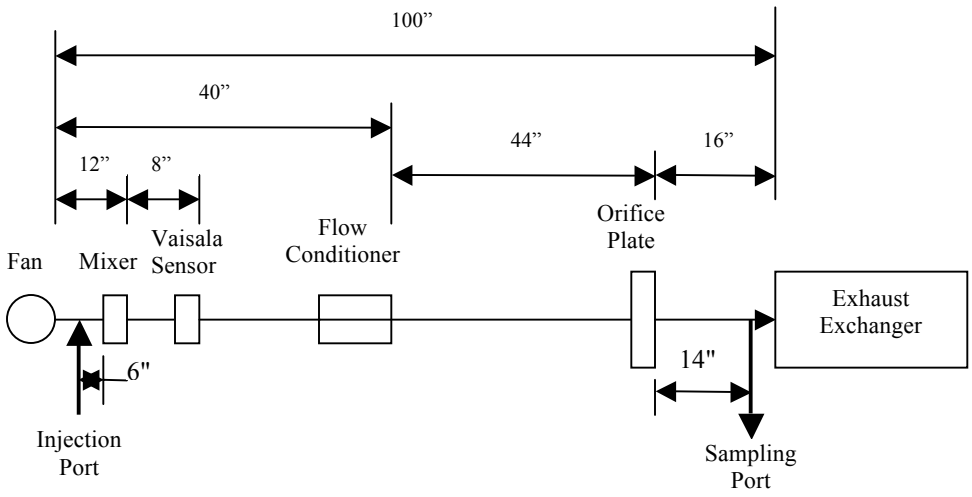

Figure 2.12: Schematic diagram of the exhaust inlet segment of RAMEE test facility

All four piping segments of the air streams consist of a 2 inch (60 mm) diameter Schedule 40 PVC piping. Air supplied by the vacuum fan passes through a mixer, which creates uniform temperature and humidity distributions in the duct. The contaminants were injected 6 inches (152 mm) upstream of the mixer to ensure turbulent mixing and uniform concentration of the contaminants in the air stream. The air samples were taken from the sampling ports located at 90 degrees around the circumference of the pipe and contaminant concentration was measured to be consistent within the experimental uncertainty. Hence, it was confirmed that the contaminants were mixed uniformly in the air stream. Vaisala temperature and humidity transmitter were located 8 inches (203 mm) downstream of the mixer to measure the temperature and RH of the air. A honeycomb grid, shown in Figure 2.13, located downstream of the Vaisala sensor helped to create a uniform velocity profile of air flow upstream of the orifice flow meter in the duct.

Figure 2.13: A honeycomb flow conditioner located upstream of the orifice plate in the RAMEE test facility

Erb (2007) has shown that the minimum and maximum air mass flow rates that can be measured with the combination of orifice plates (throat diameter range of 0.5 inch to 1.5 inch (12.5 to 38 mm)) and pressure transducer (measurement range of 1 to 5 inch of H_2O (0.25 to 1.25 kPa)) in the RAMEE test facility are 1.8×10^{-3} kg/s and 43.8×10^{-3} kg/s, respectively.

2.4.2 Liquid Desiccant Loop

A closed loop liquid desiccant flow line in the RAMEE test facility was used to circulate the liquid desiccant between the two exchangers (SE-LAMEE and EE-LAMEE). The schematic of the liquid desiccant flow loop is shown in Figure 2.14.

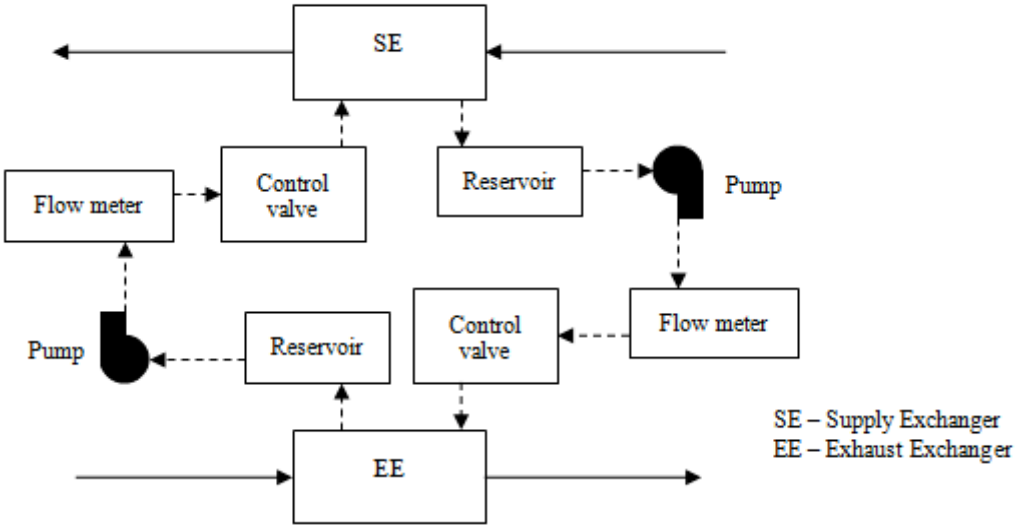

Figure 2.14: Schematic of the liquid desiccant flow loop of the RAMEE test facility

As shown in Figure 2.14, two reservoirs, one for each exchanger, were used to store the liquid desiccant. They were coated with the spray foam to minimize the heat losses/gains to/from the surroundings. Two centrifugal pumps were used to supply the liquid desiccant to each exchanger's inlet header from the reservoirs. The pumps were connected to the reservoirs under the positive suction head to reduce the risk of air locking the pumps. The outlet of each pump was connected to the magnetic flow meter. The flow rate of the liquid desiccant was controlled using the electronically actuated Belimo B3 Series Characterized Control Valve coupled to the flow meter. The controlled flow rate of the liquid desiccant was passed through the micro filters to remove any solid particles before supplying the liquid desiccant to each exchanger's liquid header. A two-way bypass valve was located downstream of each filter to discharge the liquid desiccant from the exchangers when the RAMEE system was not in operation. Shielded thermocouples were located at the inlet and outlet header of each exchanger, which were used to measure the temperature of the liquid desiccant entering and leaving the exchanger.

2.5 Summary

In this chapter, a brief explanation of the design and construction of LAMEE Prototype # 4 and Prototype # 6 is presented. The major differences between the Prototype # 4 and the Prototype # 6 are also explained briefly. The air properties (temperature, humidity ratio, and mass flow rate) and the liquid desiccant properties (temperature, salt concentration and mass flow rate) required to evaluate the RAMEE performance are identified. The instruments and sensors (T-type thermocouples, Vaisala humidity and temperature transmitters, micromanometer, mass flow meters of the liquid desiccant) used for the measurement of these properties are presented. The calibration process for each of this instrument and sensor is explained in detail. The calibration curves showing the relationship between the standard calibrator and the sensor

are found to be linear. The uncertainties of the sensors are reported based on the ASME PTC 19.1 (1998) standard using the 95% confidence interval.

The RAMEE test facility is designed according to ISO Standard 5167-1 (1991). The description of the two distinct flow loops (air side flow loop and liquid desiccant side flow loop) is presented. The details of the air flow loop of the RAMEE test facility shows the location of various devices (vacuum fans, flow mixer, flow conditioner and orifice plates) and measurement sensors. Similarly, the liquid desiccant flow loop of the test facility shows the locations of the pumps, flow meters, control valves, filters and reservoirs.

CHAPTER 3

CONTAMINANT SELECTION, INJECTION AND SAMPLING TECHNIQUE

3.1 Introduction

Hundreds of contaminants including airborne particles, vapors, and gases are found in a typical nonindustrial indoor air. Particulate contaminants cover a wide range of particle sizes, from a few nanometers to 100 μm and, for particle sizes larger than 0.3 μm, most of these can be removed using filters. It is more challenging to reduce the transfer of gaseous contaminants in energy recovery systems, as they exist as free molecules or may be adsorbed on particles in the air. Their very small size (e.g. less than 10 angstroms) makes them even more difficult to be controlled. This chapter focuses on the selection of gaseous contaminants for testing of the RAMEE prototypes. Previous reported data on the gaseous contaminants found in the buildings are used to select contaminants for RAMEE prototype testing. In addition, this chapter describes the injection mechanism used to introduce the contaminants in the RAMEE air stream. The sampling mechanism used for collecting the air samples is explained in detail. The physical principle and operation of the instrument used for the measurement of gaseous contaminant concentration is briefly described.

3.2 Selection of Gaseous Contaminants

The gaseous contaminants are a major concern compared to the particulate contaminants as they can coexist with the air as free molecules. They are often classified in to two categories, organic and inorganic compounds. Organic compounds contain carbon atoms that can combine

with air molecules to form chains, branched or ring molecular structures. Volatile Organic Compounds (VOCs) belong to the organic compound category and hence, they exhibit similar molecular structures and properties as all other organic compounds. Many VOCs (e.g. benzene, *p*-Xylene, *n*-decane) are also known for their adverse health effects on building occupants. Hence, VOCs are chosen as gaseous contaminants for testing of the RAMEE system. However, more than 300 compounds of VOCs have been identified in indoor air (VanOsdell, 1994). Numerous sources list VOCs that are most often found in office buildings (Brown et al., 1994; Hodgson, 1995; Maroni et al., 1995; Wal et al., 1998). Since it is not possible to test the RAMEE system with each of these VOCs for contaminant transfer, it is important to choose the most significant VOCs for testing in the RAMEE system. The criteria used to select VOCs to be used in the tests are as follows:

1. Concentration of VOCs found in buildings and in the outside air,
2. Physical and chemical characteristics of VOCs, and
3. Ability to measure the concentration of VOCs.

3.2.1 Existence of VOCs in Buildings

Building materials, ventilation system and occupants and their activities are major sources for emission of VOCs resulting in higher indoor concentration of VOCs than that exists in the outdoor air. Zuraimi et al. (2002) showed that occupants of air-conditioned offices and their activities contribute 73% of total VOC emissions in the buildings. Moreover, the age of the building also influences the indoor concentration of VOCs. Brown (2002) showed that the indoor concentration of Total Volatile Organic Compounds (TVOC) was reduced by almost 50% from day 2 to day 19 after the construction of a new home, while the outdoor TVOC concentration remained constant. The TVOC concentration in new office buildings at the time of initial

occupancy can be 50 to 100 times that present in outdoor air (Sheldon et al., 1988a, 1988b). Hence, the emission of VOCs is a major concern in the newly constructed buildings compared to old buildings. With adequate outdoor air ventilation, indoor/outdoor ratio of total VOCs in new buildings has been shown to fall by less than 20% after 4 to 5 months of aging. Although the complete removal of VOCs from indoor air is not possible due to their continuous emission from various indoor sources over many years. ASHRAE (2005) lists the major chemical families of organic gaseous air contaminants found in the nonindustrial environments, which are listed in Table 3.1.

Table 3.1: Major chemical families of organic gaseous contaminants (ASHRAE, 2005)

n-Alkanes (e.g. methane)	Ethers (e.g. ethyl ether)	Heterocylics (e.g. nicotine)
Branched alkanes (e.g. 2-methyl pentane)	Aldehydes (e.g. formaldehyde)	Organophosphates (e.g. malathion)
Alkenes and cyclic hydrocarbons (e.g. cyclohexane)	Ketones (e.g. acetone)	Amines (e.g. trimethylamine)
Chlorofluorocarbons (e.g. trichlorofluoromethane)	Esters (e.g. ethyl acetate)	Monomers (e.g. ethylene)
Chlorinated hydrocarbons (e.g. chloroform)	Nitrogen compounds other than amines (e.g. nitromethane)	Mercaptans and other sulfur compounds (e.g. carbon disulfide)
Halide compounds (e.g. methyl bromide)	Aromatic hydrocarbons (e.g. toluene)	Organic acids (e.g. formic acid)
Alcohols (e.g. methanol)	Terpenes (e.g. limonene)	Miscellaneous (e.g. phosgene)

VOCs are found in the wide range of chemical families; however, it is possible that all of them may or may not be present in the indoor air. Roulet et al. (2002) have listed the most common VOC classes and their concentration found in buildings, which are shown in Table 3.2.

Table 3.2: List of VOC classes and concentration found in buildings

VOC classes	Mean concentration ranges ($\mu g/m^3$) (Roulet et al., 2002)	Reason for selection for testing
Aromatic hydrocarbons	1-80	Most common
Aldehydes	1-40	Polar
Cycloalkenes	1-30	No reason
Alkanes, cycloalkanes and alkenes	1-20	No reason
Chlorinated hydrocarbons	1-10	No reason
Alcohols	1-2	No reason
Ketones	1	No reason
Others: organic acids, amines and glycols	<1	No reason

From Table 3.2, it is evident that VOCs from aromatic hydrocarbons and aldehydes chemical families are found at the highest concentration in indoor air. Hence, these chemical classes of VOCs are of some concern for indoor air quality. Some chemical compounds possess an electric charge separation between the atoms that causes higher chemical affinity with water, a well-known polar molecule. This results in higher water solubility of polar VOC molecular compounds (ASHRAE, 2005). VOCs from the aldehydes chemical family are strongly polar, which makes them more likely to be transferred between the air streams along with transfer of water vapor in the RAMEE system. Hence, VOCs from aromatic hydrocarbon and aldehyde chemical families appear to be more appropriate for testing of the RAMEE system.

ASHRAE (2008) has listed the example generation of various gaseous contaminants including VOCs by building materials, human activities and indoor equipment. From the list it is evident that toluene and formaldehyde, which belongs to aromatic hydrocarbon and aldehyde chemical families of VOCs respectively, are generated in significant amounts by various sources such as adhesives, lacquer carpet, paint, particle board, underlay, and plywood. Brightman et al. (1996) developed a list of contaminants, as shown in Table 3.3, that should be measured in indoor air and they included toluene and formaldehyde in their contaminant target list.

Table 3.3: Contaminant target list (Brightman et al., 1996)

Benzene	m,p-xylene	1,2,4-trimethylbenzene
n-octane	n-decane	n-dodecane
Butyl acetate	Chloroform	Trichloroethylene
Trichlorofluoromethane	Dimethyl disulfide	4-methyl-2-pentanone
Limonene	Propane	2-butoxyethanol
Isopropanol	Formaldehyde	Toluene
Styrene	p-dichlorobenzene	n-undecane
n-nonane	Ethyl acetate	Dichloromethane
1,1,1-trichloroethane	Tetrachloroethylene	Carbon disulfide
Acetone	2-butanone	Methyl tertiary butyl ether
Naphthalene	4-phenyl cyclohexene	Butane
Ethanol	Phenol	Siloxanes

Concentration of contaminants in outdoor air is also important as they may determine the indoor concentration of contaminants in the absence of indoor sources. A considerable amount (20 $\mu g/m^3$) of toluene and formaldehyde is found in some outdoor air. At high concentrations, both of these VOCs can cause health risks when inhaled for long durations. The National Institute for Occupational Safety and Health (NIOSH, 1997) has established standards for the occupational exposure limit for numerous hazardous chemicals. The Time Weighted Average (TWA) and Short Term (ST) exposure limits for toluene and formaldehyde are shown in Table 3.4.

Table 3.4: Occupational exposure limit for toluene and formaldehyde (NIOSH, 1997)

Exposure limit	Toluene	Formaldehyde
Time Weighted Average (TWA)	100 ppm	0.016 ppm
Short Term (ST)	150 ppm	0.1 ppm

As shown in Table 3.4, toluene and formaldehyde can be of concern even at very low concentration in indoor air. Concentration of VOCs can accumulate to a risky level in indoor air if they are transferred from the exhaust air stream to the fresh intake air stream of the RAMEE. Therefore, it is very important to quantify their transfer between the air streams in the RAMEE.

3.2.2 Physical and Chemical Properties of VOCs

In order for contaminants to be transferred between the air streams of the RAMEE system, first they need to transfer to the membrane surface by convection and diffusion through the air stream. These contaminants need to diffuse through the porous membrane in the exhaust LAMEE. Then the contaminants need to dissolve in the liquid desiccant and flow in the bulk liquid flow to the supply LAMEE where again they need to diffuse through the porous membrane and transfer in to the supply air stream by convection and diffusion. The contaminants dissolve and diffuse to/from the liquid desiccant due to their partial pressure difference created by concentration gradient of contaminants between the air stream and the liquid desiccant. The physical and chemical properties of contaminants play very important role in their transfer. VOCs that have their physical and chemical properties similar to water have a higher probability of transfer between the air streams because the RAMEE is designed to transfer heat and moisture between the supply and exhaust air streams using an aqueous salt solution as the run- around fluid. Comparison between some of the physical and chemical properties of water (H_2O), formaldehyde (HCHO) and toluene (C_7H_8) are shown in Table 3.5 below.

Table 3.5: Comparison between physical and chemical properties of water and contaminants (Treybal, 1980; Green and Perry, 2007; Fisk et al., 1985)

Property	Water	Formaldehyde	Toluene
Molecular weight (g/mol)	18.01	30.03	92.14
Approx. molecular diameter (^oA)	2.60	3.70	NA
Diffusivity in air – calculated (m^2/s)	2.2×10^{-5}	1.9×10^{-5}	6.57×10^{-6}
Water solubility at 25 ^oC (g/g_{water})	---	0.46	0.00058

Refer to Appendix A for detailed calculations of the contaminant diffusivity in the air. From the data in Table 3.5, it is clear that the molecular diameter and diffusion coefficient of formaldehyde do not differ greatly from those of water vapor in air. Since formaldehyde is highly soluble in water, it has tendency to be transferred with water in the liquid desiccant loop. Although toluene has lower diffusion coefficient and lower water solubility compared to

formaldehyde, it is one of the highly emitted VOCs belonging to the aromatic hydrocarbon chemical family. A study performed by ECA (1997) on the nonindustrial indoor air environment reported that toluene was always observed in more than 75% of studies.

The solubility of VOCs in water is important because liquid desiccant is a water-salt solution, which connects two remotely located LAMEEs. VOCs with higher solubility in the liquid desiccant may be transferred as the liquid desiccant is circulated between the supply and exhaust LAMEEs. The solubility characteristics of VOCs in the liquid desiccant depend on the following three parameters:

1. Partial pressure of VOC in contact with the liquid desiccant;
2. Temperature of liquid desiccant;
3. Dissolved solids (e.g. salts) in the liquid desiccant.

From Dalton's law for a mixture of perfect gases (Brown et al., 1994), the total pressure of a gas mixture is the sum of the partial pressures of each individual gas in the mixture. Hence, the partial pressure of a gas in the gas mixture is equal to the pressure it would exert if it occupied the same volume alone at the same temperature and it can be calculated as shown in equation (3.1).

$$P_i = x_i \times P \tag{3.1}$$

Here,

P_i = the partial pressure of individual gas in the gas mixture (Pa),

x_i = the mole fraction of individual gas in the gas mixture, and

P = the total pressure of the gas mixture (Pa).

If the partial pressure of a VOC in the air is higher than the partial pressure of VOC in the liquid desiccant, then the VOC will flow into the liquid desiccant and vice versa. At larger partial

pressure differential, the flow rate of VOCs will also be higher resulting in higher VOC transfer fraction. The partial pressure of VOCs in the air also affects the dissolution of VOCs in the liquid desiccant. At a constant temperature, the amount of gas that dissolves in the given volume of liquid is directly proportional to the partial pressure of that gas in equilibrium with that liquid. This relationship is known as Henry's law and it is given by equation (3.2).

$$C_s = k_s \times P_i \tag{3.2}$$

Here,

C_s = the saturation concentration of the gas in the liquid (g/L),

k_s = the absorption coefficient (mol/Latm), and

P_i = the partial pressure of the gas in the mixture (Pa).

The absorption coefficient of toluene (C_7H_8) and formaldehyde (HCHO) in the water at 25^{o}C is listed in Table 3.6. If the concentration of toluene or formaldehyde in the air at the atmospheric pressure is 10 ppm, then the partial pressure of the contaminant in the air can be calculated as 1.01 Pa using equation (3.1). Using the values of absorption coefficient given in the Table 3.6 and the partial pressure value of 1.01 Pa for toluene and formaldehyde, the saturation concentration of both contaminants in the water is calculated and it is shown in Table 3.6.

Table 3.6: The absorption coefficient and the saturation concentration of toluene (C_7H_8) and formaldehyde (HCHO) in the water at 25^{o}C (Robbins et al., 1993; Zhou and Mopper, 1990)

Property	**C_7H_8**	**HCHO**
Absorption coefficient (mol/Latm)	0.15	3100
Saturation concentration in water at 25 ^{o}C (mg/L_{water})	0.14	927.9

From Table 3.6 it is evident that the absorption coefficient of formaldehyde in water is much higher than that of toluene. This results in higher saturation concentration of formaldehyde in the water compared to toluene.

Water solubility of VOCs also depends on the liquid desiccant solution temperature. Figure 3.1 shows the variation in solubility of toluene and formaldehyde in water with change in temperature.

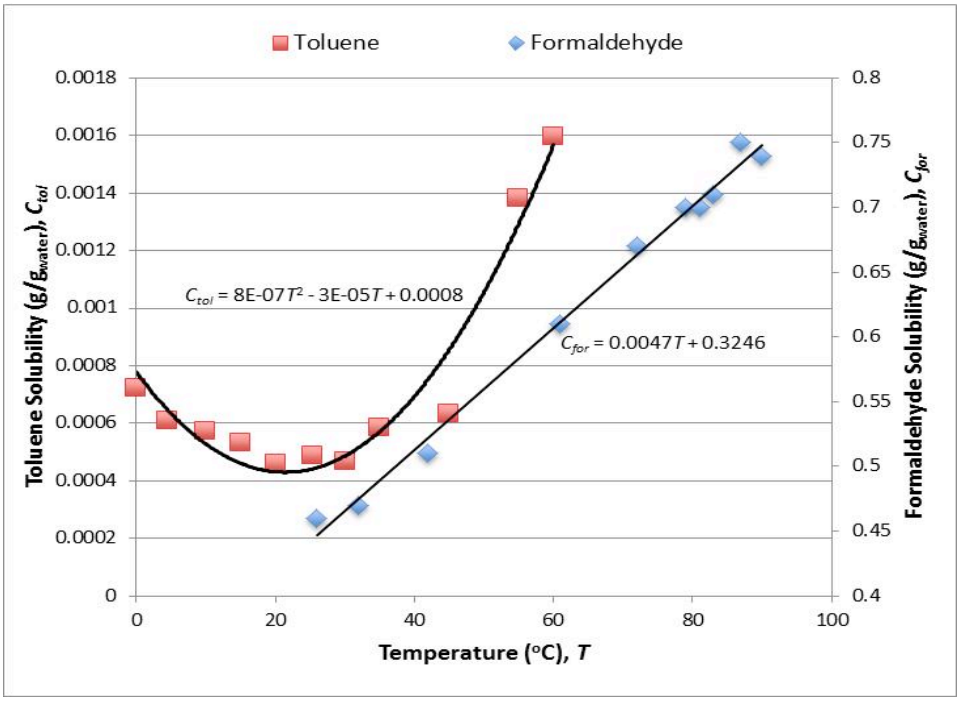

Figure 3.1: Dependence of water solubility of toluene and formaldehyde on water temperature (Yalkowsky and He, 2003; Grutzner and Hasse, 2004)

As shown in Figure 3.1, formaldehyde has very high solubility in water and this solubility increases linearly with increasing temperature. Hence, a significant amount of formaldehyde may transfer in the RAMEE at higher liquid desiccant temperatures. The solubility of toluene in water decreases initially with increasing temperature below 20^{o}C and starts to increase with temperature from 22^{o}C. The solubility of toluene is very small compared to that for formaldehyde over the temperature range of 0^{o}C to 90^{o}C. Hence, it is expected that toluene may transfer in considerably less amount compared to formaldehyde even at higher liquid desiccant temperature.

Another important parameter, which plays very important role in determination of solubility of VOCs in the liquid desiccant, is the salt concentration of the liquid desiccant. The solubility of gaseous organic compounds (e.g. toluene, formaldehyde) decreases in inorganic salt solutions (e.g. $MgCl_2$, NaCl) due to an effect known as salting-out. Addition of inorganic salts in water causes the formation of hydration shells around the salt ions, which effectively reduces the availability of free water molecules to dissolve the VOCs (Poulson et al., 1999). An empirical relationship between the solubility of an organic compound and the salt concentration is given by equation (3.3).

$$\log(C_o / C_{salt}) = S \times K_s \tag{3.3}$$

Here,

C_0 = the solubility of the organic compound in the distilled water,

C_{salt} = the solubility of the organic compound in the salt solution,

S = the salt concentration, and

K_s = the salting or Setschenow constant.

The values of K_s are dependent upon the salt composition, molar volume of the organic compound, and the magnitude of any possible interaction between the organic compound and dissolved salts (Sanemasa et al., 1984). Poulson et al. (1999) also mentioned that there could be a relationship between the availability of free water molecules to dissolve an organic compound and the value of K_s. Several empirical models have been developed to estimate the value of K_s based on experimental results. Schumpe (1993) proposed a model shown in equation (3.4) to estimate the value of gas solubility in a mixture of salt solutions comprised of various types of ions.

$$\log(C_0 / C_{salt}) = \sum (h_i + h_G) c_i \tag{3.4}$$

Here,

h_i = the ion-specific parameter,

h_G = the gas specific parameter, and

c_i = the concentration of ion i in the salt solution.

Hermann et al. (1995) calculated the values of Setschenow constant (K_s) for 319 different gas-salt systems from the experimental data reported by various investigators. These results were used to evaluate the ion-specific (h_i) and gas-specific (h_G) parameters for 45 ions and 22 different gases at 298.2 K. However, the gas-specific parameters (h_G) for toluene and formaldehyde are not reported by Hermann et al. (1995). Hence, it is not possible to theoretically estimate the solubility of toluene and formaldehyde in a particular salt solution. Poulson et al. (1999) performed experiments to measure the solubility of toluene in distilled water and in various inorganic salt solutions and the results are shown in Figure 3.2.

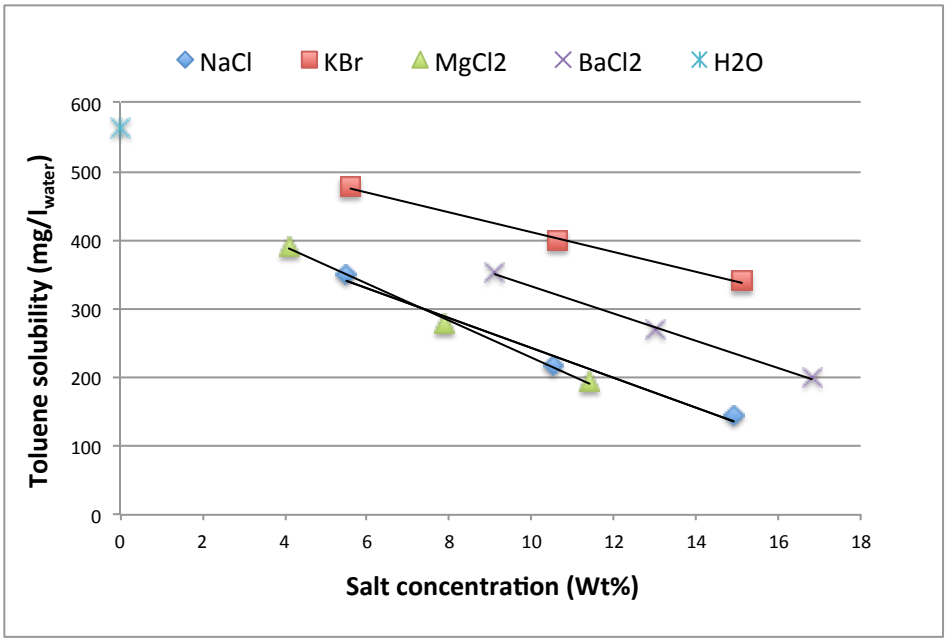

Figure 3.2: Variation of toluene solubility versus salt concentration for various inorganic salts (Poulson et al., 1999)

The solubility of toluene in pure distilled water is 562.9 mg/L but it is clear from Figure 3.2 that the solubility of toluene in the water decreases as salt concentration increases. The toluene solubility in the water is decreased by 65% when $MgCl_2$ salt concentration in the water is increased to 11.4 wt.%. Toluene is least soluble in $MgCl_2$ and NaCl salt solutions among the four inorganic salt solutions shown in Figure 3.2. Similar to toluene, formaldehyde solubility in the salt solution is also expected to decrease with increasing salt concentration.

From the above discussion, it follows that formaldehyde and toluene are two VOCs that need to be tested for their transfer between the air streams of the RAMEE. Different VOCs may exhibit different characteristics and no clear relationship has been found between the transfer ratio of VOCs and the type of chemical compound. However, the transfer mechanism of the RAMEE suggests that the VOCs most effectively transferred in the RAMEE are VOC molecules that are small, polar, and water soluble with high diffusion coefficients in air. Toluene and formaldehyde fulfill these requirements and therefore they are chosen as test VOCs for contaminant transfer experiments on the RAMEE system. Additionally, sulfur hexafluoride (SF_6) is also chosen as a non-organic tracer gas to determine any gaseous cross contamination due to air leakage during the testing of the RAMEE.

3.3 Contaminant Injection Technique

In order to perform the contaminant transfer experiments in the RAMEE in a controlled laboratory environment, contaminants need to be introduced into the air stream from an external source. A proper injection technique was required to inject the contaminants at a constant rate during the experiments. Various authors have used different techniques for injection of contaminants into an experimental system. The most common technique used for tracer gas

experiments is to inject the calibrated concentration of tracer gas at a constant rate into the air stream to generate the desired amount of tracer gas concentration in the air stream.

3.3.1 Calibrated Gas Mixture Injection Technique

Schaeffler et al. (1988) and Shang et al. (2001) performed experiments on regenerative rotary wheels using nitrous oxide (N_2O) as a tracer gas. The volume flow rate of N_2O was adjusted with a flow meter to achieve the concentration of about 150 ppm of N_2O. Sparrow et al. (2001) used a pressurized cylinder of carbon dioxide to perform contaminant transfer experiments on an enthalpy plate exchanger. A calibrated orifice plate was used to measure and control the flow of carbon dioxide to achieve the desired concentration in the air.

Two commercially available pressurized cylinders containing individual calibrated mixtures for toluene and formaldehyde were used to achieve the desired concentration of respective contaminant in the air stream of the RAMEE. Figure 3.3 shows the schematic diagram of the injection mechanism.

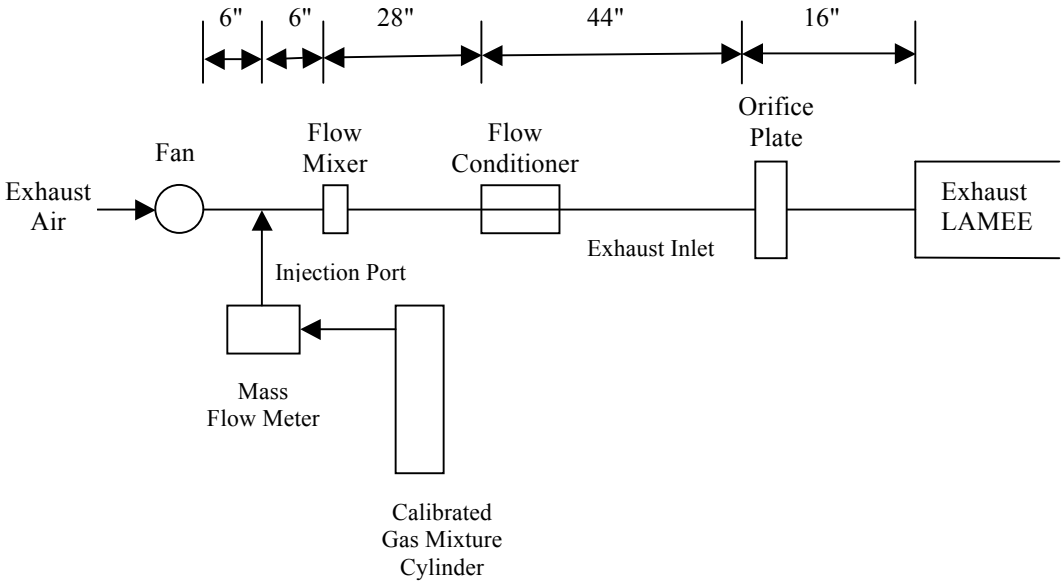

Figure 3.3: Schematic diagram of injection mechanism using calibrated gas mixture

A cylinder containing 142 ft^3 (4.02 m^3) volume of toluene at 150 ppm was used to inject the toluene, and a cylinder containing 73 ft^3 (2.07 m^3) volume of formaldehyde at 30 ppm was used as an external source for formaldehyde injection. The flow rate of each contaminant was controlled using an Omega mass flow meter to achieve the desired concentration of each contaminant in the inlet air stream of the exhaust LAMEE. The contaminants were injected upstream of the flow mixer to ensure turbulent mixing of the contaminant with the air. One contaminant was injected at a time for testing.

The desired concentrations for toluene and formaldehyde were obtained at the sampling port of the exhaust inlet duct using the injection technique shown in Figure 3.3; however, the limited amount of contaminant volume in the cylinder constrained the duration of experiments. At higher air flow rate, higher injection flow rate of contaminant was required to maintain the same concentration of the contaminant in the air stream (Refer to Appendix B for the detailed calculation of injection flow rate). This emptied the cylinders of the contaminants very quickly before the RAMEE system reached steady state. Additionally, it was very expensive to obtain the commercial cylinders containing calibrated mixtures of toluene and formaldehyde. Hence, another alternative was required, which was less expensive and could be used over the longer period of experiments.

3.3.2 Contaminant Evaporation Technique

Roulet et al. (2000) performed experiments of VOC transfer in a rotating heat exchanger by using an evaporation method to inject the VOCs. A liquid cocktail was prepared by mixing equal masses of 7 different liquid VOCs. One milliliter of cocktail was injected by syringe within about 30 seconds into the exhaust duct. Hot air at 200 ^oC was blown to ensure the evaporation of all the VOCs in the cocktail before it entered the exhaust duct. The pulse injection technique was

used to be able to control the quantity of each injected VOC, to limit the amount of injected compounds, and to shorten the duration of experiment. Wolfrum et al. (2008) used a syringe pump assembly to inject the desired amount of liquid mixture of toluene and formaldehyde. The transfer air stream was used to evaporate the liquid mixture. Then the transfer air stream was mixed with the main air stream to achieve the desired concentration of toluene and n-hexane in the air stream. Similarly, liquid toluene and formaldehyde were used as a second alternative for contaminant transfer experiments in the RAMEE. Two individual solutions containing 100% liquid toluene and 37% (vol%) liquid formaldehyde (mixed with 63% water) were used for the experiments as shown Figure 3.4.

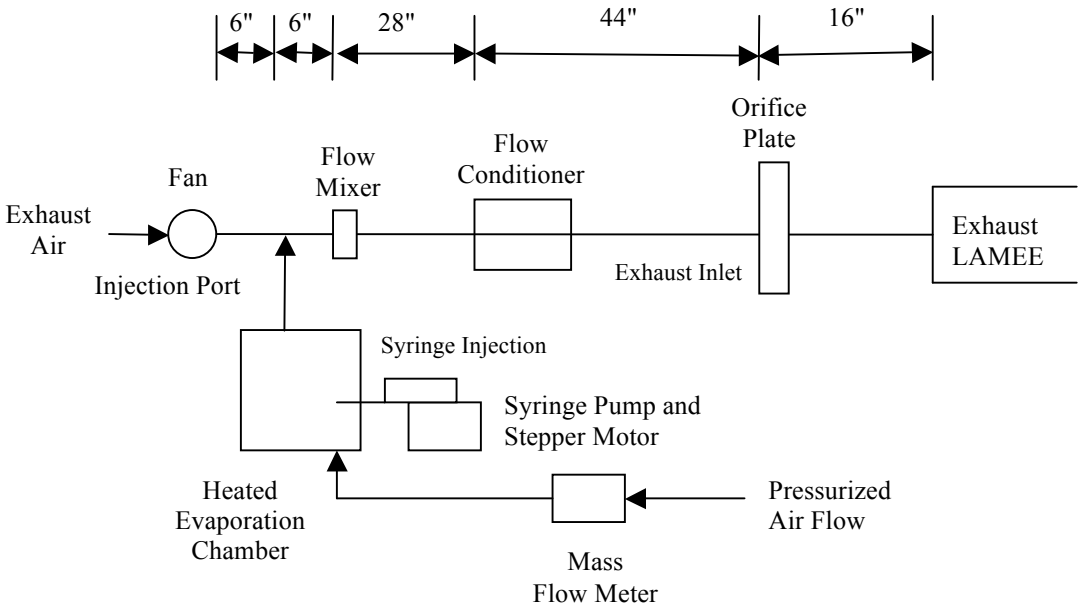

Figure 3.4: Schematic diagram of injection mechanism using evaporative method

As shown in Figure 3.4, the evaporation method was used to inject the liquid toluene or formaldehyde individually in the exhaust inlet duct. The liquid toluene or formaldehyde was injected continuously from a syringe into the evaporation chamber using a syringe pump (LongerPump model: NE 300). The syringe pump is a microcontroller based system, which

continuously drives the syringe plunger using a drive-screw and drive-nut mechanism operated by the stepper motor. The micro-stepping ability of the stepper motor allows it to produce wide range of pumping flow rates ranging from 0.73 μL/hr to 1500 mL/hr with high accuracy. The pressurized air was supplied to the heated evaporation chamber from the bottom at a constant flow rate. An Omega mass flow meter was used to regulate the flow rate of the air. The air was supplied into the evaporation chamber through a nozzle to increase its velocity. The location of the syringe was adjusted such that the needle of the syringe was located exactly above the nozzle. The high velocity air coming from the nozzle evaporated the toluene or formaldehyde solution injected from the syringe.

The air containing evaporated toluene or formaldehyde flows out from the top of the evaporation chamber and was injected into the exhaust inlet duct. The desired concentration of toluene or formaldehyde was achieved by adjusting the flow rate of the syringe pump (Refer to Appendix B for the detailed calculation of injection flow rate). It requires a very small amount of liquid contaminant to create the desired concentration of a particular contaminant in the air. Hence, this evaporation method of contaminant injection allows the experiments to be conducted for longer duration. Moreover, the liquid toluene and formaldehyde solution are safer, less expensive, and easier to handle compared to calibrated toluene or formaldehyde gas. Due to these reasons, the evaporation method was used as the injection technique for the majority of the experiments.

3.4 Sampling Technique

The measurement of gaseous contaminants at very low concentration requires special sampling techniques and costly analytical equipment. The sampling technique of contaminants can be mainly divided into two tasks. First is the sample collection/sample preparation and the

second is identification and quantification of contaminant components in the sample. ASHRAE (2005) has listed several methods for sample collection of gaseous contaminants. Collection of sample in non-rigid containers such as plastic bags using a pump is relatively simple and rapid compared to other methods. A wide range of VOCs can be identified by conducting the replicated analysis on the sample collected in the plastic bag. However, the chemical reactions of contaminants within the plastic bag, physical absorption by the walls of the plastic bag and the dissolution of contaminant in the water condensed in the plastic bag may lead to inaccurate measurement of contaminant concentration (Hsieh et al., 2003).

To minimize these causes, Tedlar or Teflon sampling bags were used for collection of the sample. Hsieh et al. (2003) showed that the half-lives of 56 VOCs, including several highly reactive alkenes in Tedlar bags, were generally in excess of 30 days. Batterman et al. (1998) also showed that collection of contaminants in the Tedlar or Teflon sampling bag is the method of choice for sampling and storing reactive compounds such as terpenes and aldehydes. Hence, the samples of contaminants from the RAMEE were collected in Teflon sampling bags. Experiments were conducted to check whether Teflon sampling bags are inert to contaminants and the results are presented in Chapter 4.

Once the samples are collected in the sampling bags, they are analyzed to identify and obtain the concentration of contaminants in the collected sample. ASHRAE (2005) has listed various methods, including Gas Chromatography (GC), Mass Spectroscopy (MS), Infrared Spectroscopy (IR), and High Performance Liquid Chromatography (HPLC), for measurement of contaminant concentration in the sample. Several researchers have used different methods to measure the concentration of contaminants. Roulet et al. (2000) used GC method to measure the concentration of 7 different contaminants (n-decane, n-butanol, hexanal, limonene, m-xylene,

mesitylene, and acetone). Air samples were collected in a small tube with an absorbing medium. Contaminants accumulated by absorption in the small tube were desorbed by heating the tube and stored in a cold trap. A flame ionization detector (FID) was used to detect and measure the amount of each compound, while a mass spectrograph was used to help identify each compound in the cold trap.

Schaeffler et al. (1988) and Andersson et al. (1993) used an infrared spectrophotometer (MIRAN 1A) to determine the concentration of nitrous oxide (N_2O). The air samples were collected using a vacuum pump and a metal tube with 45^o capped end. The tube was inserted into the duct and placed perpendicular to the air stream such that the inclined capped end of the tube remained in the middle of the duct with the open area facing the air flow. Wolfrum et al. (2008) also used a vacuum pump to collect the air sample into a manifold containing 10 sorbent tubes (100 mg of Tenax TA 35/60). A thermal desorption unit (Perkin-Elmer ATD 400) was used to create a concentrated sample by desorbing the sorbent tubes. These concentrated gas samples were analyzed by a gas chromatograph (Agile 6890N) with a flame ionization detector. Sparrow et al. (2001) used a commercially available TSI CO_2 meter (Q-TRAK 8550) to measure the concentration of carbon dioxide in the air samples. Fisk et al. (1985) used infrared analyzers for real-time measurement of propane (C_3H_8) and sulfur hexafluoride (SF_6). A microprocessor based solenoid valve system was used which directed the air samples into the analyzers from the air stream.

Since toluene and formaldehyde have absorption bands in the infrared region of the electromagnetic spectrum, infrared spectroscopy can be used to analyze the air samples containing toluene or formaldehyde. A Fourier Transform Infrared Spectroscopy (FTIR) gas analyzer available in the Thermal Science Laboratory at the University of Saskatchewan was

used for analysis of air samples collected from the RAMEE. Figure 3.5 shows the sampling mechanism used for the collection of air samples from the RAMEE.

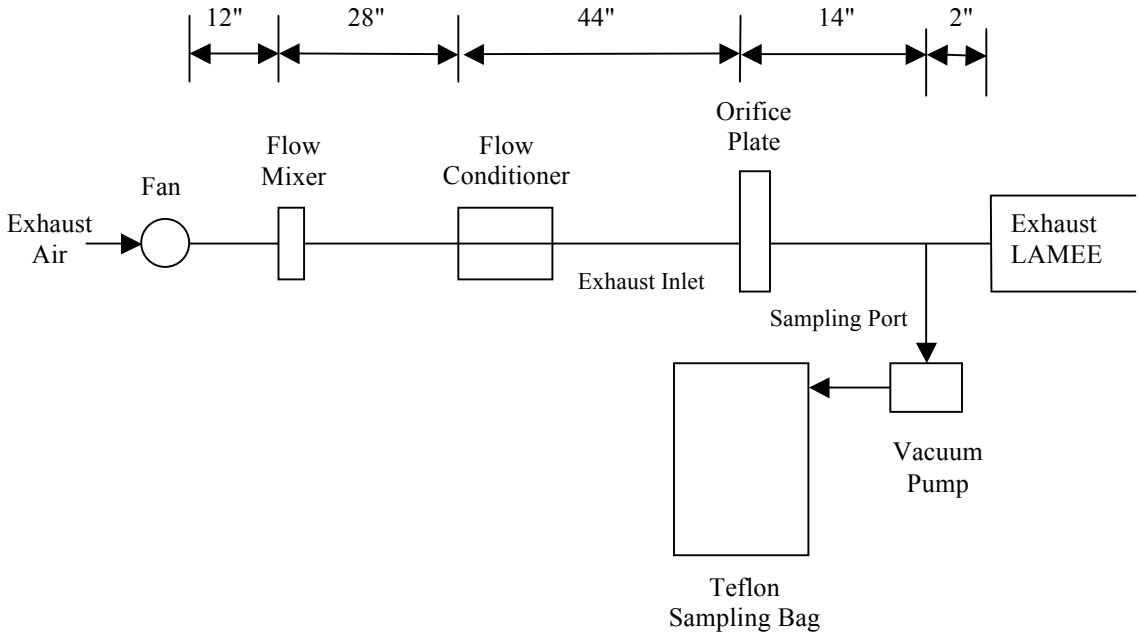

Figure 3.5: Schematic diagram of the sampling scheme

As shown in Figure 3.5, the air samples were collected using a vacuum pump (model: 1LAA-10M-1000X, GAST, USA). The oil-less operation of the vacuum pump ensured that the air samples were not contaminated. Air at the four locations (exhaust inlet, exhaust outlet, supply inlet, and supply outlet) was sampled using the vacuum pump. Straight Teflon tubing used to take the air samples was inserted perpendicular to the air stream such that the open end of the tube is located in the middle of the duct. Teflon tubing minimizes the chemical reactions or absorption of contaminants in the sampling lines. However, if the sampling lines are long and the flow is laminar, which often is the case, these sampling lines need to be flushed every time before collecting the air sample to remove any contaminants remaining in the sampling line from the previous test. Air was allowed to run through the Teflon tubing for 1 minute each time before collecting the air sample. The sampling rate was 20 liter of air per minute. Since the volume in

the Teflon tubing is very small (0.25 L), the Teflon tubes are flushed 80 times before sample collection. Air samples were collected in the 100 L Teflon gas sampling bags, as these bags are chemically inert to wide range of compounds including VOCs. The experiments were conducted to identify whether 100 L of sample gas is enough to accurately determine the concentration of contaminants in the sample gas. The results of these experiments are presented in Chapter 4. The air samples collected in the sampling bags were passed through Gasmet™ FTIR gas analyzer (model: CR-100M) sample cell as shown in Figure 3.6, which detects and measures the concentration of each compound in the air samples.

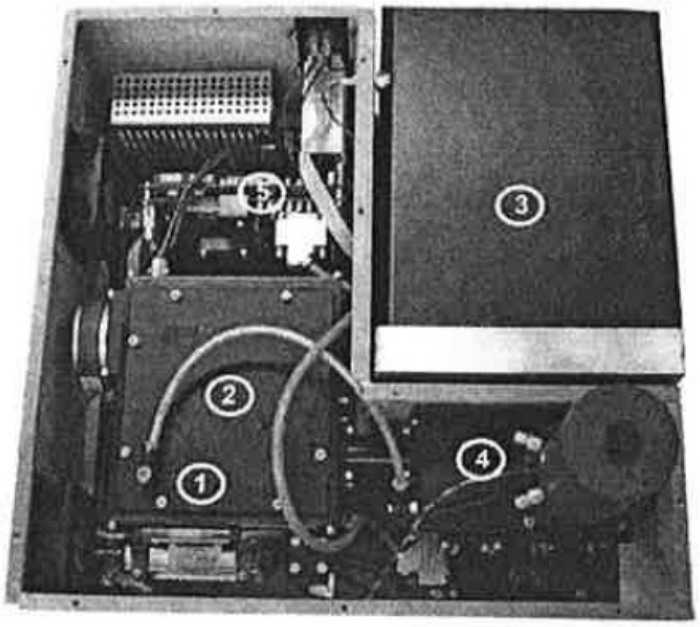

Figure 3.6: Inner components of Gasmet™ CR-100M FTIR gas analyzer. Components are 1) Infrared Source 2) Interferometer 3) Sample cell (multi-pass with fixed path length of 100 m) 4) Detector 5) Signal processing electronics (Gasmet™ Technologies Oy, 2006)

3.4.1 Zero Calibration of the FTIR Gas Analyzer

The working principle of Gasmet^{TM} CR-100M FTIR gas analyzer is described in detail in Appendix C. The gas analyzer was calibrated by measuring the background spectrum. This background spectrum was used as the zero level, to which the actual sample measurements were later compared. The process of measuring the background spectrum is called “Zero Calibration”

(Gasmet^{TM} Technologies Oy, 2006). For the zero calibration measurement, the sample cell of the gas analyzer was flushed with monoatomic gases (such as noble gases He, Ne, Ar, Kr and Ra) or diatomic homonuclear gases (such as N_2, O_2, H_2 and Cl_2) because they are not infrared-active and thus give rise to no infrared spectrum. Typically, the sample cell is flushed with ultrapure N_2 for a few minutes before initiating the background measurement. Once the sample cell was flushed by the zero calibration gas (i.e. N_2) with three times the volume of the sample cell (i.e. 100 L as the volume of the sample cell is 30 L), the background spectrum was measured for the nitrogen gas sample. The background spectrum shows the actual absolute intensity of the infrared radiation that is transmitted through the sample cell containing zero gas. Hence, it shows the absorbance with respect to a black body spectrum at same temperature of the source. The background spectrum is used as a reference level, to which actual sample measurements are compared at later stages. A typical background spectrum is presented in Figure 3.7.

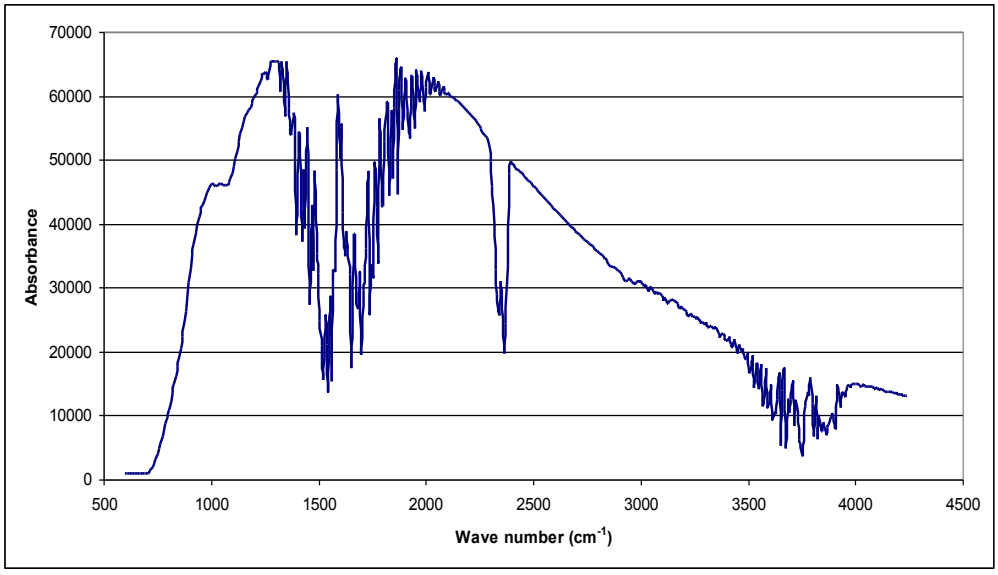

Figure 3.7: A typical background spectrum of Gasmet^{TM} CR-100M FTIR gas analyzer

The spectrum in infrared spectroscopy is commonly shown as a function of wave number, which is the reciprocal of the wavelength of the infrared radiation. In the background

spectrum, the absorbance peak at 2350 cm^{-1} is observed due to CO_2 that is typically present in the optical path inside the spectrometer. The peaks at 1300-1800 and 3500-4000 cm^{-1} result from water vapor. While measuring the background spectrum there is only N_2 present in the sample cell, however, there is always some air along the optical path in the other parts of the instrument. Therefore, CO_2 and H_2O bands are usually visible in the background spectrum.

3.5 Summary

This chapter covers the major topics of contaminant selection, injection techniques, sampling mechanisms and the gas analyzer calibration. Based on the literature on contaminants and their concentrations found in indoor air, toluene (C_7H_8) and formaldehyde (CHOH) belonging to aromatic hydrocarbons and aldehydes chemical families were chosen as contaminants for testing of the RAMEE. Additionally, sulfur hexafluoride (SF_6) was chosen as a tracer to determine any leakage in the RAMEE. Further analysis on the selection of toluene and formaldehyde was carried out by finding out the physical and chemical properties of both these contaminants.

Two kinds of injection mechanisms used for injection of contaminants in the RAMEE system are discussed in detail; however, evaporative method of contaminant injection was found to be less expensive and longer lasting compared to calibrated gas mixture. Various sampling mechanisms used to collect the air samples are briefly discussed. An oil-less vacuum pump was used to collect the air samples from the RAMEE into Teflon sampling bags, as these bags are chemically inert to wide range of contaminants.

The methods used to measure the concentration of various contaminants are listed. Infrared Spectroscopy was chosen as a method for determination of contaminant concentration because toluene and formaldehyde have absorption frequencies in the infrared region of the

electromagnetic wavelength. The principles of infrared spectroscopy are explained briefly. A Gasmet™ CR-100M FTIR gas analyzer was used to measure the concentration of contaminants in the air sample. The operation of gas analyzer's components is described along with some preliminary results (e.g., background calibration).

CHAPTER 4

EXPERIMENTAL RESULTS AND DISCUSSION

4.1 Introduction

In this chapter, contaminant transfer in the RAMEE with counter-cross flow exchangers is evaluated. To begin with, the Gasmet^{TM} CR-100M FTIR gas analyzer is used to perform the single component analysis of the carbon dioxide (CO_2) sample and the multi-component analysis of ambient air. The accuracy of the gas analyzer is tested through numerous experiments using ambient air as the sample gas. Then, the air samples containing contaminants are collected from the RAMEE test facility to determine the fraction of contaminant transfer in the RAMEE prototypes. Experiments are conducted on two different RAMEE prototypes (Prototype #4 and Prototype # 6), using the RAMEE test facility described in Chapter 2. Contaminant transfer for the selected contaminants (described in Chapter 3) in the RAMEE is quantified using *EATR* and *EATR** (equations (1.2) and (1.4) respectively) while the RAMEE is operating under AHRI summer and winter conditions. Effects of various process parameters like air flow rate (inferred from the value of *NTU*), liquid desiccant flow rate (inferred from the value of *Cr**), and latent effectiveness (calculated as ε_l) on the contaminant transfer in both prototypes are also evaluated in this chapter.

4.2 Gasmet™ CR-100M FTIR Gas Analyzer Testing

Once the Gasmet™ CR-100M FTIR gas analyzer is calibrated using the "Zero Calibration" procedure described in Section 3.4.1, it can be used to determine the concentration of various gas molecules in the sample gas. The volume of sample gas required to determine the gas concentration can vary widely depending on the technique used for analysis of the sample gas. Hence, it is important to determine the volume of sample gas required to obtain accurate concentration of each gas compound used in the FTIR gas analyzer.

4.2.1 Air Sample Size Determination

The Gasmet™ operating manual recommends that the sample cell of the CR-100M gas analyzer needs to be flushed with 3 times the volume of the sample cell by the sample gas to accurately measure the gas compound concentration. The volume of the sample cell of the CR-100M gas analyzer is 30 L (Gasmet™ Technologies Oy, 2006). Hence, the sample cell needs to be flushed with a minimum of 90 L of sample gas.

Experiments were conducted to determine the minimum volume of air sample that is required to obtain an accurate concentration of gas compounds in the air sample. Sulfur hexafluoride (SF_6) was used as a tracer gas in these experiments. A fixed volume of air sample containing 8 ppm of SF_6 was passed through the sample cell of the gas analyzer and then the concentration of SF_6 was measured by the gas analyzer. Before conducting the next experiment with a different volume of air with the same concentration (8 ppm) of SF_6, the sample cell was flushed completely with nitrogen (i.e. more than 90 L) to remove the entire air sample used in the previous measurement. The concentration of SF_6 measured by the gas analyzer for different air sample volumes is shown in Figure 4.1.

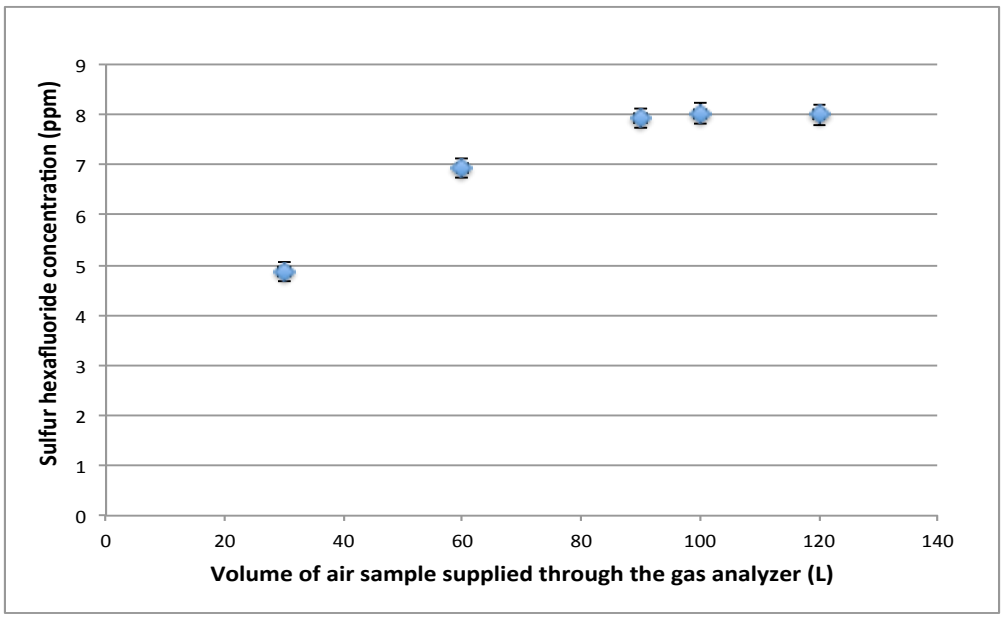

Figure 4.1: Concentration of sulfur hexafluoride (SF_6) measured by Gasmet^{TM} CR-100M FTIR analyzer for different air sample volumes

As shown in Figure 4.1, the concentration of SF_6 measured by the gas analyzer increases as the air sample volume increases. This is due to the fact that supplying higher volume of the air sample flushes the sample cell completely and displaces the majority of the gas previously contained in the sample cell. A smaller volume of the air sample is not able to flush the sample cell completely and hence, it is diluted with the gas already existing in the sample cell (which is nitrogen in this case since the sample cell is flushed with nitrogen in between the two consecutive measurements). If too small a volume is used to flush out the instrument, the above data show that the concentration data will indicate a lower concentration measurement of the gas compound. There is no significant change in the measured concentration of SF_6 (8 ppm) when the air sample volume is increased beyond 90 L. Hence, the minimum volume of air sample required for testing is at least 90 L and this limitation determines the size of sampling bags (100 L) required for air sample collection from the RAMEE.

4.2.2 Single Component Analysis

Initially, the gas analyzer was tested for single component analysis. The sample cell of the gas analyzer was supplied with 100 L of carbon dioxide (CO_2). The calibrated concentration of CO_2 was 500 ± 0.5 ppm for experiments and it was stated by the supplier Praxair Inc. The sample spectrum created by the gas analyzer for CO_2 is shown in Figure 4.2.

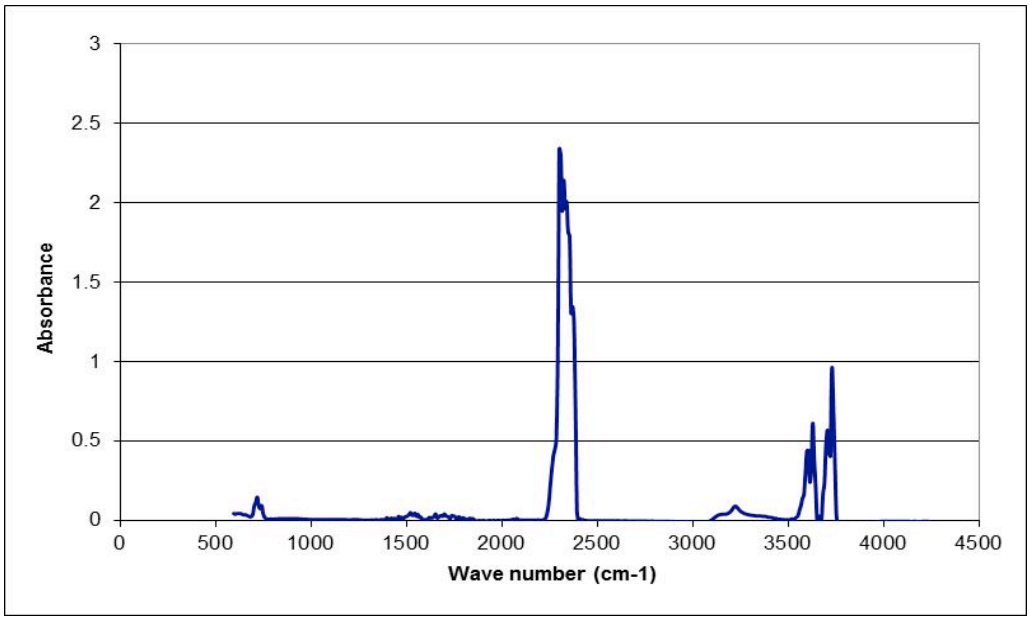

Figure 4.2: Sample spectrum of 500 ppm CO_2 data measured using the Gasmet^{TM} CR-100M FTIR gas analyzer

Figure 4.2 shows that the absorbance peak is near the spectrum wave number 2350 cm^{-1} and that there are some other peaks in the range 3500-3700 cm^{-1} and near 700 cm^{-1}, which indicates the presence of CO_2 in the sample cell. By analyzing the sample spectrum, the concentration of CO_2 is calculated to be 495.62 ppm that differs by 0.9% m the calibrated test sample concentration. Gasmet^{TM} Technologies Oy (2006) has stated the accuracy of the gas analyzer as $\pm 2\%$ and hence, the measured concentration is within the accuracy range of the gas analyzer.

4.2.3 Multi-component Analysis of Ambient Air

Similar to the single component analysis of CO_2 sample, the multi-components analysis of the air sample containing VOCs can be performed to calculate the concentration of VOCs in the air sample. The degree of absorption of infrared radiation at each wavelength relates quantitatively to the number of absorbing molecules in the sample gas (Gasmet^{TM} Technologies Oy, 2006). Beer's law (equation (C.1)) shows that there is a linear relationship between the absorbance and the concentration of a particular gas compound (the fraction of absorbing molecules) in the sample gas. Hence, the quantitative multi-component analysis of the sample gas is feasible using FTIR gas analyzer.

To perform multi-component analysis of the ambient air, air was pumped into the sample cell of the gas analyzer using the vacuum pump. An Omega mass flow meter was used to maintain the constant air flow rate. Once the sample cell was flushed with 100 L of ambient air, it was analyzed to create the sample spectrum of the ambient air as shown in Figure 4.3.

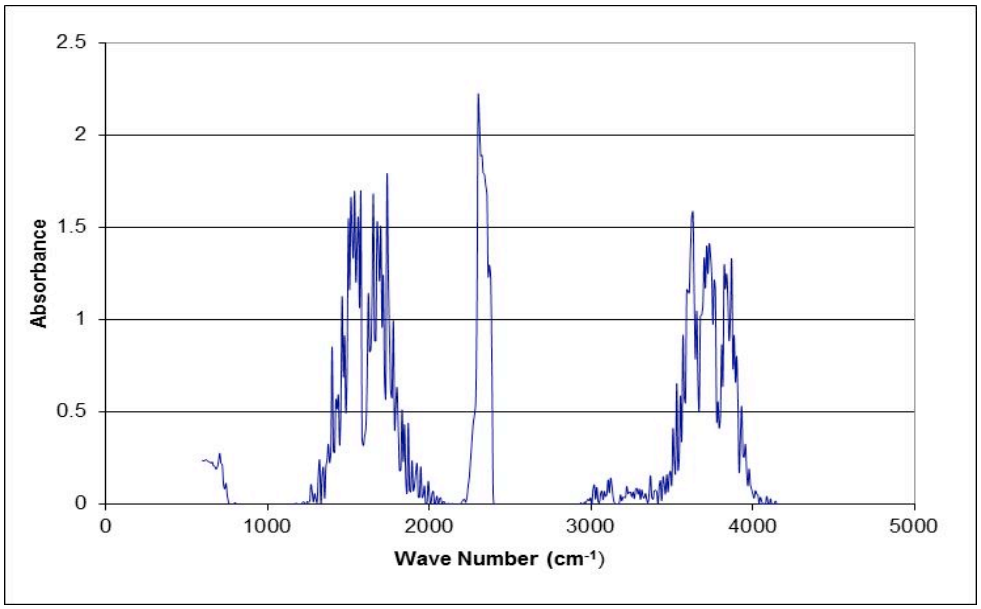

Figure 4.3: Multi-component sample spectrum of ambient air measured by Gasmet^{TM} CR-100M FTIR gas analyzer

Figure 4.3 shows a major absorbance peak at 2350 cm^{-1}, which indicates the presence of CO_2 in the ambient air. There are few peaks in the region of 3500 to 4000 cm^{-1} and 1400 to 2000 cm^{-1}, which are due to water vapor (H_2O) present in the ambient air. Hence, these results show that CO_2 and H_2O are the two major components present in the ambient air.

In addition to CO_2 and H_2O, a few other gas components are also present in the ambient air. Reference spectra of all the gas components that may exist in the ambient air are required to determine the concentration of various gas components in the ambient air. A reference spectrum is a spectrum of one single gas component of specific concentration. In multi-component analysis, these reference spectra are combined with appropriate multipliers to get a spectrum that is as close as possible to the ambient air. Since the concentration of single gas components in the reference spectrum are known, the concentration of each gas component in the ambient air can be calculated using the multipliers of the individual reference spectrum.

The reference spectra of 11 different gases (water vapor (H_2O), carbon dioxide (CO_2), sulfur hexafluoride (SF_6), nitrous oxide (N_2O), toluene (C_7H_8), formaldehyde (CHOH), methane (CH_4), carbon monoxide (CO), sulfur dioxide (SO_2), nitrogen dioxide (NO_2), and ammonia (NH_3)) at known concentrations are stored in the library of gases of the gas analyzer. These reference spectra are applied with appropriate multipliers and then combined by Calcmet (the multi-component analysis software) to obtain a spectrum as close as possible to the sample spectrum of the ambient air shown in Figure 4.3. Thus, the concentration of these 11 gas components in the ambient air is calculated and the results are shown in Table 4.1.

In addition, a Vaisala Carboncap® carbon dioxide meter (GM 70) containing the probe GMP 70 was used to measure the concentration of CO_2 in the ambient air. The Vaisala GM-70 can simultaneously be used with the Vaisala dew point probe DMP 74, to determine the amount

of H_2O in the ambient air. Table 4.1 shows the comparison between the gas component concentrations measured by the Gasmet^{TM} CR-100M gas analyzer and Vaisala Carboncap® GM-70 meter at atmospheric pressure and temperature. The water vapor concentration measured by the gas analyzer was in volume percentage, which is converted to humidity ratio. The Vaisala dew point probe (DMP 74) measures the water vapor in the ambient air as relative humidity and it is also converted into the humidity ratio for comparison purposes.

Table 4.1: Comparison between the gas compound concentrations measured by the Gasmet^{TM} CR-100M gas analyzer and Vaisala Carboncap® GM-70 meter

Gas Compound	Concentration measured by Gasmet^{TM} CR-100M gas analyzer	Concentration measured by Vaisala Carboncap® GM-70
Water vapor (H_2O)	1.61 ± 0.09 g_{water}/kg_{air}	1.61 ± 0.33 g_{water}/kg_{air}
Carbon dioxide (CO_2)	517 ± 20 ppm	520 ± 85 ppm
Carbon monoxide (CO)	0.07 ± 0.5 ppm	---
Methane (CH_4)	2.2 ± 0.2 ppm	---
Nitrous oxide (N_2O)	0.3 ± 0.2 ppm	---
Nitrogen dioxide (NO_2)	0.06 ± 0.5 ppm	---
Sulfur dioxide (SO_2)	0.00 ± 0.25 ppm	---
Ammonia (NH_3)	0.00 ± 0.25 ppm	---
Sulfur hexafluoride (SF_6)	0.00 ± 0.2 ppm	---
Toluene (C_7H_8)	0.00 ± 0.2 ppm	---
Formaldehyde (CHOH)	0.00 ± 0.04 ppm	---

The Gasmet^{TM} CR-100M gas analyzer has a bias uncertainty of ±2% of the measurement range of the gas component and precision uncertainty of ±0.01% of the measurement range of the gas component. Using these values, the overall uncertainty at 95% confidence interval of the gas analyzer is calculated as shown in Table 4.1. The bias uncertainty of the Vaisala carbon dioxide probe (GMP 70) is 75 ppm + 2% of reading and that of the Vaisala dew point probe (DMP 74) is 0.2 g/m^3 + 10% of reading. From Table 4.1, it is evident that the concentration of CO_2 and H_2O measured by the gas analyzer and Vaisala GM-70 are in agreement within the uncertainty range. The lowest concentration detection limit of the gas analyzer is 0.05 ppm.

Hence, gas compounds such as sulfur dioxide (SO_2), ammonia (NH_3), sulfur hexafluoride (SF_6), toluene (C_7H_8) and formaldehyde (CHOH) are not detected by the gas analyzer because they exist at very low concentration in the ambient air. The ambient air also contains numerous inert gases (such as Helium (He), Neon (Ne), Argon (Ar), Krypton (Kr), Nitrogen (N_2), Oxygen (O_2), Hydrogen (H_2)), but the gas analyzer does not detect them because these inert gases are not infrared active and thus give rise to no infrared absorption spectrum.

4.3 Sampling Bag Experiments

Teflon sampling bags were used to collect the air samples from the RAMEE because they are chemically inert to a wide range of gas compounds. If there is any chemical reaction between the sampling bag and the gas compounds present inside, it could alter the concentration of gas compounds. Experiments were conducted to check whether Teflon sampling bags are chemically inert to various gas compounds present in the ambient air. In the first experiment, air from the ambient atmosphere was pumped directly in to the gas analyzer and the concentration of different gas compounds was measured. In the second experiment, the ambient air was pumped into the sampling bag and left in the bag for one day to allow for any chemical interaction between the gas compounds and the sampling bag. The ambient air from sampling bag was then supplied to the gas analyzer to measure the concentration of various gas compounds. Table 4.2 shows the concentration of various gas compounds measured during both experiments.

Table 4.2: Comparison between the gas compound concentrations measured in the ambient air sample and the ambient air sample collected in the Teflon sampling bag

Gas Compound	Concentration measured in the ambient air sample	Concentration measured in the Teflon sampling bag air sample
Water vapor (H_2O)	1.61 ± 0.09 g_{water}/kg_{air}	1.60 ± 0.09 g_{water}/kg_{air}
Carbon dioxide (CO_2)	517 ± 20 ppm	509 ± 20 ppm
Carbon monoxide (CO)	0.07 ± 0.5 ppm	0.05 ± 0.5 ppm
Methane (CH_4)	2.2 ± 0.2 ppm	2.3 ± 0.2 ppm
Nitrous oxide (N_2O)	0.3 ± 0.2 ppm	0.4 ± 0.2 ppm
Nitrogen dioxide (NO_2)	0.05 ± 0.5 ppm	0.06 ± 0.5 ppm
Sulfur dioxide (SO_2)	0.00 ± 0.25 ppm	0.00 ± 0.25 ppm
Ammonia (NH_3)	0.00 ± 0.25 ppm	0.00 ± 0.25 ppm
Sulfur hexafluoride (SF_6)	0.00 ± 0.2 ppm	0.00 ± 0.2 ppm
Toluene (C_7H_8)	0.00 ± 0.2 ppm	0.00 ± 0.2 ppm
Formaldehyde (CHOH)	0.00 ± 0.04 ppm	0.00 ± 0.04 ppm

From Table 4.2, it is clear that there is no significant difference in the gas compound concentration measured during the two experiments. Hence, it is concluded that the Teflon sampling bags are chemically inert to majority of the measured gas compounds (H_2O, CO_2, CO, CH_4, N_2O and NO_2) present in the ambient air and it can be used to collect the air samples from the RAMEE. The vacuum pump used for air sample collection cannot pump out the entire air sample and evacuate the sampling bag completely. If sampling bag is used twice consecutively to collect the air sample, then the gas compounds remained from the previous air sample can mix with the following air sample resulting in false experimental data. Hence, once the sampling bags are filled with the air sample, they need to be flushed with inert gas like nitrogen (N_2) before they can be used again to collect the next air sample.

Experiments were conducted using SF_6 as a tracer gas to determine how many times the sampling bag needs to be flushed before collecting the next air sample. Initially, the sampling bag was filled with the air sample containing 8 ppm SF_6, which was pumped out using the vacuum pump. The sampling bag was then filled with nitrogen to mix with the air sample containing SF_6 remained from previous experiment. This nitrogen mixture (containing mostly

nitrogen and some SF_6, if any) was passed through the gas analyzer to determine the concentration of SF_6. The sampling bag was consecutively filled with pure nitrogen and the procedure was repeated until no SF_6 was detected in the nitrogen mixture. Figure 4.4 shows the traces of SF_6 detected in the nitrogen mixture each time the sampling bag is flushed with pure nitrogen.

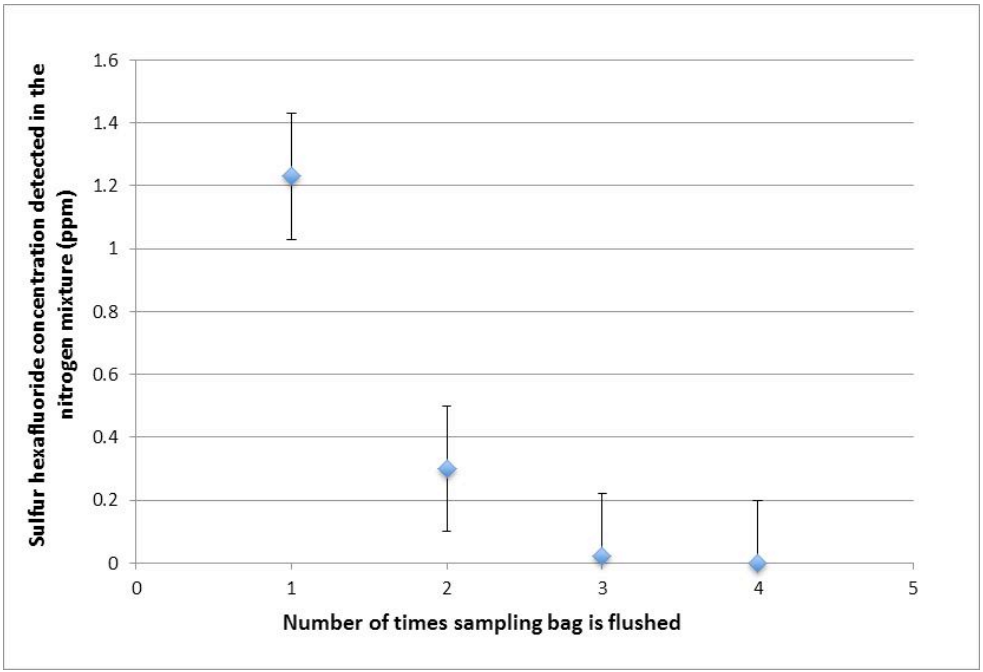

Figure 4.4: Traces of sulfur hexafluoride (SF_6) detected in the nitrogen mixture obtained from the sampling bag

As shown in Figure 4.4, some SF_6 is detected in the nitrogen mixture when it is passed through the gas analyzer after the first flushing. With the subsequent flushing of sampling bag with pure nitrogen, traces of SF_6 detected in the nitrogen mixture are reduced. From Figure 4.4, it is concluded that the sampling bag needs to be flushed at least three times with nitrogen before the bag can be used to collect a new sample.

4.4 Test conditions

To evaluate the amount of contaminant transfer in the RAMEE, tests were conducted on Prototype #4 and Prototype #6 over a range of *NTU* and heat capacity ratio (*Cr**) values. The different *NTU*s were created by varying the air flow rate through each LAMEE. When the air flow rate is kept constant (i.e., constant *NTU*), the heat capacity of the air and the liquid desiccant are nearly constant. Hence, the ratio of heat capacities (*Cr**) is proportional to the mass flow rate of the liquid desiccant. The different values of *Cr** were created by varying the liquid desiccant flow rate. Both prototypes were tested for AHRI summer and winter test conditions. Figure 4.5 shows the AHRI standard supply inlet (SI) and exhaust inlet (EI) air conditions and actual experimental conditions superimposed on the psychrometric chart.

(a) (b)

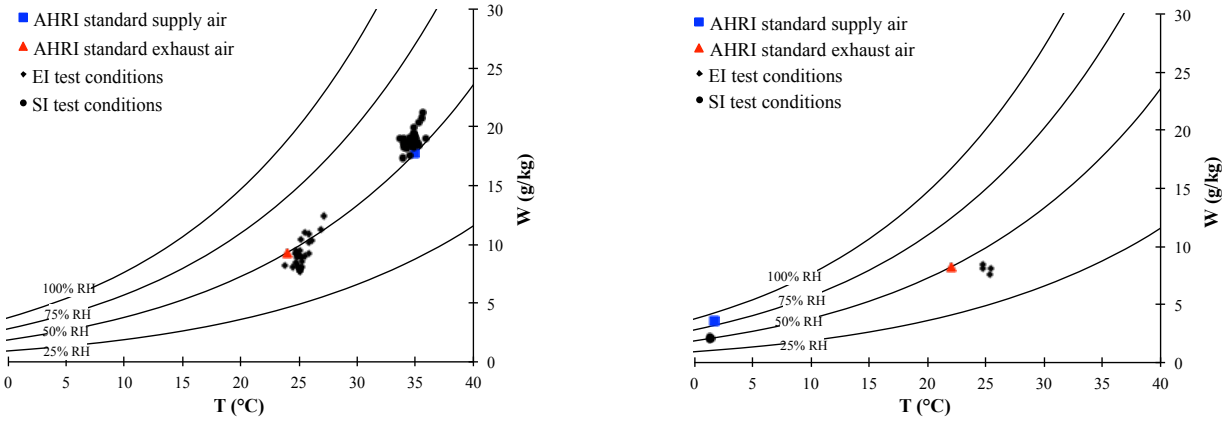

Figure 4.5: AHRI standard and experimental (a) summer and (b) winter test conditions superimposed on a psychrometric chart

Figure 4.5 shows that the experimental supply inlet (SI) and exhaust inlet (EI) air conditions are slightly different than AHRI standard conditions. Since the supply inlet (SI) air was drawn from the environmental chamber, it was conditioned closer to AHRI standard SI conditions than the exhaust inlet (EI) air, which was drawn from the laboratory room that was

conditioned by the building HVAC system. Moreover, the vacuum fans used to supply the exhaust air in the RAMEE test facility also add heat resulting in higher temperature of the exhaust inlet (EI) air than the AHRI standard EI conditions.

Beriault (2011) conducted experiments to test the performance of Prototype #4. The experimental results showed that the effectiveness (sensible, latent and total) of the exchanger increased with increase in Cr^*. The highest effectiveness was measured at Cr^*=4.5 and there was no significant change in the effectiveness when Cr^* was increased beyond 4.5. Also, the exchangers performed better at higher *NTU* (*NTU* = 12.3) than at lower *NTU* (*NTU* = 5). It is suspected that the contaminant transfer may occur in the RAMEE in similar fashion to water vapor transfer. Thus, the high latent effectiveness operating conditions are chosen for testing to allow for maximum contaminant transfer in the RAMEE.

Both prototypes were tested for different *NTUs* varying from 3.2 to 12.2 at the highest constant Cr^* to investigate the effect of change in air flow rate on the contaminant transfer. Similarly, both prototypes were tested for different Cr^* values varying from 1.0 to 4.5 at highest constant *NTU* to investigate the effect of change in desiccant flow rate on the contaminant transfer. Additionally, the effect of change in environmental conditions was analyzed by testing both prototypes for AHRI summer and winter conditions. Tables 4.3 and 4.4 show the experimental test conditions for Prototype #4 and Prototype #6, respectively.

Table 4.3: Experimental test conditions for Prototype #4

Test Index	Test Condition	NTU	Cr*	Contaminant	Temperature (°C)		RH (%)		Dry air mass flow rate (kg/s)		Face velocity (m/s)		Solution flow rate (l/min)
					EI	SI	EI	SI	EI	SI	EI	SI	
Change in air flow rate (NTU) at constant Cr*													
1	Summer	12.1	4.5	SF_6	25.2	34.6	49	51	0.015	0.015	0.45	0.44	1.20
				C_7H_8	25.9	34.6	42	50	0.016	0.015	0.46	0.45	1.20
				HCHO	24.7	33.7	45	54	0.015	0.015	0.45	0.44	1.21
2		8.5	4.5	C_7H_8	25.3	33.9	40	49	0.021	0.021	0.62	0.63	1.71
				HCHO	26.1	34.1	46	53	0.022	0.021	0.64	0.63	1.70
3		4.9	4.5	C_7H_8	24.8	34.2	43	52	0.046	0.045	1.34	1.36	1.93
				HCHO	25.0	34.3	38	50	0.046	0.045	1.34	1.35	1.94
Change in Cr* at constant air flow rate (NTU)													
4	Summer	12.2	1.0	C_7H_8	24.5	34.1	40	52	0.015	0.015	0.45	0.45	0.38
				HCHO	25.1	34.5	38	48	0.015	0.015	0.45	0.45	0.39
5		12.2	2.0	C_7H_8	25.9	35.2	49	49	0.016	0.015	0.46	0.44	0.54
				HCHO	24.7	34.9	46	51	0.015	0.015	0.45	0.45	0.53
6		12.1	3.0	C_7H_8	25.1	35.6	45	53	0.015	0.015	0.45	0.46	0.84
				HCHO	25.5	35.3	51	48	0.016	0.015	0.46	0.45	0.84
7		12.2	4.5	C_7H_8	27.1	34.6	52	51	0.015	0.015	0.45	0.45	1.21
				HCHO	26.9	34.1	48	52	0.015	0.015	0.44	0.46	1.20
Change in environmental condition													
8	Winter	12.1	4.5	C_7H_8	25.4	1.4	38	49	0.015	0.015	0.45	0.46	1.21
				HCHO	24.7	1.5	41	47	0.016	0.015	0.46	0.44	1.21

Table 4.4: Experimental test conditions for Prototype #6

Test Index	Test Condition	NTU	Cr*	Contaminant	Temperature (°C)		RH (%)		Dry air mass flow rate (kg/s)		Face velocity (m/s)		Solution flow rate (l/min)
					EI	SI	EI	SI	EI	SI	EI	SI	
Change in air flow rate (NTU) at constant Cr*													
1	Summer	8.9	3.0	SF_6	25.1	35.0	37	51	0.018	0.018	0.54	0.55	1.03
				C_7H_8	25.3	34.8	42	52	0.018	0.019	0.54	0.53	1.02
				HCHO	24.9	34.9	39	50	0.019	0.018	0.55	0.55	1.02
2		6.1	3.1	C_7H_8	25.3	34.8	38	49	0.026	0.027	0.77	0.77	1.58
				HCHO	24.8	35.3	40	53	0.026	0.026	0.76	0.78	1.59
3		3.2	3.0	C_7H_8	23.8	34.6	42	50	0.049	0.050	1.49	1.50	2.39
				HCHO	24.7	35.7	45	54	0.051	0.049	1.49	1.48	2.37
Change in Cr* at constant air flow rate (NTU)													
4	Summer	8.8	1.0	C_7H_8	25.9	35.1	46	50	0.018	0.018	0.53	0.54	0.36
				HCHO	25.1	34.5	43	52	0.018	0.017	0.54	0.54	0.36
5		8.9	2.0	C_7H_8	24.7	34.9	41	52	0.017	0.018	0.54	0.55	0.69
				HCHO	24.9	34.1	44	51	0.018	0.019	0.54	0.56	0.68
6		8.8	2.9	C_7H_8	25.1	35.0	38	49	0.018	0.018	0.53	0.54	1.02
				HCHO	25.5	35.9	42	48	0.017	0.018	0.53	0.54	1.01
7		8.8	4.5	C_7H_8	25.0	34.6	37	51	0.018	0.017	0.55	0.53	1.59
				HCHO	24.9	34.9	44	53	0.019	0.018	0.53	0.54	1.59
Change in environmental condition													
8	Winter	8.9	3.1	C_7H_8	25.3	1.3	36	47	0.018	0.019	0.54	0.55	1.03
				HCHO	24.8	1.4	39	45	0.018	0.018	0.55	0.55	1.02

4.5 Transient Testing of the Contaminants

The environmental chamber was started and allowed to reach close to AHRI standard summer condition at the beginning of each test. Once the environmental chamber was conditioned, the air was supplied to the exchangers. When the air was stabilized close to AHRI summer condition, the liquid desiccant flow was started. At the same time, sulfur hexafluoride (SF_6) was also injected into the exhaust inlet air stream using the injection technique shown in Figure 3.3. Prototype #4 and prototype #6 were tested at the conditions of Test 1 shown in Tables 4.3 and 4.4, respectively. The experiments were repeated using toluene (C_7H_8) and formaldehyde (HCHO) individually at the conditions of Test 1 on both prototypes. The pressurized cylinders containing specific calibrated concentrations of each individual contaminant were used in these experiments. The air samples were taken from all four sampling ports (Figure 2.11) every hour to evaluate the transient behavior of contaminant transfer in the RAMEE. The air samples were analyzed using the gas analyzer to determine the transfer fraction of each contaminant in both prototypes. The detailed experimental data on concentration of each contaminant measured at each sampling port are shown in Appendix D. Figure 4.6 shows the *EATR* (for sulfur hexafluoride) and $EATR_i$* (i = 1 for toluene and i = 2 for formaldehyde) measured over the period of 6 hours in both prototypes. Please note that the data are slightly offset from each other to help distinguish the uncertainty bars that overlap each other. Also, note that each data point represents one single measurement.

(a) (b)

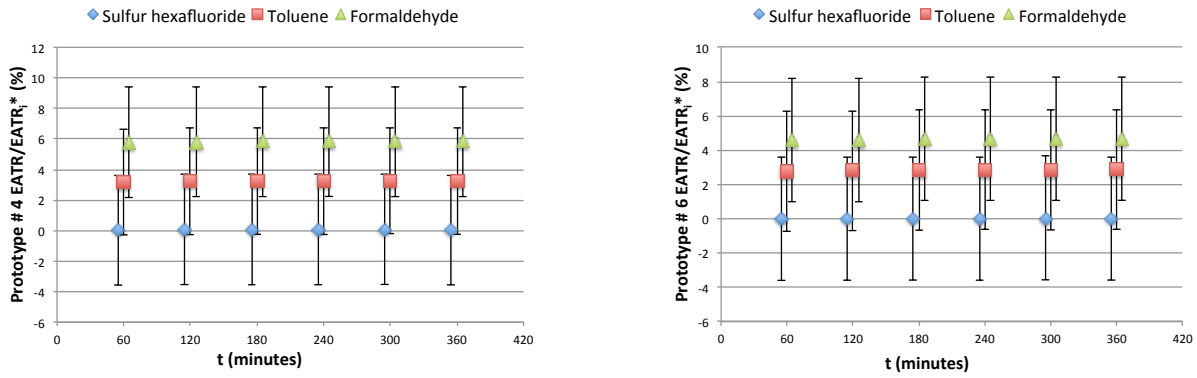

Figure 4.6: *EATR* for sulfur hexafluoride and $EATR_i$* for toluene and formaldehyde measured in (a) Prototype # 4 (*NTU* = 12.1 and *Cr** = 4.5) and in (b) Prototype # 6 (*NTU* = 8.9, *Cr** = 3)

It is evident from Figure 4.6 that there is negligible transfer of sulfur hexafluoride in both prototypes. This is mainly due to very low solubility of sulfur hexafluoride in water. At 25^{o}C sulfur hexafluoride has the lowest solubility in water among the three tested contaminants and hence, there is no transfer of sulfur hexafluoride by dissolution in the liquid desiccant or by air leakage between the air streams. Hence, these sulfur hexafluoride results show that the air leakage between the air streams is negligible in both prototypes. The transfer fraction of toluene in each prototype is higher than that of the sulfur hexafluoride. Toluene results show that dissolution transfer for a low solubility VOCs like toluene is very small and within the 95% uncertainty bounds of measurement.

As shown in Table 3.3, the solubility of formaldehyde in water is about 800 times higher than toluene, which makes it highly vulnerable to dissolution in the liquid desiccant and transfer to the supply air stream. Figure 4.6 shows that the transfer fraction ($EATR_i$*) values of formaldehyde exceeds its 95% uncertainty limits, which means that there is a small transfer of formaldehyde, but slightly higher than that of toluene, in both prototypes. The reduction in the solubility of contaminants in the liquid desiccant occurs due to the salting out effect. As shown

in Figure 3.2, Poulson et al. (1999) showed that toluene solubility in 11.4 wt% $MgCl_2$ salt solution is decreased by 65% compared to pure water. The liquid desiccant used in the experiment is nearly saturated (34~35 wt%) $MgCl_2$ salt solution. At such high salt concentration, there are less water molecules available for contaminants to dissolve, resulting in reduction of the solubility of contaminants by a large amount. Moreover, the temperature of the liquid desiccant during the test is observed to be 22 to 26^{o}C. As shown in Figure 3.1, toluene and formaldehyde have low solubility in water within this temperature range causing the minimal dissolution and subsequent transfer of these contaminants in both prototypes. Hence, the transfer fraction of toluene ($2.3-3.4\pm3.5\%$) and formaldehyde ($4.5-6.4\pm3.6\%$) in the RAMEE prototypes is smaller than 71% toluene and 8-15% formaldehyde measured in the desiccant wheel (Wolfrum et al. (2008)) and the energy wheel (Fisk et al. (1985), Andersson et al. (1993)), respectively.

Figure 4.6 also shows that there is negligible amount of change in the transfer fraction of all three contaminants over the period of 6 hours. Formaldehyde has the highest solubility among the tested contaminants and its transfer fraction is changed by negligible amount in 6 hours of testing. This is because the salting out effect reduces the solubility of contaminants causing very small dissolution and hence, the contaminant transfer is limited by mass equilibrium of contaminants in the liquid desiccant. These results agree with Wolfrum et al. (2008), who observed that the contaminant transfer was limited by the adsorption equilibrium of contaminants with the desiccant wheel. These results conclude that dissolution transfer is the contaminant transfer mechanism where the small amount of contaminants transfer from the exhaust air stream to the liquid desiccant and they are dissolved in the liquid desiccant and transported to the other LAMEE where they are transferred through the membrane to the supply air stream.

The transfer fraction of contaminants is slightly lower in Prototype #6 than in Prototype #4 indicating that the diffusion coefficient of the tested contaminants through Prototype #6 membrane (GE ePTFE QL822^{TM}) is lower than that of Prototype #4 membrane (AY Tech^{TM} ePTFE). The mass balance inequality for all three contaminants is checked and it is showed in Appendix D. It satisfies the 15% limit set by ASHRAE Standard 84 (2012). This indicates that the measurements of concentration and mass flow rate are reasonably accurate in both prototypes.

4.6 Evaporation Chamber Testing

For the evaporation chamber testing, contaminants were obtained in the liquid form and evaporated as shown in Figure 3.4 before injecting in the exhaust inlet air stream. Evaporation chamber testing was employed to allow for longer duration of contaminant testing because the pressurized cylinders of contaminants used for transient tessting were getting emptied very quickly. Moreover, it is very economical to obtain the contaminants in the liquid form. Only toluene and formaldehyde were tested using the evaporation method because sulfur hexafluoride was only used as tracer gas to indicate any air leakage in the exchangers.

If the liquid contaminants are not evaporated properly before injecting in the exhaust inlet air stream, then it could result in large fluctuation of contaminant concentration. Once all the process parameters (i.e. flow rate of the air stream, injection rate of liquid contaminants) were set, the air samples were taken every hour from the exhaust inlet stream (sampling port 1) and analyzed using the gas analyzer. Figure 4.7 shows the concentration of toluene and formaldehyde measured in the air samples with time.

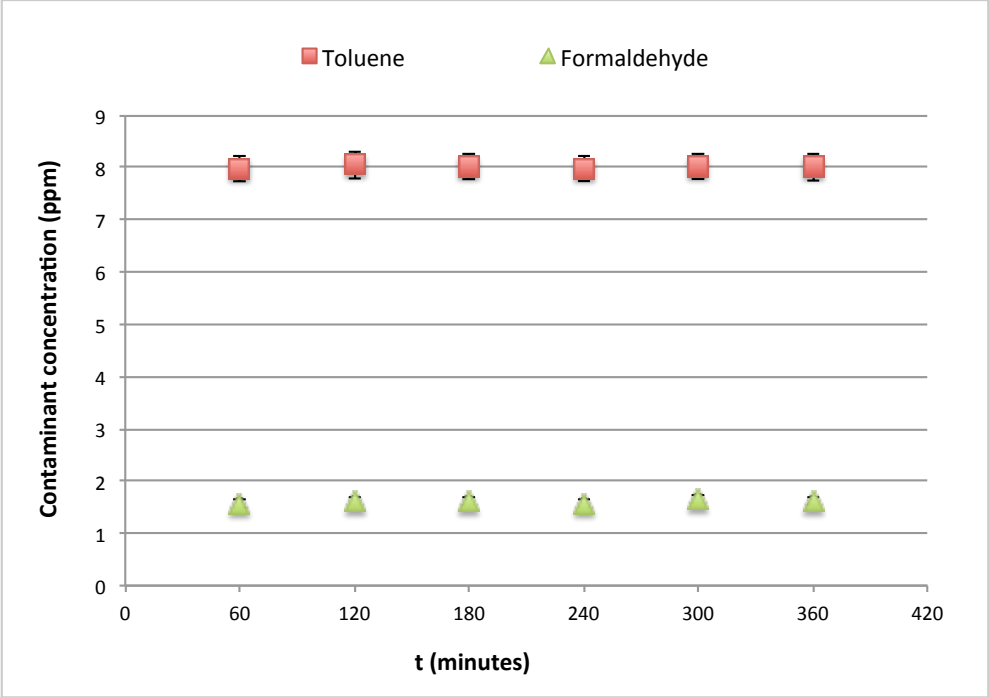

Figure 4.7: Concentration of toluene and formaldehyde measured in the air sample with time

It is clear from Figure 4.7 that the measured concentration of toluene and formaldehyde remains fairly constant with time indicating that both contaminants (toluene and formaldehyde) are evaporated properly before entering in the air stream.

4.6.1 Effect of Change in the Air Flow Rate on $EATR_i$*

Prototype #4 and Prototype #6 were tested over a range of air flow rate (Test 1 to 3 in Table 4.3 and Table 4.4) to investigate the effect of change in *NTU* on the transfer fraction ($EATR_i$*) of toluene and formaldehyde. The liquid desiccant flow rate (*Cr**) was maintained constant during these experiments. Both prototypes were tested at AHRI standard summer condition. The air samples were taken after 6 hours of continuous injection of contaminants to allow the liquid desiccant to be saturated with contaminants. Figure 4.8 shows the effect the change in the air flow rate on contaminant transfer in both prototypes. The data are slightly offset to help distinguish the uncertainty bars that overlap each other.

(a) (b)

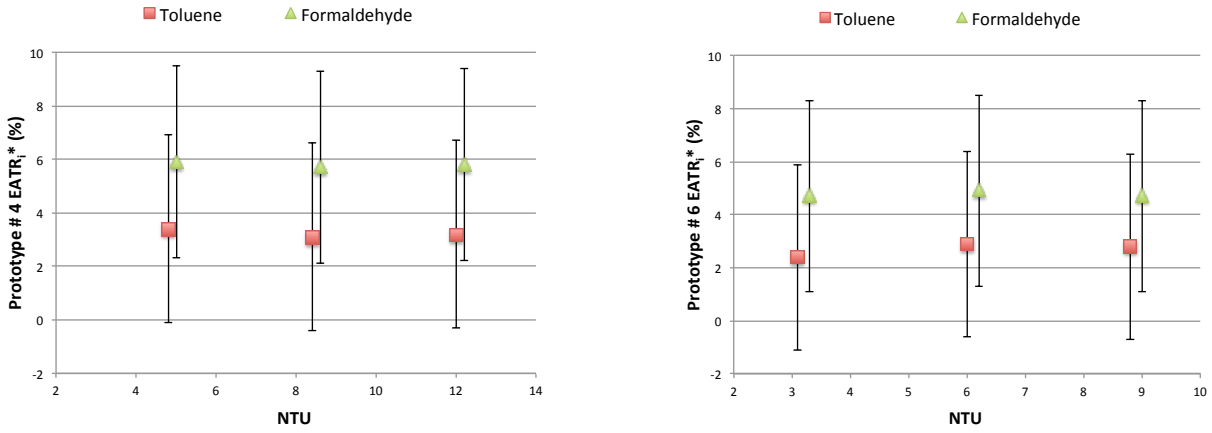

Figure 4.8: Effect of change in the air flow rate (*NTU*) on $EATR_i$* for toluene and formaldehyde in (a) Prototype #4 at constant $Cr^* = 4.5$ and in (b) Prototype #6 at constant $Cr^* = 3$

The latent effectiveness of the RAMEE increases with increase in *NTU* because at higher *NTU* the mass flow rate of air is smaller allowing more water vapor to transfer to/from air stream to/from the liquid desiccant. Since the transfer mechanism of contaminants is expected to be similar to water vapor, contaminants could also transfer at higher rate at higher *NTUs*. However, results from Figure 4.8 show that there is negligible change in the transfer fraction of toluene or formaldehyde over the range of *NTU*s in both prototypes.

As shown in Table D.1 in Appendix D, there is only 5-10% increase in the latent effectiveness from *NTU* = 4.9 to *NTU* = 12.1 for Prototype #4. Similarly, as per Table D.3 in Appendix D, the latent effectiveness of Prototype #6 is increased by 8-12% when *NTU* is increased from *NTU* = 3.2 to *NTU* = 8.9. The change in latent effectiveness is quite small over this range and therefore it has a negligible effect on the transfer fraction of contaminants in both prototypes. The air leakage in the exchangers also depends on the air flow rate because the air pressure changes with the air flow rate. Since the transfer fraction of contaminants remains fairly constant over the range of *NTU*s, it indicates that there is negligible air leakage. These results

conclude that the contaminant transfer in the RAMEE is nearly unaffected compared to a heat wheel in which the carry over rate of nitrous oxide was increased by 10-20% when the air flow was increased from 3000 m^3/h to 3500 m^3/h (Schaeffler et al., 1988).

4.6.2 Effect of Change in the Liquid Desiccant Flow Rate on $EATR_i$*

The liquid desiccant flow rate through the exchanger was varied at constant air flow rate (Test 4 to 7 in Table 4.3 and Table 4.4) to investigate the effect of change in *Cr** on the transfer fraction of toluene and formaldehyde. The experiments were performed at AHRI standard summer condition and the air samples were collected are 6 hours of continuous operation of the RAMEE prototypes. Figure 4.9 shows the effect of change in the liquid desiccant flow rate on contaminant transfer in Prototype #4 and Prototype #6. The experimental data are slightly offset to help distinguish the uncertainty bars of the data.

(a) (b)

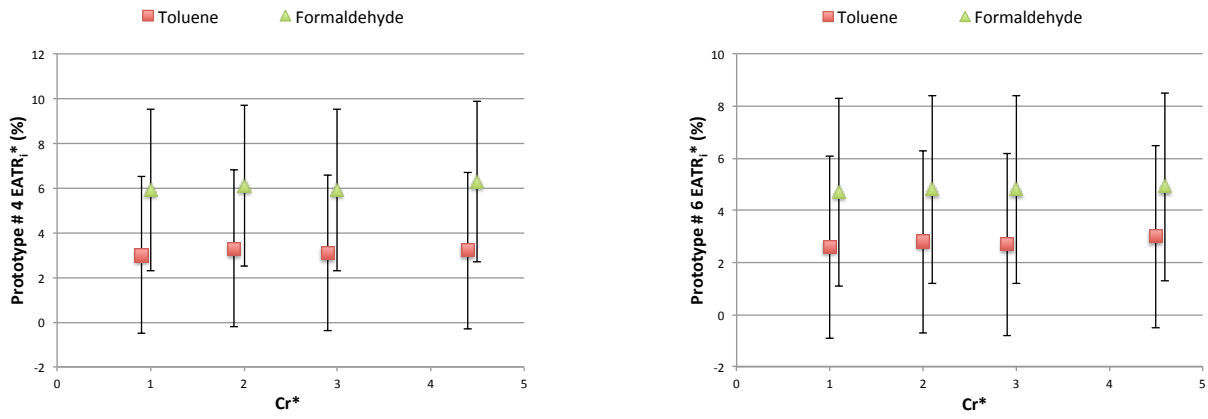

Figure 4.9: Effect of change in the liquid desiccant flow rate (*Cr**) on $EATR_i$* for toluene and formaldehyde in (a) Prototype #4 at constant *NTU* = 12.2 and in (b) Prototype #6 at constant *NTU* = 8.8

At higher *Cr** values (i.e. higher liquid desiccant flow rate), more liquid desiccant is being circulated between the two LAMEEs. One of the mechanisms of contaminant transfer in

the RAMEE system is by dissolution in the liquid desiccant. Thus, at higher liquid desiccant flow rate, there could be higher contaminant transfer. Figure 4.9 shows that there is negligible change in $EATR_i^*$ of toluene and formaldehyde over the range of Cr^*.

The latent effectiveness of Prototype #4 increases from 32% at $Cr^* = 1$ to 46% at $Cr^* = 4.5$ as shown in Table D.1 in Appendix D. This small change in latent effectiveness means that the contaminant transfer in Prototype #4 is not significantly affected by Cr^* for the range of test conditions studied. The latent effectiveness of Prototype #6 increases from 26% at $Cr^* = 1$ to 62% at $Cr^* = 4.5$ as shown in Table D.3 in Appendix D. This large change in the latent effectiveness of Prototype #6 is accompanied by a very slight increase in $EATR_i^*$ of toluene and formaldehyde, but these $EATR_i^*$ values are constant within the experimental uncertainties because the liquid desiccant used in the RAMEE is saturated salt solution (34~35 wt% $MgCl_2$ salt solution) resulting in the reduced solubility of contaminants. These results conclude that the RAMEE is negligibly affected by increase in the liquid desiccant flow rate compared to heat wheel (Schaeffler et al. (1988)) or desiccant wheel (Wolfrum et al. (2008)) in which the contaminant transfer is increased quadratic or linearly as the wheel rotation speed increases.

4.6.3 Effect of Change in the Latent Effectiveness on $EATR_i^*$

The latent effectiveness of Prototype #4 and Prototype #6 was measured over the range of air flow rate (NTU) and the liquid desiccant flow rate (Cr^*) shown in Table 4.3 and Table 4.4. These latent effectiveness values measured during each test are presented in Appendix D. The contaminant transfer in both prototypes is plotted as a function of latent effectiveness and it is shown in Figure 4.10. The data are slightly offset to help distinguish the uncertainty bars that overlap each other.

(a) (b)

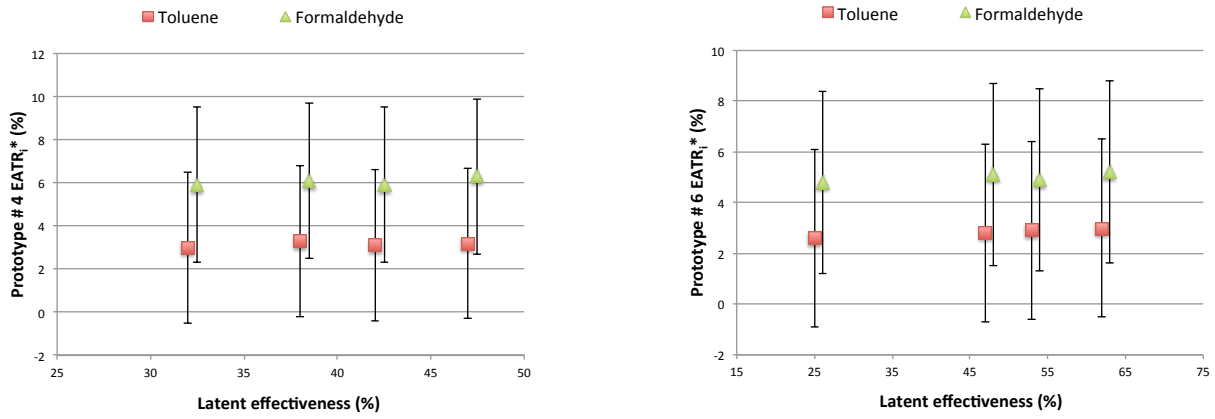

Figure 4.10: Effect of change in the latent effectiveness (ε_l) on $EATR_i$* for toluene and formaldehyde in (a) Prototype #4 and (b) Prototype #6

Figure 4.10 shows that the transfer fraction of toluene and formaldehyde in both prototypes increases slightly as the latent effectiveness increases. However, the measured values of $EATR_i$* are constant within the experimental uncertainties. Therefore, there may be a trend, but it cannot be determined because the experimental uncertainties are too high. Moreover, the transfer fraction of contaminants in Prototype #6 is measured to be lower than that of Prototype #4 even at higher latent effectiveness, which indicates that the RAMEE can provide higher effectiveness (sensible, latent and total) with minimal transfer of contaminants if the exchangers are made with minimal air leakage and the membrane with the smaller diffusion coefficient of contaminants. These results eliminate the suspicion that the RAMEE may transfer higher amount of contaminants at higher latent effectiveness.

4.6.4 Effect of Change in the Environmental Condition on $EATR_i$*

During the summer outdoor conditions, warm and humid outdoor air is passed through the supply LAMEE and it is dehumidified before supplying to the building. Hence, the water vapor is transferred from the supply LAMEE to the exhaust LAMEE. Contrary to that, water

vapor is transferred from the exhaust LAMEE to the supply LAMEE during the winter outdoor conditions because outdoor air is dry and less humid than indoor air. The contaminants may be transferred from the exhaust air stream to the supply airstream in the energy recovery systems. Hence, the contaminant transfer gradient is in the same direction as water vapor during winter outdoor conditions but it is in the opposite direction during the summer outdoor conditions.

The experiments were conducted on Prototype #4 and Prototype #6 to check whether contaminant transfer in the RAMEE is affected by the direction of water vapor gradient. The environmental conditions were changed while keeping the air flow rate (*NTU*) and the liquid desiccant flow rate (*Cr**) constant (Test 1 and 8 in Table 4.3 and Table 4.4). The air samples were collected after 6 hours of continuous injection of contaminants. Figure 4.11 shows the effect of change in environmental conditions on the transfer fraction of contaminants in both prototypes. Please note that the data are slightly offset to help distinguish the uncertainty bars that overlap each other.

(a) (b)

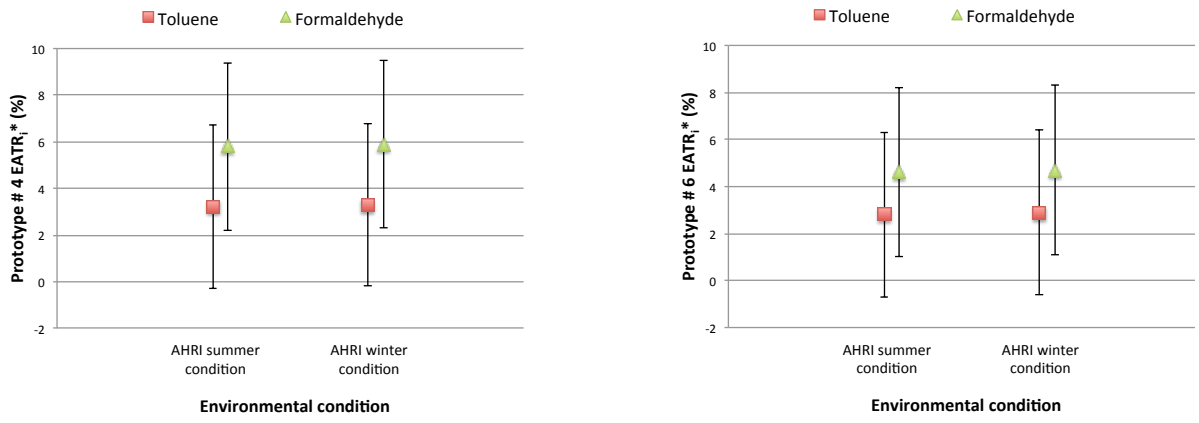

Figure 4.11: Effect of change in the environmental condition on $EATR_i$* for toluene and formaldehyde in (a) Prototype #4 and (b) Prototype #6

Figure 4.11 shows that there is slightly higher $EATR_i$* in the winter conditions than in the summer conditions; however, the difference is much smaller than the uncertainty in the measured $EATR_i$* values. These results indicate that the change in the environmental condition does not affect the transfer fraction of toluene and formaldehyde in the RAMEE prototypes. The directional gradient of water vapor has negligible impact on the contaminant transfer and hence, it eliminates the possibility of higher contaminant transfer during the winter outdoor conditions.

4.7 Summary

In this chapter, the experimental results are presented for the Gasmet™ CR-100M gas analyzer testing and the contaminant transfer testing of the Prototype #4 and Prototype #6. Some preliminary experiments were conducted to ensure that a 100 L air sample is appropriate to accurately measure the concentration of contaminants using the Gasmet™ CR-100M gas analyzer. A single component analysis of air sample containing calibrated concentration of carbon dioxide was carried out using the Gasmet™ CR-100M gas analyzer. The multi-component analysis of ambient air was performed using the gas analyzer and results were compared with Vaisala Carboncap® GM-70 meter. The concentration of water vapor and carbon dioxide measured by both devices was found to be in agreement within their uncertainty limits. The Teflon sampling bags were checked whether they are inert to gas compounds present in ambient air and they were found to be inert to majority of gas compounds present in the ambient air. The experimental results also indicated that the Teflon sampling bags need to be flushed at least three times with an inert gas like nitrogen (N_2) before collection of a new air sample.

The transient testing of contaminant transfer was performed on the both RAMEE prototypes and it is shown that there is negligible amount of change in the transfer fraction of contaminants over a 6-hour period. Moreover, the transfer fraction was measured to be lower in

Prototype #6 than Prototype #4. It was found that a very small amount of contaminants is transferred from the exhaust inlet air stream to the liquid desiccant and transported to the other LAMEE. The transfer fraction of toluene was smaller than formaldehyde in both prototypes because toluene has lower air diffusion coefficient and water solubility than formaldehyde. The effects of various process parameters like the change in the air flow rate (*NTU*), the change in the liquid desiccant flow rate (*Cr**), and the change in the environmental conditions on the contaminant transfer were also evaluated. It was found that the transfer fraction of contaminants is nearly insensitive to all these process parameters. The transfer fraction of all three contaminants in the RAMEE prototypes was found to be smaller than in enthalpy plate, energy wheel or the desiccant wheel.

CHAPTER 5

SUMMARY, CONCLUSIONS AND RECOMMENDATIONS

5.1 Summary

An air-to-air energy recovery system can reduce the energy consumption of an HVAC system by preconditioning the outdoor air. A Run-Around Membrane Energy Exchanger (RAMEE) is a novel design of such an air-to-air energy recovery system which is capable of transferring heat and moisture between two remotely located air streams. Since the ducts for the supply and exhaust airstream of the RAMEE can be non-adjacent, it is suitable for retrofit HVAC applications. However, just like any other energy recovery system, the RAMEE may also transfer contaminants between the air streams. This study is a part of large research project of design, testing and prototype development of the RAMEE and the overall objective of this study is to quantify and compare the contaminant transfer in two different RAMEE prototypes. The Exhaust Air Transfer Ratio (*EATR*) defined by ANSI/ASHRAE Standard 84 (2012) is used to determine the transfer fraction of contaminants in the RAMEE. The objectives of the present research are divided into three main categories as shown in Chapter 1. The following sections describe how these objectives are addressed in different chapters of the thesis.

The design and construction of two different prototypes (Prototype #4 and Prototype #6) of the RAMEE are discussed in Chapter 2. Prototype #4 of the RAMEE consists of two counter-cross-flow liquid-to-air membrane energy exchangers (LAMEEs). Prototype #4 has 10 liquid

desiccant channels (1/8 inch (3.18 mm) thick) separated from the air channels (1/4 inch (6.35 mm) thick) by AY Tech^{TM} ePTFE laminated membrane. Prototype #6 also has as counter-cross-flow configuration but it is built longer and wider than Prototype #4. Prototype #6 has 23 liquid desiccant channels (1/16 inch (1.59 mm) thick) and 24 air channels (1/4 inch (6.35 mm) thick) separated by GE ePTFE QL822^{TM} membrane. The two LAMEEs of each prototype are then coupled with a liquid desiccant line running in a closed loop between the two exchangers. A saturated $MgCl_2$ salt solution (34~35 wt%) is used as a liquid desiccant.

Both prototypes of the RAMEE were tested using the test facility developed by Erb (2007). A TSI DP-CALC™ micromanometer and the orifice plates were used to measure the mass flow rate of air. Thermocouples were used to measure the air and the liquid desiccant temperature. Vaisala humidity sensors and RTDs upstream and downstream of each LAMEE measured the humidity ratio and temperature of air. Omega FMG 220 magnetic flow meters in conjunction with electronically actuated flow control valves were employed to measure and control the liquid desiccant flow rate. An environmental chamber was used to control the temperature and humidity of the supply inlet air stream close to AHRI standard conditions. The exhaust inlet air stream conditions were found slightly different than AHRI standard conditions because it is mainly controlled by the building HVAC system.

The selection of Volatile Organic Compounds (VOCs) for testing of the RAMEE prototypes is discussed in Chapter 3. Three criteria were used to select the most significant VOCs out of more than 300 compounds of VOCs. Toluene and formaldehyde belonging to aromatic hydrocarbons and aldehydes group were selected as VOCs for testing of the RAMEE prototypes. In addition, sulfur hexafluoride was used for tracer gas experiments. These VOCs were injected into the exhaust inlet air stream for contaminant transfer experiments. Two

different methods were used for injection of VOCs. In the first method, a commercially available pressurized cylinder containing calibrated concentration of desired contaminant was used. The flow rate of each contaminant was controlled to achieve the desired concentration of contaminant in the exhaust inlet air stream. In the second method, the contaminants were obtained in the liquid form and they were evaporated into the air stream. The injection rate of contaminants was varied to achieve the desired contaminant concentration. Only toluene and formaldehyde were tested using the evaporation technique. The air samples were collected in the Teflon sampling bags from all four air streams of the RAMEE test facility and analyzed using the Gasmet™ FTIR CR-100M gas analyzer to determine the concentration of contaminant in the air sample.

Various experiments were conducted using the Gasmet™ FTIR gas analyzer to determine its bias and precision uncertainty. In addition, a few experiments were conducted to find out the air sample volume that needs to be collected, and to check for inertness of the Teflon sampling bags. Both prototypes of the RAMEE were tested over the range of operating conditions. Since the contaminants were suspected to transfer by similar mechanism as water vapor, high latent effectiveness operating conditions (higher *NTU* and higher *Cr**) were chosen for testing. The effect of various process parameters like change in the air flow rate (*NTU*), change in the liquid desiccant flow rate (*Cr**), change in the latent effectiveness (ε_l), and change in the environmental conditions on contaminant transfer were also evaluated.

5.2 Conclusions

The following conclusions are drawn from the work presented in this thesis.

- Toluene and formaldehyde are chosen as VOCs for testing of the RAMEE prototypes based on the criteria of concentration of contaminants found in typical non-industrial

indoor and outdoor air, and the transfer mechanism of contaminants in the RAMEE. Sulfur hexafluoride is used as a tracer gas for testing air leakage.

- The concentration of contaminants measured in the ambient air sample agreed with the ambient air sample collected and kept for one day in the Teflon sampling bag indicating that the Teflon sampling bags are chemically inert to majority of chemical compounds present in the ambient air.
- The minimum volume of air sample required by Gasmet™ CR-100M gas analyzer for accurate measurement of contaminant concentration is 90 L and hence, 100 L Teflon sampling bags are suitable for collection of the air sample.
- Teflon sampling bags need to be flushed at least 3 times with inert gas like nitrogen before collecting a new air sample.
- The concentration of water vapor and carbon dioxide in the ambient air measured by Gasmet™ CR-100M gas analyzer agreed with those measured by Vaisala Carboncap® GM-70 meter within their uncertainty range.
- The bias and precision uncertainty of Gasmet™ CR-100M gas analyzer are 2% and 0.01% of the measurement range, respectively. This results in total uncertainty of 3.6% for *EATR* values of sulfur hexafluoride, 3.5% for $EATR_i$* values of toluene and 3.6% for $EATR_i$* values of formaldehyde.
- *EATR* values of sulfur hexafluoride are measured to be nearly $0 \pm 3.6\%$ in Prototype #4 and Prototype #6 and therefore, it can be concluded that there is negligible air leakage in both prototypes.
- $EATR_i$* values of toluene and formaldehyde in the RAMEE prototypes are measured to be in the range of $2.3 - 3.4 \pm 3.5\%$ and $4.5 - 6.4 \pm 3.6\%$, respectively. These values are

smaller than 71% toluene and 8-15% formaldehyde measured in the desiccant wheel (Wolfrum et al., 2008) and the energy wheel (Fisk et al., 1985, Andersson et al., 1993), respectively. The transfer fraction of toluene is lower than formaldehyde in both RAMEE prototypes because toluene has lower air diffusion coefficient and water solubility compared to formaldehyde.

- The transient testing of Prototype #4 and Prototype #6 shows that the transfer fraction of toluene, formaldehyde and sulfur hexafluoride remains unchanged over a time duration of 6 hours. It is concluded that the salting out effect reduces the solubility of contaminants causing very small dissolution of contaminants for high concentration of salt solutions. Hence, the contaminant transfer is limited by mass equilibrium of contaminants in the liquid desiccant.
- The transfer fraction of contaminants in Prototype #6 is measured to be lower than in Prototype #4 indicating that the diffusion coefficient of the tested contaminants through Prototype #6 membrane (GE ePTFE QL822^{TM}) is lower than that of Prototype #4 membrane (AY Tech^{TM} ePTFE).
- The measured transfer fraction of toluene and formaldehyde in Prototype #4 and Prototype #6 remains nearly unchanged over the range of tested process parameters like the air flow rate (*NTU*) and the liquid desiccant flow rate (*Cr**). This is because the small increase in latent effectiveness over the range of *NTU* and *Cr** does not have significant effect on the transfer fraction of toluene and formaldehyde.
- The transfer fraction of toluene and formaldehyde is measured to be slightly higher in winter than in summer conditions, but the difference in values is much smaller than the uncertainty.

- The transfer fraction of toluene and formaldehyde increases slightly as the latent effectiveness increases; however, the values are constant within the experimental uncertainties.
- The mass balance inequality defined by ANSI/ASHRAE Standard 84 (2012) is satisfied for all of the contaminant transfer testing on Prototype #4 and Prototype #6.

5.3 Recommendation for Future Work

There are still many tasks that need to be studied to evaluate the contaminant transfer in the RAMEE. Some of the topics are suggested based on the work of this thesis and they are as follows:

- Determine the contaminant transfer in the RAMEE prototypes using different contaminants and liquid desiccant solutions
- Develop a numerical model to simulate the transfer of contaminants in the RAMEE so that the experimental results could be compared with the numerical results. The numerical model could also be useful to perform the sensitivity study for contaminant transfer.
- Manufacture a new leak proof RAMEE prototype so that the liquid desiccant is not leaking into the air channels inside LAMEE.

LIST OF REFERENCES

Afshin, M., Simonson, C.J., and Besant, R.W., 2010. Crystallization limits of LiCl-Water and $MgCl_2$-Water salt solutions as operating liquid desiccant in the RAMEE system. ASHRAE Transactions, vol. 116(2), p. 494-506.

AHRI STANDARD 1060, 2011. Performance rating for air-to-air exchangers for energy recovery ventilation equipment. Arlington: Air-Conditioning & Refrigeration Institute.

Ali, A., Vafai, K. and Khaled, A.-R.A., 2004. Analysis of heat and mass transfer between air and falling film in a cross flow configuration, International Journal of Heat and Mass Transfer, vol. 47, p. 743-755.

Andersson, B., Andersson K., Sundell J., and Zingmark, P.A., 1993. Mass Transfer of contaminants in rotary enthalpy exchanger. Indoor Air, vol. 3, p. 143-148.

American Conference of Governmental Industrial Hygienists (ACGIH), 1988. Threshold Limit Values (TLVs) and Biological Exposure Indices for 1988-1989. Cincinnati, USA.

ANSI/ASHRAE STANDARD 55, 2004. Thermal environmental conditions for human occupancy. Atlanta: American Society of Heating, Refrigerating, and Air-Conditioning Engineers.

ANSI/ASHRAE STANDARD 62.1, 2004. Ventilation for acceptable indoor air quality. Atlanta: American Society of Heating, Refrigerating, and Air-Conditioning Engineers.

ANSI/ASHRAE STANDARD 84, 2012. Method of test for air-to-air heat/energy exchangers. Atlanta: American Society of Heating, Refrigerating, and Air-Conditioning Engineers.

ANSI/ASHRAE STANDARD 90.1, 2007. Energy standards for buildings except for low- rise residential buildings. Atlanta: American Society of Heating, Refrigerating, and Air-Conditioning Engineers.

ASHRAE, 2005. ASHRAE Handbook-Fundamentals. Atlanta: American Society of Heating, Refrigerating, and Air-Conditioning Engineers.

ASHRAE, 2008. ASHRAE Handbook-HVAC Systems and Equipments. Atlanta: American Society of Heating, Refrigerating, and Air-Conditioning Engineers.

ASME Performance Test Code 19.1, 1998. Test uncertainty: Instruments and Apparatus. New York: American Society of Mechanical Engineers.

Batterman, S.A., Zhang, G.Z., and Baumann, M., 1998. Analysis and stability of aldehydes and terpenes in electropolished canisters. Atmospheric Environment, vol. 32, p. 1647-1655.

Berglund, B., Johansson, I., Lindvall, T. and Lundin, L., 1989. Air quality and symptoms in a sick library building with a return-air ventilation system. Proceedings of Clinia 2000, Amersfoort, Netherlands, REHVA, vol. 111, p. 13-18

Beriault, D.A., 2011. Run-Around Membrane Energy Exchanger Prototype 4: Design and laboratory testing, M.Sc. Thesis, Department of Mechanical Engineering, University of Saskatchewan, SK.

Besant, R.W. and Simonson, C.J., 2003. Air-to-air energy recovery. ASHRAE Journal, vol. 45(4), p. 42-52

Brightman, H.S., Womble, S.E., Ronca, E.L., and Girman, J.R., 1996. Baseline information on indoor air quality in large buildings (BASE '95). Proceedings of Indoor Air, vol. 3, p. 1033-1038.

Brown, S. K., 2002. Volatile organic pollutants in new and established buildings in Melbourne, Australia. Indoor Air, vol. 12, p. 55-63.

Brown, S.K., Sim, M.R., Abramson, M.J., and Gray, C.N., 1994a. Concentrations of Volatile Organic Compounds in indoor air – A review. Indoor Air, vol. 4, p. 123-134.

Brown, T., LeMay, E. and Burston, B., 1994b. Chemistry: The Central Science. Englewood Cliffs, NJ: Prentice Hall, Inc.

D & R International, 2009. Buildings Energy Data Book. The Buildings Technologies Program, Energy Efficiency and Renewable Energy, U.S. Department of Energy.

Erb., B., 2007. Run-around membrane energy exchanger prototype-2 testing, Summer work report. Saskatoon, Saskatchewan: Department of Mechanical Engineering, University of Saskatchewan.

European Collaborative Action (ECA) on Indoor Air Quality and its Impact on Man, 1997. Total volatile organic compounds (TVOC) in indoor air quality investigations. Report no 19, EUR 17675EN. Luxembourg Office for Official Publications of the European Community.

Fan, H., 2005. Modeling a run-around heat and moisture recovery system, M.Sc. Thesis, Department of Mechanical Engineering, University of Saskatchewan, Saskatoon.

Fan, H., Simonson, C.J., Besant, R.W. and Shang, W., 2005. Run-around heat recovery system using cross-flow flat-plate heat exchangers with aqueous ethylene glycol as the coupling fluid, ASHRAE Transactions, vol. 111(1), p. 901-910.

Fang, L., Clausen, G. and Fanger, P.O., 2000. Temperature and humidity: important factors for perception of air quality and for ventilation requirements. ASHRAE Transactions, vol. 106, p. 503-510.

Fisk, W.J., Pederson, B.S., Hekmat, D., Chant, R.E., Kaboli, H., 1985. Formaldehyde and tracer gas transfer between air streams in enthalpy air-to-air heat exchanger. ASHRAE Transactions, Pt 1B, p. 173-186.

Gasmet™ Technologies Oy, 2006. In-Lab Series Instruction & Operating Manual for the Gasmet CR-100M FT-IR gas analyzer model. Gasmet Technologies Oy, Helsinki, Finland.

Green, D.W., and Perry, R.H., 2007. Perry's Chemical Engineer's Handbook, Eighth Edition. New York, McGraw-Hill.

Grutzner, T., and Hasse H., 2004. Solubility of formaldehyde and trioxane in aqueous solutions. Journal of Chemical Engineering Data, vol. 49(3), p. 642-646

Hemingson, H., 2005. Preliminary testing for run around heat and moisture exchanger, Summer work report. Saskatoon, Saskatchewan: Department of Mechanical Engineering, University of Saskatchewan.

Hermann, C., Dewes, I., and Schumpe, A., 1995. The estimation of gas solubilities in salt solutions. Chemical Engineering Science, vol. 50(10), p. 1673-1675.

Hodgson, A.T., 1995. A review and limited comparison of methods for measuring total volatile organic compounds in indoor air. Indoor Air, vol. 5, p. 247-257.

Hsieh, C.C., Horng, S.H., and Liao, P.N., 2003. Stability of trace-level volatile organic compounds stored in canisters and Tedlar bags. Aerosol Air Quality Research, vol. 3, p. 17–28

Hundell, K., Otto, D., and House, D., 1993. Time course of odor and irritation effects in humans exposed to a mixture of 22 volatile organic compounds. Proceedings of Indoor Air '93, Helsinki. International Conference on Indoor Air Quality and Climate, vol. 1, p. 567-572.

Incropera, F.P. and Dewitt, D.P., 2002. Fundamentals of Heat and Mass Transfer. 5th edn. New York, McGraw-Hill.

ISO Standard 5167-1, 1991. Measurement of Fluid Flow by Means of Pressure Differential Devices. International Organization for Standardization.

Johnson, A.B., Besant, R.W., and Schoenau, G.J., 1995. Design of multi-coil run-around heat exchanger systems for ventilation air heating and cooling. ASHRAE Transactions, vol. 101(2), p. 967-78.

Kjaergaard, S., Molhave, L., and Pederson, O., 1991. Human reactions to a mixture of indoor air volatile organic compounds. Atmospheric Environment, vol. 25A(8), p. 1417-1426.

Kosonen, R. and Tan, F., 2004. The effect of perceived indoor air quality on productivity loss. Energy and Buildings, vol. 36(10), p. 981-986.

Larson, M.D., 2006. The performance of membrane in a newly proposed run-around heat and moisture exchanger, M.Sc Thesis, Department of Mechanical Engineering, University of Saskatchewan, Saskatoon.

Mahmud, K., 2009, Design and performance testing of counter-cross-flow Run- Around Membrane Energy Exchanger System, M.Sc. Thesis, Department of Mechanical Engineering, University of Saskatchewan, SK.

Maroni, M., Seifert, B., and Lindvall, T., 1995. Indoor air quality: A comprehensive reference book. Air Quality Monographs, vol. 3, p. 1049.

Mesquita, L.C.S., Harrison, S.J. and Thomey, D., 2006. Modeling of heat and mass transfer in parallel plate liquid –desiccant dehumidifiers, Solar Energy, vol. 80, p. 1475-1482.

Mishra, M., Das, P.K. and Sarangi, S., 2004. Transient behavior of cross-flow heat exchangers with longitudinal conduction and axial dispersion. Journal of Heat Transfer, vol. 126(3), p. 425-433.

Molhave, L. (1986). Indoor air quality in relation to sensory irritation due to volatile organic compounds. ASHRAE Transactions, vol. 92 Part 1 (Paper 2954).

Molhave, L. (1991). Volatile organic compounds, indoor air quality and health. Indoor Air, vol. 4, p. 357-376

Molhave, L., Kjaergaard, S., Pederson, O., Jorgensen, A., and Pederson, A., 1993b. Human response to different mixtures of volatile organic compounds. In: Proceedings of Indoor Air ’93, Helsinki. International Conference on Indoor Air Quality and Climate, vol. 1, p. 555-560.

Molhave, L., Liu, Z., Jorgensen, A., Pederson, O., and Kjaergaard, S., 1993a. Sensory and physiological effects on humans of combined exposures to air temperature and volatile organic compounds. Indoor Air, vol. 3, p. 155-169.

NIOSH, 1997. NIOSH pocket guide to chemical hazards. DHHS (NIOSH) Publication 97-10. U.S. Department of Labor, Occupational Safety and Health Administration, Washington, D.C.

Otto, D., Hundell, K., House, D., and Prah, J., 1993. Neurobehavioral and subjective reactions of young men and women to a complex mixture of volatile organic compounds. In: Proceedings of Indoor Air ’93, Helsinki. International Conference on Indoor Air Quality and Climate, vol. 1, p. 59-64.

Park, M.S., Howell, J.R., Vliet, G.C. and Peterson, J., 1994. Numerical and experimental results for coupled heat and mass transfer between a desiccant film and air in cross flow, International Journal of Heat and Mass Transfer, vol. 37(1), p. 395–402.

Popescu, M., and Ghosh, T.K., 1999. Dehumidification and Simultaneous Removal of Selected Pollutants from Indoor Air by a Desiccant Wheel Using a 1M Type Desiccant. Journal of Solar Energy Engineering, vol. 121, p. 1-13.

Poulson, S., Harrington, R., and Drever, J., 1999. The solubility of toluene in aqueous salt solutions. Talanta, vol. 48, p. 633-641.

Prah, J., Hazucha, M., Horstman, D., Garlington, R., Case, M., Ashley, D., and Tepper, J., 1993. Purmonary, respiratory and irritant effects of exposure to a mixture of VOCs at three concentrations in young men. In: Proceedings of Indoor Air '93, Helsinki. International Conference on Indoor Air Quality and Climate, vol. 1, p. 607-612.

Redlich, C., A., Spacer, J. and Cullen. M., R., 1997. Sick-building syndrome. Occupational medicine, vol. 349(1), p. 1013-1016.

Robbins, G.A., Wang, S., and Stuart, J. D., 1993. Using the headspace method to determine Henry's law constants. Analytical Chemistry, vol. 65, p. 3113-3118.

Sanemasa, I., Arakawa, S., Araki, M., and Deguchi, T., 1984. The effects of salts on the solubilities of benzene, toluene, ethylbenzene, and propylbenzene in water. Bulletin of the Chemical Society of Japan, vol. 57, p. 1539-1544.

Schaeffler, A., Schultz, U., Beckert, J., 1988. Carry over of pollutants in rotary air-to-air heat exchangers (Regenerative Heat Recovery Systems). Systems Material and Policies for Healthier Indoor Air, vol. 2, p. 113-119.

Schumpe, A., 1993. The Estimation of Gas Solubilities in Salt Solutions. Chemical Engineering Science, vol. 48(1), p. 153-158.

Seyed Ahmadi, M., 2008. Modeling the transient behaviour of a run-around heat and moisture exchanger system, M.Sc Thesis, Department of Mechanical Engineering, University of Saskatchewan, Saskatoon.

Shang, W., Wawryk, M., and Besant, R.W., 2001. Air crossover in rotary wheels used for air-to-air heat and moisture recovery. ASHRAE Transactions: Research, 4463 (RP-862), p. 72-83.

Sheldon, L., Handy, R.W., Hartwell, T., Whitmore, R.W., Zelon, H., and Pellizzari, E.D., 1988a. Indoor Air Quality in public buildings, Vol. I. EPA/600/S6-88/009a. Environmental Protection Agency, Washington, D.C.

Sheldon, L., Zelon, H., Sickles, J., Easton, C., Hartwell, T., and Wallace, L., 1988b. Indoor Air Quality in public buildings, Vol. II. EPA/600/S6-88/009b. Environmental Protection Agency, Research Triangle Park, NC.

Simonson, C.J., 2007. Heat and energy wheels, Encyclopedia of Energy Engineering and Technology, Volume 2, Edited by Barney Capehart, CRC Press, Boca Raton, FL, p. 794-800.

Sparrow, E.M., Abraham, J.P., Martin, G.P., and Tong, J.C.Y., 2001. An experimental investigation of a mass exchanger for transferring water vapor and inhibiting the transfer of other gases. International Journal of Heat and Mass Transfer, vol. 44, p. 4313-4321.

Spiga, G. and Spiga, M., 1987. Two-dimensional transient solutions for cross-flow heat exchangers with neither gas mixed. Journal of Heat Transfer, vol. 109(2), p. 281-286.

Srihari, N. and Das, S.K., 2008. Experimental and theoretical analysis of transient response of plate heat exchangers in presence of nonuniform flow distribution. New York, N.Y.: American Society of Mechanical Engineers.

Treybal, R. E., 1980. Mass Transfer Operations. New York, McGraw Hill.

Vali., A., 2009. Modeling a run-around heat and moisture exchanger using two counter/cross flow exchangers, M.Sc Thesis, Department of Mechanical Engineering, University of Saskatchewan, Saskatoon.

VanOsdell, D.W. 1994. Evaluation of test methods for determining the effectiveness and capacity of gas-phase air filtration equipment for indoor air applications – Phase 1: Literature review and test recommendations. ASHRAE Research Project RP-674.

Wal, J.F.v.d., Hoogenvenn, A.W. and Leeuwen, L.V., 1998. A quick screening method for sorption effects of volatile organic compounds on indoor materials. Indoor Air, vol. 8, p. 103-112.

Wolfrum, E.J., Peterson, D., and Kozubal, E. 2008. The Volatile Organic Compound (VOC) Removal Performance of Desiccant-Based Dehumidification Systems: Testing at Sub-ppm VOC Concentrations, HVAC&R Research, vol. 14(1), p. 129-140.

Wolkoff, P., Clausen, P.A., Jensen, B., Neilsen, G.D., and Wilkins, C.K. 1997. Are we measuring the relevant indoor pollutants? Indoor Air, vol. 7, p. 92-106.

World Health Organization (WHO), 1989. Indoor air quality: organic pollutants. EURO reports and studies no 111. World Health Organization, Regional Office for Europe, Copenhagen.

Wu, X.P., Johnson, P. and Akbarzadeh, A., 1997. Application of heat pipe heat exchangers to humidity control in air-conditioning systems. Applied Thermal Engineering, vol. 17(6), p. 561-568.

Yalkowsky, S.H., and He, Y., 2003. Handbook of aqueous solubility data, First Edition, New York, CRC Press.

Zhang, L.Z. and Niu, J.L., 2002. Effectiveness correlations for heat and moisture transfer processes in an enthalpy exchanger with membrane cores, ASME Journal of Heat Transfer, vol. 124, p. 922-929.

Zhou, X. and Mopper, K., 1990. Apparent partition coefficients of 15 carbonyl compounds between air and seawater and between air and freshwater; Implications for air-sea exchange. Environment Science Technology, vol. 24, pp. 1864-1869

Zuraimi, M.S., Tham, K.W., and Sekhar, S.C., 2002. Identification and quantification of VOCs Sources in air-conditioned office buildings in singapore. Proceedings of the 9th International Conference on Indoor Air Quality and Climate. Monterey, CA, USA, 183.

APPENDIX A

CONTAMINANT PROPERTIES CALCULATION

The chemical and physical properties of contaminants play important role in the contaminant transfer in the RAMEE. The diffusivity in air, the water solubility and the saturation concentration of contaminant in the water are some of the most important properties. This is due to the fact that for contaminants to be transferred between the air streams in the RAMEE, the contaminants need to diffuse through the air and dissolve in the liquid desiccant circulated between the exchangers. The water solubility data for toluene and formaldehyde are shown in Section 3.2.2. The calculation of the contaminant saturation concentration is also explained in Section 3.2.2. The calculation of the contaminant diffusivity in the air is shown in this Appendix.

An expression for estimating the diffusivity of contaminant in the air in the absence of experimental data is given by equation (A.1) (Treybal, 1980, page 31).

$$D_{AB} = \frac{10^{-4}\left(1.084 - 0.249\sqrt{\frac{1}{M_A}+\frac{1}{M_B}}\right)T^{3/2}\sqrt{\frac{1}{M_A}+\frac{1}{M_B}}}{P\left(r_{AB}\right)^2 f\left(\frac{kT}{\varepsilon_{AB}}\right)} \qquad \text{(A.1)}$$

Here,

D_{AB} = the diffusivity of the contaminant (A) through the air (B) (m^2/s),

M_A = the molecular weight of the contaminant (kg/kmol),

M_B = the molecular weight of the air (kg/kmol),

T = the absolute temperature (K),

P = the absolute pressure (N/m^2),

r_{AB} = the molecular seperation at collision (nm),

$$= \frac{r_A + r_B}{2} \qquad \text{(A.2)}$$

k = the Boltzman's constant (J/K),

ε_{AB} = the energy of molecular attraction, and

$$= \sqrt{\varepsilon_A \varepsilon_B} \qquad \text{(A.3)}$$

$f\left(\frac{kT}{\varepsilon_{AB}}\right)$ = the collision function.

The value of the collision function can be calculated using the collision function for the diffusion chart given by Treybal (page 32, 1980). The values of r and ε can be estimated for each component empirically as shown in equation (A.4) and (A.5) below.

$$r = 1.18 v^{1/3} \qquad \text{(A.4)}$$

Here,

v = the molal volume of liquid at normal boiling point (m^3/kmol)

$$\frac{\varepsilon}{k} = 1.21 T_b \qquad \text{(A.5)}$$

Here,

T_b = the normal boiling point of the component (K)

The values of toluene, formaldehyde and water vapor diffusivity in the air are calculated using the method described here and they are given in Table 3.5.

APPENDIX B

CONTAMINANT INJECTION FLOW RATE CALCULATION

Two different contaminant injection techniques are employed for the contaminant transfer experiments. This appendix describes the calculation of the required injection flow rate of contaminant in both injection techniques to achieve the desired concentration of the contaminant in the air stream.

B.1 Calibrated Gas Mixture Injection of Cotaminants

Erb (2007) showed that the minimum and maximum mass flow rate of air that can be measured using the combination of orifice plates and pressure transducers in the RAMEE test facility are 1.8×10^{-3} kg/s and 43.8×10^{-3} kg/s. These values correspond to the dry air volumetric flow rate of 1.47×10^{-3} m^3/s (3 cfm) and 0.036 m^3/s (76 cfm) at standard pressure and temperature conditions. The mass flow meter that is used to control the flow rate of contaminants has the controllable range of 10 L/min to 200 L/min. Also, the Gasmet™ CR-100M FTIR gas analyzer used to measure the contaminant concentration in the air sample can measure formaldehyde up to 2 ppm and toluene and sulfur hexafluoride up to 10 ppm only in the air sample. The injection flow rate of each contaminant is calculated by considering all the experimental constraints explained above.

Formaldehyde is obtained as the pressure cylinder containing calibrated gas mixture of nitrogen and formaldehyde at 30 ppm concentration. The injection flow rate for formaldehyde is calculated as follows:

- Concentration of formaldehyde in the calibrated gas mixture is:

  $C_{f,m}$ = 30 ppm = 3×10^{-5} m^3 of formaldehyde/m^3 of mixture

- Flow rate of this calibrated gas mixture containing formaldehyde is set to:

  q_m = 15 L/min = 2.51×10^{-4} m^3 of mixture/s

- This results in the flow rate of formaldehyde as:

  $q_f = C_{f,m} \times q_m = 7.52 \times 10^{-9}$ m^3 of formaldehyde/s

If this gas mixture is injected into the air stream having the flow rate of 10 cfm (4.72×10^{-3} m^3 of air/s), then the resulting concentration of formaldehyde in the air stream is:

$$C_{f,a} = \frac{q_f}{q_a} = \frac{7.52 \times 10^{-9} m^3 of formaldehyde / s}{4.72 \times 10^{-3} m^3 of air / s} = 1.59 ppm$$

The RAMEE prototypes are tested to the maximum air flow rate of 70 cfm (0.033 m^3 of air/s). Under these circumstances, the flow rate of the formaldehyde gas mixture is also increased by 7 times (105 L/min) to maintain the same concentration of formaldehyde (1.59 ppm) in the air stream. The injection flow rates of toluene and sulfur hexafluoride are determined in a similar fashion. The air is assumed to be dry and at standard pressure and temperature conditions in these calculations. Hence, the actual measured concentration of contaminants in the air stream is slightly different than the calculated concentration; however, it is very close to the calculated amount.

B.2 Evaporation Chamber Injection of Contaminants

The contaminants are obtained as liquids and they are evaporated in the evaporation chamber. The air mixture containing evaporated contaminants is then mixed with the exhaust inlet air stream in the RAMEE test facility. Toluene is obtained as 100% liquid solution but formaldehyde is obtained as 37% liquid solution containing 63% water. The injection flow rate of both of these contaminants is calculated considering the same experimental constrains mentioned in Section B.1.

- The desired concentration of formaldehyde in the exhaust inlet air stream is:

  $C_{f,a}$ = 1.6 ppm = 1.97 mg of formaldehyde/m^3 of air

- Considering the exhaust inlet air stream flow rate of 10 cfm (4.72×10^{-3} m^3 of air/s), the mass flow rate of formaldehyde in this air stream can be calculated as:

  $\dot{m}_{f,a} = C_{f,a} \times q_a = 0.0093$ mg of formaldehyde/s

- For 37% formaldehyde solution, the concentration of formaldehyde can be given as:

  $C_{f,s} = 0.37$ mg of formaldehyde/mg of solution

- To maintain the same mass flow rate of formaldehyde as given by $\dot{m}_{f,a}$, the formaldehyde solution mass flow rate can be calculated as:

  $$\dot{m}_{f,sol} = \frac{\dot{m}_{f,a}}{C_{f,s}} = 0.025 \text{ mg of solution/s}$$

- Using the specific gravity of 37% formaldehyde solution (1.08), the volumetric injection flow rate for formaldehyde solution can be calculated as:

  $$q_{f,sol} = \frac{\dot{m}_{f,sol}}{SG_{f,sol}} = 1.39 \text{ μl/min}$$

The syringe pump is set to inject such low volume of formaldehyde continuously. When the air stream flow rate is increased to 70 cfm (0.033 m^3 of air/s), the injection rate of formaldehyde is also increased by 7 times to maintain the same concentration of formaldehyde in the air stream. The injection rate of liquid toluene is also calculated in a similar manner.

APPENDIX C

GASMET™ CR-100M FTIR GAS ANALYZER

The Gasmet™ CR-100M FTIR gas analyzer works on the principles of infrared spectroscopy. When a beam of infrared light is passed through the sample gas, gas molecules absorb specific frequencies, known as characteristic absorption frequencies, corresponding to the frequencies of molecular vibrations occurring in the infrared region of the electromagnetic spectrum (Gasmet™ Technologies Oy, 2006). An absorption spectrum, showing the characteristic absorption frequencies of gas molecules, demonstrates graphically to what extent the sample gas absorbs the different wavelengths of the infrared radiation (Gasmet™ Technologies Oy, 2006). The quantitative analysis of the absorption spectrum detects and measures the concentration of each compound in the sample gas (Gasmet™ Technologies Oy, 2006). Beer's law (also known as Beer-Lambert law) is the basic law for spectroscopic quantitative analysis. It shows how the concentration of the sample gas is related to the measured absorbance spectrum.

$$\log(I_0 / I) = \log(1/T) = A = abc \tag{C.1}$$

Here,

I_0 = intensity of infrared radiation entering the gas sample,

I = intensity of infrared radiation that has passed through the sample,

T = transmittance,

A = absorbance,

a = absorptivity (m^2/mol),

b = optical path length (m), and

c = sample concentration (ppm).

For each wavelength, the transmittance (T) is the intensity of the infrared radiation that has passed through the sample gas divided by the intensity of the infrared radiation that has entered the sample gas (Gasmet™ Technologies Oy, 2006). When there is no absorption, the value of transmittance (T) is 1, which indicates that 100% of the infrared radiation at that wavelength goes through the sample gas. The absorptivity (a) characterizes the capacity of the molecule to absorb infrared radiation. The value of absorptivity (a) varies from one molecule to another and as a function of wavelength; however, it is constant for a given molecule at a given wavelength (Gasmet™ Technologies Oy, 2006). The value of the optical path length (b) for the Gasmet™ CR-100M FTIR is 100 m and it is the distance the infrared radiation beam traverses in the gas sample. The quantity c indicates the concentration of the gas molecules in the sample gas (Gasmet™ Technologies Oy, 2006).

If the optical path length is constant, Beer's law states that the absorbance is directly proportional to the concentration of the sample gas at a given wavelength. Since Beer's law is additive, the total absorbance (A) is equal to the sum of the values of absorbance of each gas component. Additionally, to measure the concentration of a gas compound, it is necessary to calculate the number of gas molecules in the sample cell. According to ideal gas law ($pV = nRT$), the number of gas molecules (n) in the sample cell depends linearly on both the gas pressure (p) and the volume of the sample cell (V), and reciprocally on the gas temperature (T). Hence, any changes in sample gas temperature and pressure in the sample cell directly affect the measured gas compound concentration. Figure C.1 shows the basic components of the Gasmet™ FTIR gas analyzer.

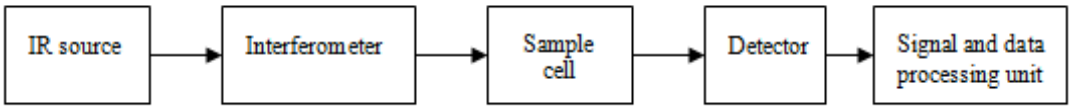

Figure C.1: Basic components of the Gasmet™ FTIR gas analyzer (Gasmet^{TM} Technologies Oy, 2006)

The infrared source produces broadband radiation, which is modulated by the interferometer. The interferometer performs an optical inverse Fourier transform of the infrared radiation emitted by the infrared source. The modulated infrared radiation passes through the sample cell where sample gas absorbs certain wavelengths of the radiation. The detector detects the intensity of transmitted infrared radiation. The A/D converter digitizes the signal and the digital signal processor (DSP) performs a mathematical Fourier transform on the digitized signal resulting in an absorbance spectrum. The Fast Fourier Transform (FFT) algorithm is used to compute the absorbance spectrum (Gasmet^{TM} Technologies Oy, 2006). Gasmet™ uses the multi-component analysis software known as Calcmet to compute the concentrations of the various components present in the sample gas from the absorbance spectrum.

APPENDIX D

TEST RESULTS

Table D.1 shows the concentration of contaminants measured at all four sampling ports during the experiments performed on RAMEE Prototype #4. The values for *EATR* or $EATR_i$* and mass balance inequality are calculated using the contaminant concentration data and mass flow rate data shown in Table 4.3. The measured latent effectiveness values are also shown in Table D.1.

Table D.1: Transfer fraction of contaminants measured in the RAMEE Prototype #4 during summer and winter testing conditions

Test Index	Test Condition	NTU	Cr*	Contaminant	Concentration of contaminant (ppm)				EATR or $EATR_i$* (%)	Latent effectiveness (%)	Mass balance inequality
					EI	EO	SI	SO			
Change in air flow rate (NTU) at constant Cr*											
1	Summer	12.1	4.5	SF_6	7.94	7.89	0.07	0.08	0.05	46	0.03
				C_7H_8	8.13	8.18	0.00	0.26	3.2	48	0.03
				HCHO	1.64	1.64	0.11	0.20	5.8	49	0.05
2		8.5	4.5	C_7H_8	7.86	7.88	0.09	0.33	3.1	43	0.03
				HCHO	1.61	1.59	0.05	0.14	5.7	41	0.05
3		4.9	4.5	C_7H_8	8.07	8.03	0.14	0.41	3.4	39	0.02
				HCHO	1.63	1.64	0.09	0.18	5.9	41	0.04
Change in Cr* at constant air flow rate (NTU)											
4	Summer	12.2	1.0	C_7H_8	7.96	7.95	0.10	0.34	3.0	31	0.03
				HCHO	1.58	1.60	0.06	0.15	5.9	32	0.07
5		12.2	2.0	C_7H_8	8.10	8.11	0.00	0.28	3.4	38	0.03
				HCHO	1.61	1.61	0.13	0.22	6.1	36	0.05
6		12.1	3.0	C_7H_8	8.17	8.18	0.09	0.34	3.1	42	0.03
				HCHO	1.59	1.63	0.07	0.16	5.9	44	0.03
7		12.2	4.5	C_7H_8	7.84	7.83	0.12	0.37	3.2	47	0.03
				HCHO	1.63	1.64	0.06	0.16	6.4	46	0.07
Change in environmental condition											
8	Winter	12.1	4.5	C_7H_8	7.88	7.85	0.00	0.26	3.3	47	0.03
				HCHO	1.59	1.55	0.06	0.15	5.9	46	0.03

Table D.2 shows the contaminant concentration measurement uncertainties and propagated uncertainties into *EATR* or $EATR_i$* and latent effectiveness for RAMEE Prototype #4.

Table D.2: Uncertainties associated with transfer fraction of contaminants measured in the RAMEE Prototype #4 during summer and winter testing conditions

Test Index	Test Condition	NTU	Cr*	Contaminant	Concentration of contaminant (ppm)				EATR or $EATR_i$* (%)	Latent effectiveness (%)
					EI	EO	SI	SO		
Change in air flow rate (NTU) at constant Cr*										
1	Summer	12.1	4.5	SF_6	0.20	0.20	0.20	0.20	3.6	4
				C_7H_8	0.20	0.20	0.20	0.20	3.4	3
				HCHO	0.04	0.04	0.04	0.04	3.6	4
2		8.5	4.5	C_7H_8	0.20	0.20	0.20	0.20	3.6	4
				HCHO	0.04	0.04	0.04	0.04	3.5	5
3		4.9	4.5	C_7H_8	0.20	0.20	0.20	0.20	3.5	4
				HCHO	0.04	0.04	0.04	0.04	3.6	3
Change in Cr* at constant air flow rate (NTU)										
4	Summer	12.2	1.0	C_7H_8	0.20	0.20	0.20	0.20	3.5	4
				HCHO	0.04	0.04	0.04	0.04	3.6	4
5		12.2	2.0	C_7H_8	0.20	0.20	0.20	0.20	3.4	3
				HCHO	0.04	0.04	0.04	0.04	3.7	5
6		12.1	3.0	C_7H_8	0.20	0.20	0.20	0.20	3.4	4
				HCHO	0.04	0.04	0.04	0.04	3.6	4
7		12.2	4.5	C_7H_8	0.20	0.20	0.20	0.20	3.6	5
				HCHO	0.04	0.04	0.04	0.04	3.5	4
Change in environmental condition										
8	Winter	12.1	4.5	C_7H_8	0.20	0.20	0.20	0.20	3.5	4
				HCHO	0.04	0.04	0.04	0.04	3.6	5

Table D.3 shows the concentration of contaminants measured at all four sampling ports during the experiments performed on RAMEE Prototype #6. The values for *EATR* or $EATR_i$* and mass balance inequality are calculated using the contaminant concentration data and mass flow rate data shown in Table 4.4. The measured latent effectiveness values are also shown in Table D.3.

Table D.3: Transfer fraction of contaminants measured in the RAMEE Prototype #6 during summer and winter testing conditions

Test Index	Test Condition	NTU	Cr*	Contaminant	Concentration of contaminant (ppm)				EATR or $EATR_i$* (%)	Latent effectiveness (%)	Mass balance inequality
					EI	EO	SI	SO			
Change in air flow rate (NTU) at constant Cr*											
1	Summer	8.9	3.0	SF_6	8.11	8.12	0.06	0.07	0.02	59	0.03
				C_7H_8	7.96	7.99	0.09	0.31	2.8	59	0.02
				HCHO	1.56	1.54	0.05	0.12	4.6	61	0.03
2		6.1	3.1	C_7H_8	8.08	8.06	0.10	0.33	2.9	54	0.06
				HCHO	1.57	1.59	0.08	0.15	4.9	53	0.06
3		3.2	3.0	C_7H_8	7.87	7.84	0.12	0.30	2.3	51	0.02
				HCHO	1.63	1.58	0.00	0.08	4.9	49	0.02
Change in Cr* at constant air flow rate (NTU)											
4	Summer	8.8	1.0	C_7H_8	7.92	7.96	0.05	0.26	2.6	25	0.02
				HCHO	1.61	1.57	0.11	0.18	4.7	26	0.03
5		8.9	2.0	C_7H_8	8.17	8.13	0.06	0.29	2.8	45	0.03
				HCHO	1.64	1.58	0.09	0.17	5.1	47	0.02
6		8.8	2.9	C_7H_8	7.97	7.93	0.13	0.32	2.4	60	0.02
				HCHO	1.60	1.63	0.07	0.14	4.6	59	0.06
7		8.8	4.5	C_7H_8	8.00	8.05	0.00	0.24	3.0	63	0.03
				HCHO	1.62	1.57	0.10	0.18	5.3	62	0.02
Change in environmental condition											
8	Winter	8.9	3.1	C_7H_8	8.12	8.06	0.06	0.29	2.9	60	0.02
				HCHO	1.63	1.59	0.09	0.16	4.5	62	0.04

Table D.4 shows the contaminant concentration measurement uncertainties and propagated uncertainties into *EATR* or $EATR_i$* and latent effectiveness for RAMEE Prototype #6.

Table D.4: Uncertainties associated with transfer fraction of contaminants measured in the RAMEE Prototype #6 during summer and winter testing conditions

Test Index	Test Condition	NTU	Cr*	Contaminant	Concentration of contaminant (ppm)				EATR or $EATR_i$* (%)	Latent effectiveness (%)
					EI	EO	SI	SO		
Change in air flow rate (NTU) at constant Cr*										
1	Summer	8.9	3.0	SF_6	0.20	0.20	0.20	0.20	3.6	4
				C_7H_8	0.20	0.20	0.20	0.20	3.5	5
				HCHO	0.04	0.04	0.04	0.04	3.7	5
2		6.1	3.1	C_7H_8	0.20	0.20	0.20	0.20	3.5	5
				HCHO	0.04	0.04	0.04	0.04	3.7	4
3		3.2	3.0	C_7H_8	0.20	0.20	0.20	0.20	3.6	4
				HCHO	0.04	0.04	0.04	0.04	3.4	5
Change in Cr* at constant air flow rate (NTU)										
4	Summer	8.8	1.0	C_7H_8	0.20	0.20	0.20	0.20	3.5	5
				HCHO	0.04	0.04	0.04	0.04	3.7	4
5		8.9	2.0	C_7H_8	0.20	0.20	0.20	0.20	3.4	4
				HCHO	0.04	0.04	0.04	0.04	3.6	5
6		8.8	2.9	C_7H_8	0.20	0.20	0.20	0.20	3.6	5
				HCHO	0.04	0.04	0.04	0.04	3.6	4
7		8.8	4.5	C_7H_8	0.20	0.20	0.20	0.20	3.5	5
				HCHO	0.04	0.04	0.04	0.04	3.6	5
Change in environmental condition										
8	Winter	8.9	3.1	C_7H_8	0.20	0.20	0.20	0.20	3.5	5
				HCHO	0.04	0.04	0.04	0.04	3.6	4